

For Reference

NOT TO BE TAKEN FROM THIS ROOM

Ex LIBRIS
UNIVERSITATIS
ALBERTAENSIS



THE UNIVERSITY OF ALBERTA

FRACTURED ROCK SUBJECTED TO DIRECT SHEAR

by



DAVID KENNETH JAMES NOONAN

A THESIS

SUBMITTED TO THE FACULTY OF GRADUATE STUDIES AND RESEARCH
IN PARTIAL FULFILMENT OF THE REQUIREMENTS FOR THE DEGREE OF
MASTER OF SCIENCE

DEPARTMENT OF CIVIL ENGINEERING

EDMONTON, ALBERTA

SPRING, 1972



Digitized by the Internet Archive
in 2019 with funding from
University of Alberta Libraries

<https://archive.org/details/Noonan1972>

Thesis
1972
111

UNIVERSITY OF ALBERTA

FACULTY OF GRADUATE STUDIES
AND RESEARCH

The undersigned certify that they have read, and recommend to the Faculty of Graduate Studies for acceptance, a thesis entitled FRACTURED ROCK SUBJECTED TO DIRECT SHEAR submitted by David Kenneth James Noonan in partial fulfilment of the requirements for the degree of Master of Science.

ABSTRACT

All engineering projects related directly to a fractured rock mass require a knowledge of the strength and deformation characteristics of the fractured rock mass in order that a rational analysis can be made. The direct shear test is the most useful method available for determining these characteristics.

Fractured coal samples have been obtained and subjected to direct shear to study the behaviour when the fractures are oriented at varying angles to the direction of the applied shear load. It was found that the shear strength of fractured rock is anisotropic and the shear parameters ϕ and c are affected in different ways. ϕ was found to be dependent upon the anisotropic strength of the unfractured material and c was found to be dependent upon the continuity of the fractures.

A method of determining Young's Modulus from the direct shear test has been developed and applied successfully. E was found to vary in direct relation to variations in ϕ .

ACKNOWLEDGEMENTS

The author wishes to acknowledge Dr. N.R. Morgenstern, research supervisor, for his constant enthusiasm and guidance in all aspects of the thesis work.

In addition, the author wishes to thank:

the personnel of Alberta Coal Ltd. and Calgary Power Ltd. for allowing access to the Highvale Mine;

Messrs. Orville Wood, Gerard Cyre, Allan Muir and Angus Hoecherl for their expert technical assistance;

Mr. John F. Nixon for his invaluable assistance with the finite element analysis;

Dr. D.M. Cruden for his assistance in the geologic mapping.

A special thanks is reserved for my wife, Arlene, for her assistance, especially in typing the original and final copies of this manuscript.

TABLE OF CONTENTS

	Page
Title Page	i
Approval Sheet	ii
Abstract	iii
Acknowledgements	iv
Table of Contents	v
List of Tables	viii
List of Figures	ix
CHAPTER I INTRODUCTION	1
CHAPTER II MECHANICAL PROPERTIES OF FRACTURED ROCK	3
2.1 GEOLOGICAL PROPERTIES	3
2.2 STRENGTH PROPERTIES	5
CHAPTER III SAMPLING PROGRAM	27
3.1 SAMPLE REQUIREMENTS AND SITE SELECTION	27
3.2 GEOLOGY	29
3.2.1 Location and Access	29
3.2.2 Topography and Drainage	31
3.2.3 General Geology	31
3.2.4 Structure	33
3.3 FIELD INVESTIGATIONS	34
3.3.1 Location	34

	3.3.2 Mining Operation	34
	3.3.3 Detailed Geology	36
	3.3.4 Method of Sampling	38
	3.3.5 Transportation	41
CHAPTER IV	LABORATORY PROCEDURE	42
4.1	SAMPLE PREPARATION	42
	4.1.1 Storage	42
	4.1.2 Trimming	42
	4.1.3 Casting	42
4.2	TESTING PROCEDURE	44
	4.2.1 Classification Properties	44
	4.2.2 Direct Shear Tests on Pre-cut Samples	47
	4.2.3 Direct Shear Tests on Intact Samples	49
CHAPTER V	FINITE ELEMENT ANALYSIS OF SAMPLE IN DIRECT SHEAR	54
5.1	THEORETICAL ANALYSIS	54
	5.1.1 Theory	54
	5.1.2 Method of Solution	56
	5.1.3 Results	59
5.2	APPLICATION TO TEST SAMPLES	68
5.3	GENERAL APPLICATION OF METHOD	68
CHAPTER VI	RESULTS AND DISCUSSION	71
6.1	CLASSIFICATION PROPERTIES	71

6.2	DIRECT SHEAR TESTS ON PRE-CUT SAMPLES	73
6.3	DIRECT SHEAR TESTS ON INTACT SAMPLES	76
	6.3.1 Before Peak	76
	6.3.2 Peak	83
	6.3.3 After Peak	95
CHAPTER VII	CONCLUSIONS	103
	List of References	106
Appendix A:	Experimental Shear Load Versus Shear Displacement Graphs	A1
Appendix B:	Experimental Relationships of ϕ_r and i	B1

LIST OF TABLES

Table		Page
5.1	Boundary Conditions	59
6.1	Classification Properties	72
6.2	Results of Finite Element Application to Test Samples	79
6.3	Shear Strength Parameters	86

LIST OF FIGURES

Figure		Page
2.1	Shear Strength Failure Envelopes	6
2.2	Shear Strength Failure Envelope for a Horizontal Plane (after Patton, 1966)	8
2.3	Shear Strength Failure Envelope for a Plane Inclined Upward (+i) (after Patton, 1966)	10
2.4	Shear Strength Failure Envelope for a Plane Inclined Downward (-i) (after Patton, 1966)	10
2.5	The Influence of the Angle of Inclination of the Teeth on the Shear Strength Failure Envelope (after Patton, 1966)	12
2.6	Shear Strength Failure Envelopes for Specimens with Teeth of Two Different Inclinations (after Patton, 1966)	13
2.7	Shear Strength Failure Envelopes Showing the Increase in Strength Resulting from an Increase in the Number of Teeth (after Patton, 1966)	15
2.8	Shear Strength Failure Envelopes for Two Specimens with Different Internal Strengths (after Patton, 1966)	16
2.9	Calculated Maximum Strength Envelopes for Shearing Along an Irregular Rock Surface with the Teeth Inclinations of $i = 20^\circ$, 30° , and 40° , Respectively ($C_o = 15,000$ psi, $T_o = -1000$ psi, $\phi = 30^\circ$) (after Ladanyi and Archambault, 1970)	22
2.10(a)	Shear Failure by Stepping Between α Joints (the Main Set) and ψ Joints (the Secondary Set) - Long Joints (after Jennings, 1971)	24

Figure		Page
2.10(b)	Stepped Joint Failure - Short Joints (after Jennings, 1971)	24
2.11	A Comparison of Strength Theories (after Lajtai, 1969)	26
3.1	Sample Configurations	28
3.2	Location of Highvale Mine	30
3.3	Sampling Area at Highvale Mine	35
3.4	Rose Diagram of Structural Observations	37
3.5	STIHL Saw Used in Field Sampling	40
4.1	Saws Used in Laboratory for Cutting Samples	43
4.2	Samples Before and After Casting	45
4.3	Layout of Strength Testing Equipment	46
4.4	Modified Direct Shear Machine	48
4.5	Wykeham-Farrance Direct Shear Machine	50
4.6	Spacer Arrangement Within Shear Box	52
5.1	Simulation of Sample in Direct Shear	55
5.2	Finite Element Grid	58
5.3	Stress Distributions	60
5.4(a)	k Values for $\mu = 0.20$	62
5.4(b)	k Values for $\mu = 0.30$	63
5.4(c)	k Values for $\mu = 0.45$	64
5.5	Shear Stress Distribution Along the Mid-Plane for Different H/L Ratios	65
5.6	Sensitivity of Shear Stress to Grid Size	66

Figure		Page
5.7	NX Plate Bearing Device (after Goodman, 1968)	67
6.1	Shear Load Versus Shear Displacement for Pre-cut Plane	74
6.2	Residual Strength Envelope for Pre-cut Plane	75
6.3	Calculated Values of Young's Modulus	80
6.4	Complete Load - Deformation Curve Recorded Automatically During Laboratory Testing of Coal Specimens 2-ft. cube in Size in Uniaxial Compression (after Bieniawski, 1968)	81
6.5	Strength Envelopes at Peak - Category I	84
6.6	Strength Envelopes at Peak - Category II	85
6.7	Test Samples in Category I	87
6.8	Test Samples in Category II	88
6.9	Predicted Strength Envelopes with Bedding Planes Only in Sample	90
6.10	Predicted Strength Envelopes with Joint Planes and Bedding Planes in Sample	91
6.11	Percentage of the Shear Surface Composed of the Joint Plane	93
6.12	Representative Samples from Category I after Testing	96
6.13	Representative Samples from Category II after Testing	97

CHAPTER I

INTRODUCTION

It is the purpose of this thesis to investigate the behaviour of fractured rock subjected to direct shear. Direct shear tests are performed on all major civil engineering works involving rock material. The information that can be derived from these tests with regard to the strength and deformation properties of the rock mass is of particular interest when dealing with engineering problems concerning slide probability, safe foundation conditions, and structural stability in tunnels and mines. An understanding of the test along with complete knowledge of the maximum amount of data that can be obtained from the test is of paramount importance.

A review of the major publications dealing with strength and deformation properties of rock was undertaken and is presented in Chapter II. Based on this review, it was established that it is desirable to test samples in the laboratory that are representative of the rock mass as it exists in the field. This means the number of discontinuities per sample must be sufficiently large that extrapolation to field behaviour can be made. Also, the samples obtained must contain a regular geometry with respect to the

discontinuities in order that a rational analysis may be undertaken. The coal deposits south of Wabamun Lake presented an ideal material for this study.

The sampling program and laboratory procedure are discussed in detail in Chapters III and IV respectively.

A method of determining Young's Modulus from direct shear tests was derived and is presented in Chapter V. This method was applied to the coal samples tested and the results are presented and discussed in Chapter VI.

The results obtained from the direct shear tests dealing with the strength and deformation of the material are also presented and discussed in Chapter VI. The major conclusions arrived at are given in Chapter VII.

CHAPTER II

MECHANICAL PROPERTIES OF FRACTURED ROCK

2.1 GEOLOGICAL PROPERTIES

For the purposes of this study, a fractured rock is defined as one in which the rock mass contains structural discontinuities or planes of weakness. These include all geological features that separate the solid blocks of the rock mass such as joints, faults, fractures or bedding planes. (Piteau, 1970). The behaviour of rock material, particularly at the lower normal stresses depends almost exclusively on joints or other discontinuities within the rock. (Jennings, 1971).

In order that a rational study can be made of fractured rock, certain criteria must be satisfied. These are best described by Piteau (1970) in his four geological propositions which have been condensed by Jennings (1971) and are presented here.

1. Structural discontinuities, which for generality will all be referred to as joints, will exist in the rock mass as detectable features and it will be possible to describe their properties in a quantitative way, particularly as these relate to shear strength on the plane of the joint concerned.

2. In the rock mass definable boundaries exist, enclosing volumes which will be called structural regions, within which the joints occur in a systematic fashion forming one or more joint sets, each of which is designated a design set. For each design set the measurable joint properties are sufficiently similar to permit analysis to be performed.
3. A reliable model can be constructed to represent the jointing in the rock mass, i.e. sampling and analysis can be carried out on elements with reasonable expectation that similar conditions will apply to the particular portion of the rock mass under consideration.
4. Shear failure will tend to occur on planes or mean planes or combinations of such plane surfaces, i.e. there will be distinct anisotropy in shear strength, compelling failure on preferred planes.

A knowledge of the following joint properties is also required:

- (a) attitude of joints
- (b) length and width of joints
- (c) spacing of joints
- (d) frictional and cohesive shearing strength determined by roughness and continuity or gouge in the joint opening (if present)
- (e) cohesive and frictional shear strength of the intact

material

- (f) any major irregularities such as waviness of the joint surface
- (g) water pressure.

2.2 STRENGTH PROPERTIES

Once the properties of the fractured rock have been defined, the strength can be analysed. Consideration is given here only to the behaviour of fractured rock subjected to direct shear.

In a series of direct shear tests various normal loads are placed on the specimens. For each normal load, the maximum shearing force is recorded together with the shear displacements in the direction of the applied shearing force. The peak of the shearing force versus shearing displacement curve gives the maximum shearing resistance offered by the specimen. If the displacements are continued, the shear strength will decrease and then approach a horizontal asymptotic value described as the residual shearing resistance.

When several tests have been completed at different normal loads, the results can be conveniently summarized on a shear strength diagram in the form of failure envelopes. The shear strength is plotted against normal load as shown on Fig. 2.1.

The upper line gives the relationship between the shearing resistance of the sample (or its shear strength)

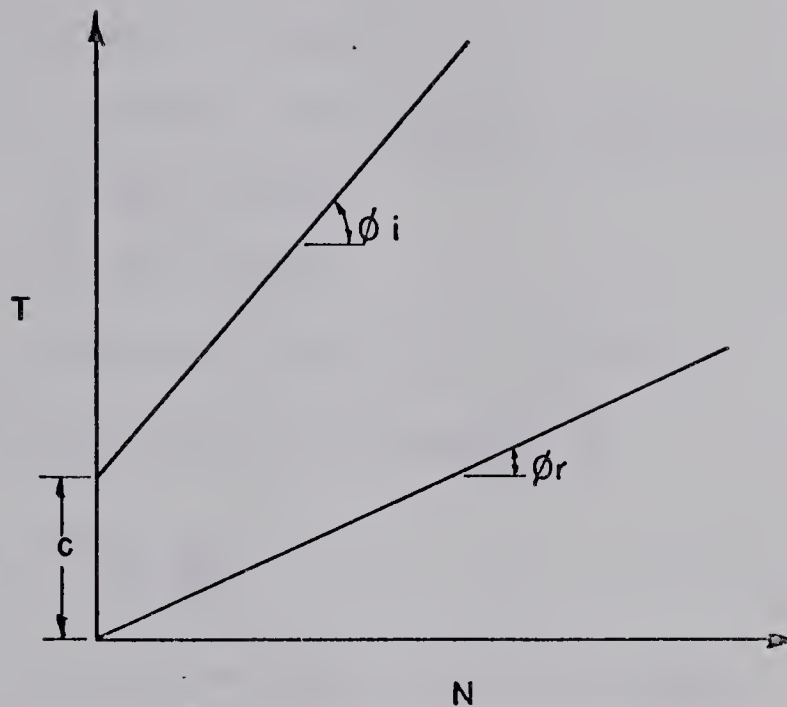


Fig. 2.1 Shear Strength Failure Envelopes.

and the normal load at failure. The inclination of this upper line is called the angle of internal shearing resistance, ϕ_i . The lower line gives the relationship between the sliding resistance or residual frictional resistance and the normal load. The inclination of the lower line is called the angle of residual shearing resistance ϕ_r . The upper line is referred to as the maximum strength failure envelope. The lower line is called the residual strength envelope and appears to correspond to the values of the frictional sliding resistance, ϕ_μ . (Patton, 1966). The upper line can be expressed by the Mohr-Coulomb equation

$$T = c + N \tan \phi_i \quad . . . \quad (2.1)$$

where T = shear strength

c = cohesion intercept or shear strength at zero
normal stress

N = normal stress

and ϕ_i = angle of internal friction.

The lower line can be expressed by

$$T = N \tan \phi_r \quad . . . \quad (2.2)$$

where ϕ_r is the residual friction angle.

In order to evaluate properly the combined sliding and shearing failure of in-situ rock masses it was necessary to develop a theoretical framework that could account for multiple modes of failure. The results of field studies on rock slopes and the related laboratory studies on rock samples indicated the importance of at least seven parameters related to combined sliding and shearing failure. These parameters were: (Patton, 1966)

- (1) the inclination of the irregularities, i
- (2) the residual angle of friction, ϕ_r
- (3) the size of the irregularities
- (4) the displacement along the failure plane
- (5) the stress level along the failure plane
- (6) the surface moisture along the failure plane
- (7) the internal strength of the material.

It was necessary to find test specimens in which the shape, size, and internal strength could be controlled. Plaster of Paris specimens whose strengths could be varied by mixing with a filler and whose surface geometry could be reproduced by casting in machined molds were specially prepared by Patton. The samples were 2.95 inches long, 1.75 inches wide, and 2.0 inches high. The following results are those given by Patton (1966).

Fig. 2.2 shows the failure envelope for a specimen with a pre-existing horizontal plane.

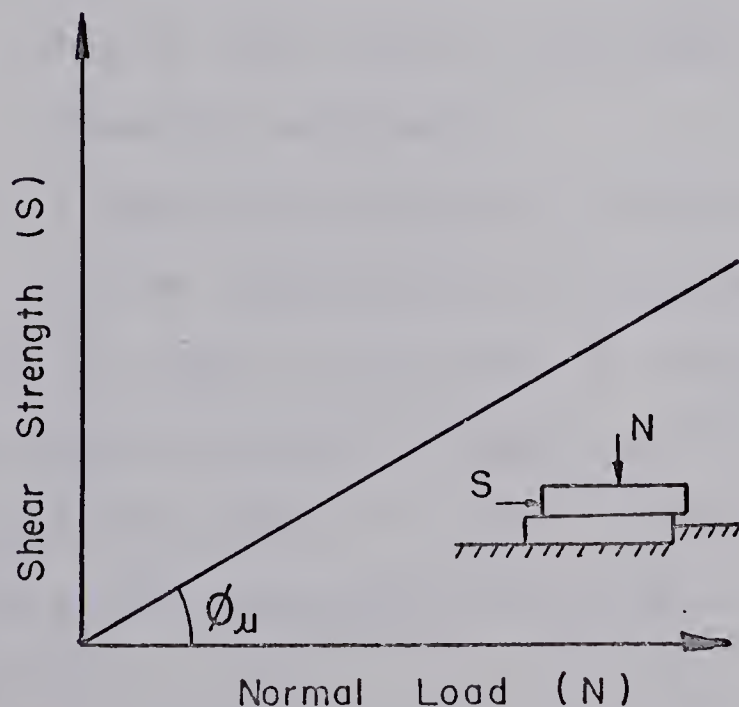


Fig. 2.2 Shear Strength Failure Envelope
for a Horizontal Plane.

(after Patton, 1966)

In this case the maximum strength failure envelope is the same as the residual strength envelope and the inclination of this line is ϕ_r .

The value of residual shearing resistance obtained for sliding along a horizontal plane is a minimum and is shown on succeeding diagrams for reference purposes. However, it is recognized that even lower values may result from:

- (1) kinetic friction
- (2) rolling friction (when rounded particles get between the sliding blocks)
- (3) excessive crushing or vertical deformation of the upper block in which some of the potential energy due to this vertical movement acts to reduce the shearing resistance
- (4) a negative or downward slope of the shearing plane in the direction of the applied shearing force.

If the plane of shearing in the previous example is inclined upward through an angle i , in the direction of the applied shearing force, it can be shown by principles of statics that the shearing resistance is increased by the relation

$$S = N \tan(\phi_r + i) \quad . . . \quad (2.3)$$

This relationship is illustrated in Fig. 2.3. Similarly if the plane of shearing is inclined downward as

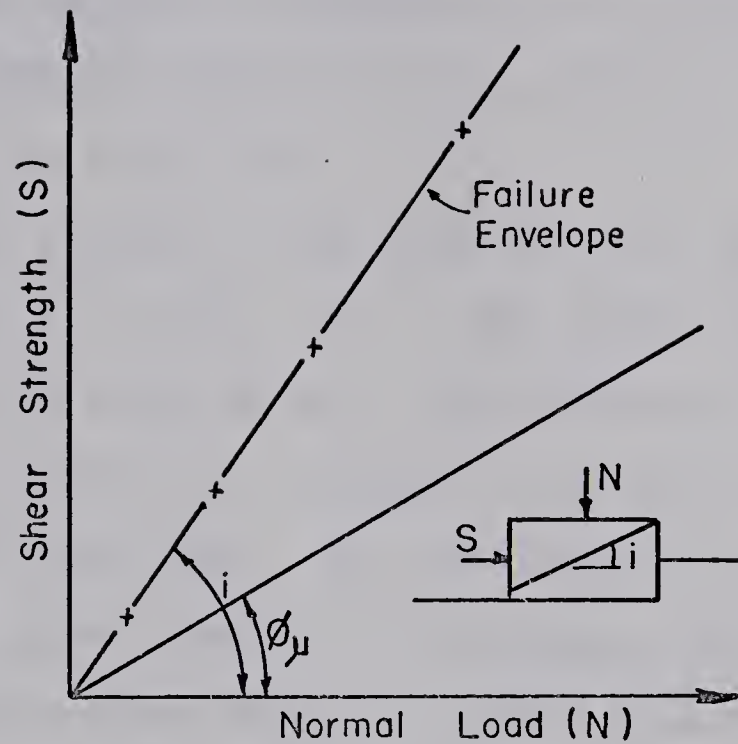


Fig.2.3 Shear Strength Failure Envelope for
a Plane Inclined Upward (+ i).
(after Patton, 1966)

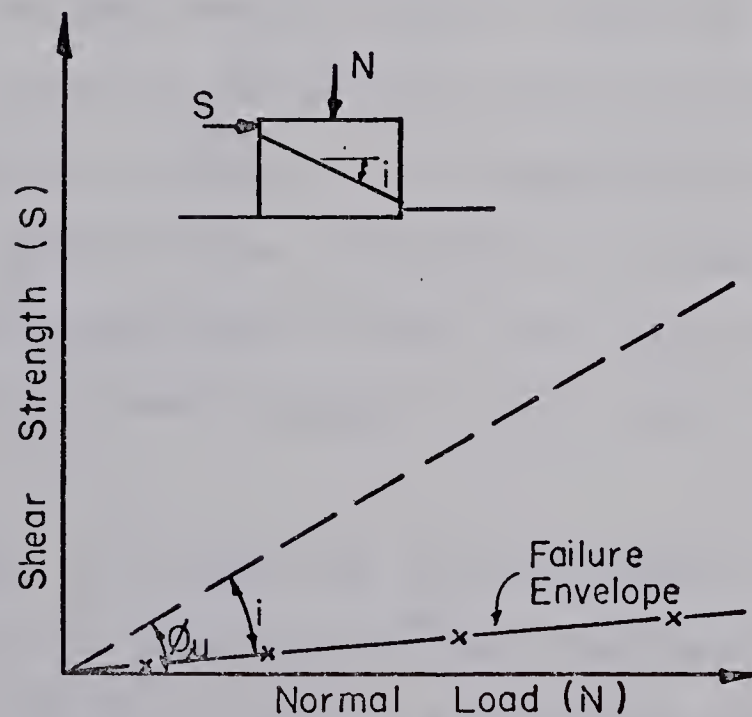


Fig.2.4 Shear Strength Failure Envelope for a
Plane Inclined Downward (- i).
(after Patton, 1966)

illustrated in Fig. 2.4, the shearing resistance is decreased.

The results of three series of tests, each series with a different angle of inclination i of the asperities are shown on Fig. 2.5.

The slopes of the lower portion of lines A, B, and C, are within 1° of $(\phi_r + i)$. The upper lines are seen to have a slope equal to ϕ_r . The change in slope of line B and C is related to a change in the mode of failure from sliding to shearing. The specimens whose results plot along the upper portion of the lines B and C did not slide along the inclined surfaces of the asperities at all before reaching their maximum load, but rather sheared off the teeth at their base. As the area of the intact material along the failure plane increases (the cross section of the intact material at the base of the 35° teeth is greater than for 45°) the load level at which the transition in the failure mode occurs becomes higher. This explains why line A is straight. The base areas of the 25° teeth are large enough that the normal load required to shear them off before sliding could occur had not been reached in the range of normal loads applied.

Fig. 2.6 shows the failure envelopes for specimens which have two teeth at 45° and two teeth at 25° . The maximum i (45°) is seen to govern the maximum strength envelope.

Fig. 2.7 shows the effect of doubling the number of

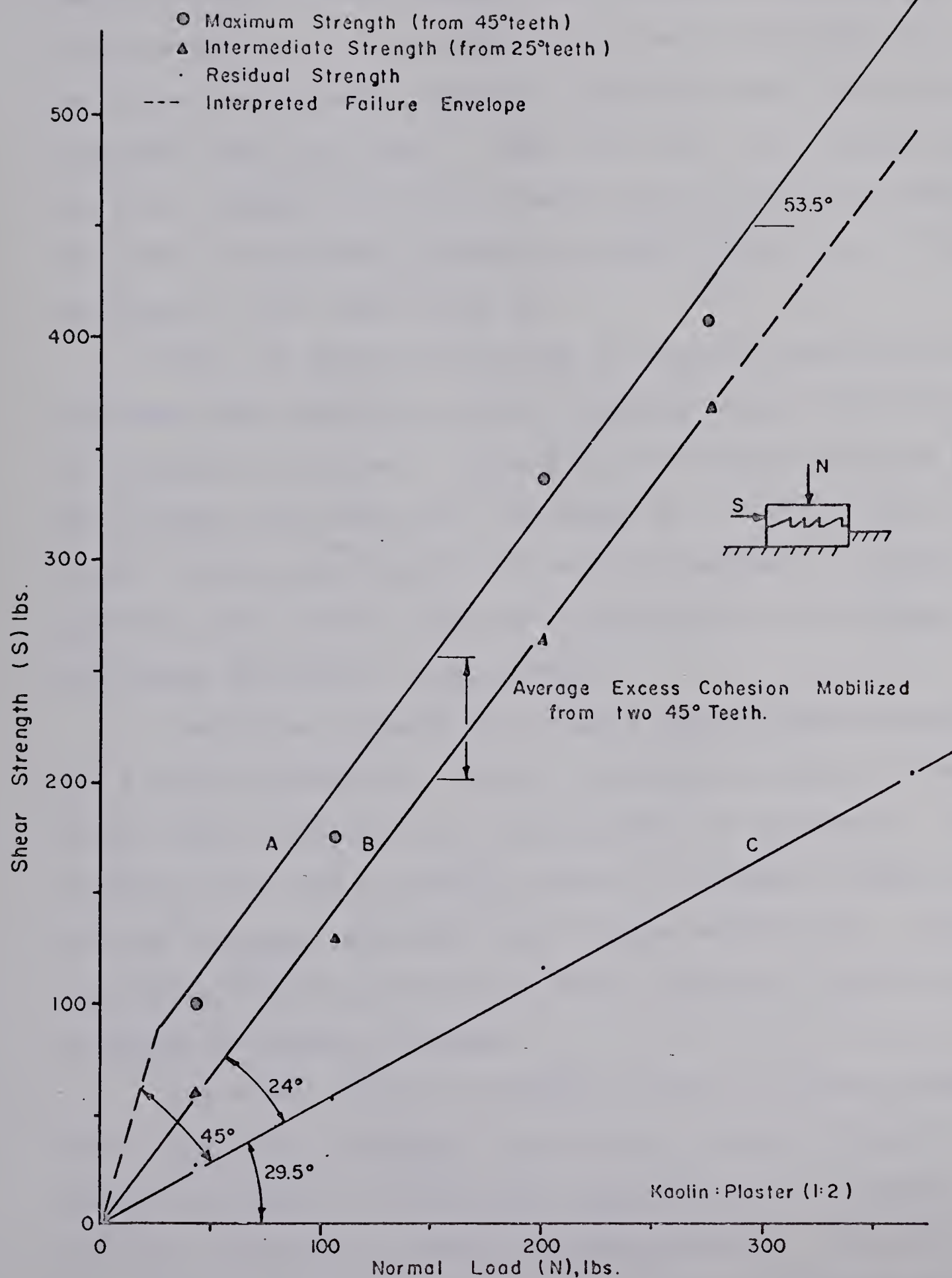


Fig. 2.6 Shear Strength Failure Envelopes for Specimens with Teeth of Two Different Inclinations. (after Patton, 1966)

teeth from two to four leaving the specimens identical in other respects. As expected, the internal strength, or the cohesion available from four teeth was about twice that available from two teeth. That is to say, the failure envelope for a specimen with four teeth (line A) is about twice as far above the residual strength envelope (line C) as is the envelope for two teeth (line B).

Fig. 2.8 shows the results of tests on two series of specimens with identical surface configurations but different internal strengths. Line A is the failure envelope for the stronger specimens with two teeth at $i = 45^\circ$. Line B is the failure envelope for the weaker specimens. Lines C and D are the residual strength envelopes for the stronger and weaker specimens, respectively.

The slopes of both the primary and secondary envelopes are slightly different. These differences reflect a change in the value of ϕ_r for the two strengths of specimens. The change in the mode of failure occurs at a higher normal stress for the stronger specimens than for the weaker ones. Thus, increasing the strength has an effect similar to that of increasing the number of teeth.

For every series of plaster of Paris specimens except those with a flat surface, the failure envelope showed a change in slope. It was found that when the inclination, internal strength, or number of irregularities within the sample varied, the transitions or changes of slope of the

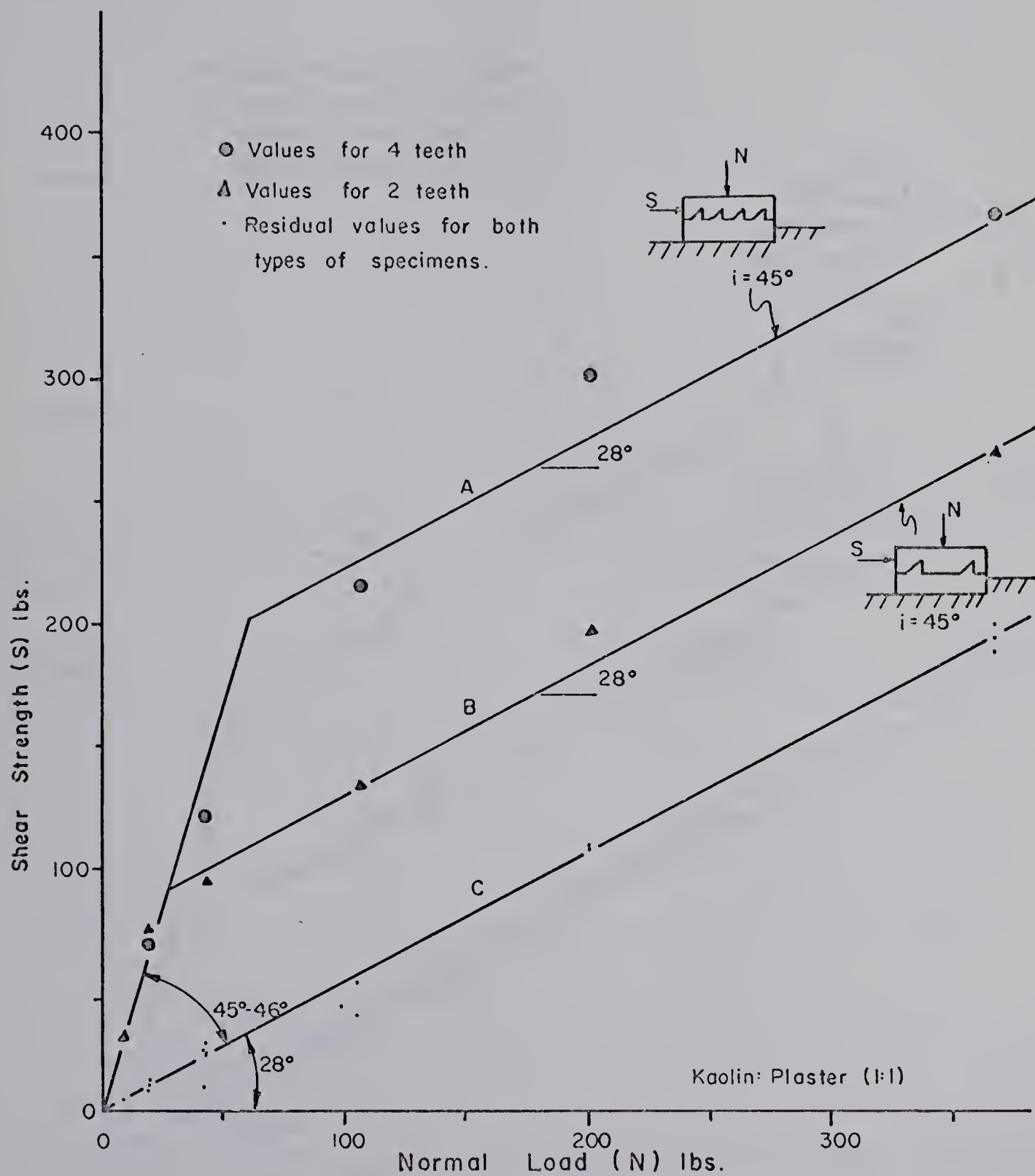


Fig.2.7 Shear Strength Failure Envelopes Showing the Increase in Strength Resulting from an Increase in the Number of Teeth.

(after Patton, 1966)

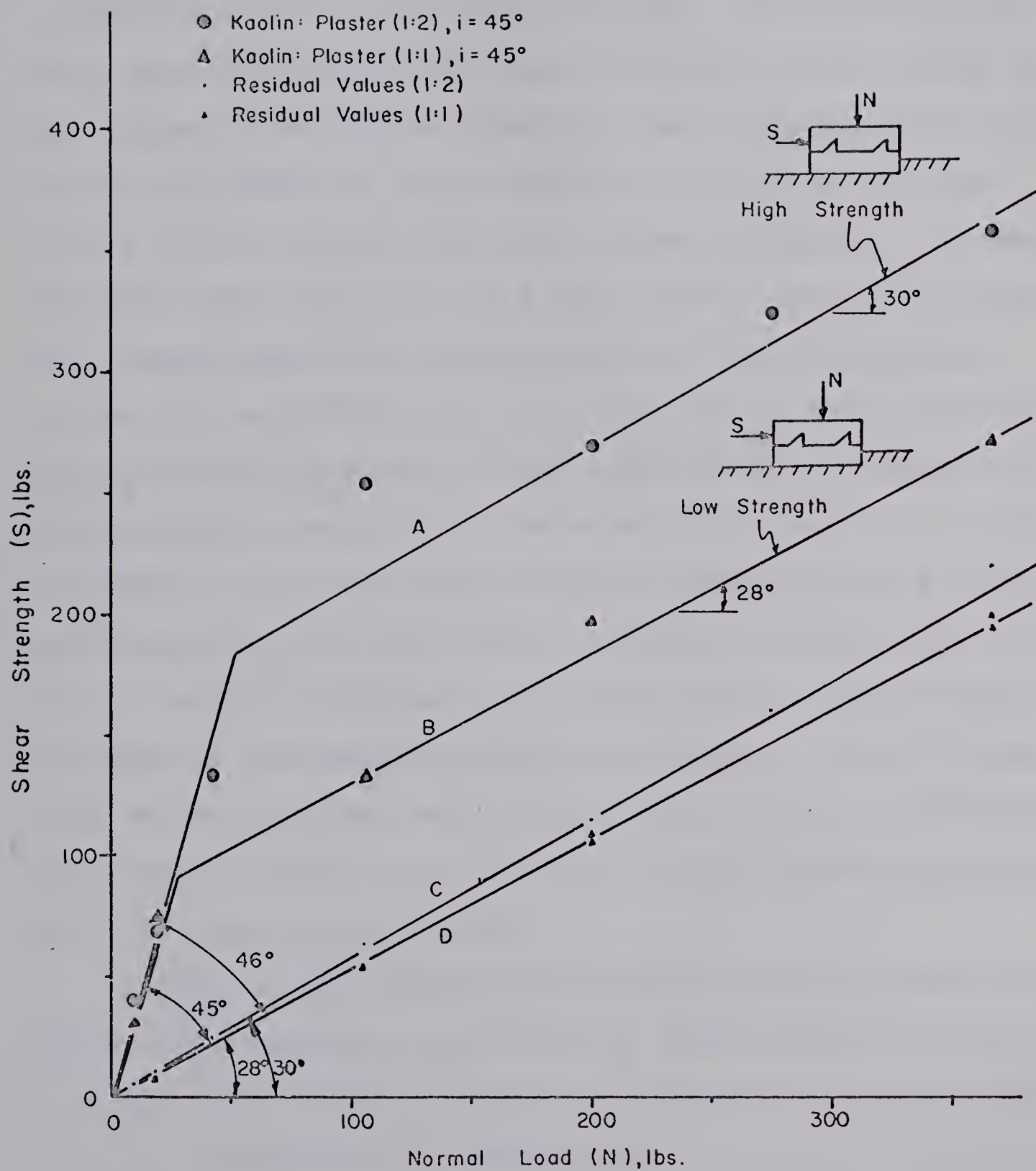


Fig.2.8 Shear Strength Failure Envelopes for Two Specimens with Different Internal Strengths.

(after Patton, 1966)

failure envelopes occurred at different stress levels. In a "typical" rock the irregularities would be expected to have a great variety of physical properties. If the failure of each type of irregularity is reflected as a small change in the slope of the failure envelope, then the cumulative effect of a large number of small changes occurring at different stress levels should result in a curved envelope. It should be noted that the values of ϕ that Patton quotes when shearing through the teeth on the plaster of Paris specimens, reflect the mobilized ϕ and not the ϕ of the intact material. The ϕ_i he determined was in the range of 52° . Because the area of intact material at the base of the teeth is so small compared to the total shear surface, the mobilized ϕ closely approximates ϕ_r and the change in mode of failure from sliding to residual shearing is reflected by the abrupt change in slope of the maximum strength envelopes. In a "typical" rock where the intact material has more effect on the strength, this abrupt change will not occur and the failure envelope will be a more regular curve.

Many of the conclusions derived from the plaster of Paris tests seemed to be covered by three generalizations:

- (1) the failure envelope is generally curved for wide variations in stress level
- (2) the change in slope of such failure envelopes is related to a change in the mode of failure
- (3) changes in the modes of failure are related to the

physical properties of the irregularities along the failure plane.

Patton undertook an extensive literature review to show the multiple modes of failure observed in the tests on plaster of Paris specimens appeared to be applicable to rock as well.

From this summary it is apparent that curved failure envelopes are the rule rather than the exception for both direct shear and triaxial compression tests on rock. This is true for in-situ tests as well as laboratory tests. The exceptions observed in the literature can be explained in one of the following ways:

- (1) the actual data points were not given
- (2) the testing procedure tended to obscure the phenomena
- (3) the rock was particularly strong and the range of normal loads used in the test was not high enough for the curved portion of the failure envelope to be encountered.

Ladanyi and Archambault (1970) analyzed the bilinear model and pointed out that it is strictly valid for shearing along a regular indented rock surface in which, at failure, the teeth have the same geometry and the degree of interlocking as at the beginning of loading in shear. They found that in reality the foregoing assumptions are rarely satisfied because a small displacement is necessary for mobilizing

the sliding friction along contact surfaces and because some teeth are usually partially broken before the maximum strength is reached giving a non-uniform stress distribution over the contact surfaces of the teeth. The same authors developed a shear equation by energy considerations, taking the foregoing into account. The following expression for the conventional shearing strength τ of the irregular surface was obtained

$$\tau = \frac{S}{A} = \frac{\sigma(1 - a_s)(\dot{v} + \tan \phi_\mu) + a_s(\sigma \tan \phi_o + s_o)}{1 - (1 - a_s)\dot{v} \tan \phi_f} \quad \dots \quad (2.4)$$

where τ = shear stress

S = total shear force

A = total projected shear area

σ = normal stress

a_s = ratio of the projected area of the asperities (A_s)
to the total projected shear area (A)

\dot{v} = rate of dilation at failure

ϕ_μ = angle of frictional sliding resistance

ϕ_o = angle of shearing resistance

s_o = cohesion intercept

ϕ_f = a statistical average value of the friction angle
when sliding occurs along the irregularities at
different orientations.

Equation (2.4) is a more general form of shear equation for an irregular rock surface than equations (2.1) and (2.3) defining the bilinear model. Equation (2.4) reduces readily to the latter in the following two extreme cases: at low normal loads, if only regular teeth are assumed $\phi_\mu = \phi_f$, $\dot{v} = \tan i$, and $a_s = 0$ and equation (2.4) yields

$$\tau = \sigma \tan (\phi_\mu + i) \quad . . . \quad (2.5)$$

At high normal loads when all the teeth are sheared off, $a_s \approx 1$ and $\dot{v} \approx 0$, so that

$$\tau = s_o + \sigma \tan \phi_o \quad . . . \quad (2.6)$$

Since the two parameters ϕ_o and s_o correspond to the slope of the linear failure envelope, Ladanyi and Archambault found it more convenient to replace the straight-line law containing the two parameters by the Fairhurst law in parabolic form. This was thought to correspond better to the actual strength behaviour of the rock substance which is a curved line.

The Fairhurst parabolic failure criterion is expressed as

$$\tau = C_o \frac{m-1}{n} \left(1 + n \frac{\sigma}{C_o} \right)^{\frac{1}{2}} \quad . . . \quad (2.7)$$

$$\text{where } n = C_o / (-T_o) \quad . . . \quad (2.8)$$

is the ratio of uniaxial compression and tensile strength of solid rock, and

$$m = (n + 1)^{\frac{1}{2}} \quad . . . \quad (2.9)$$

When the straight line law is expressed by equation (2.7), equation (2.4) may be written as

$$\tau = \frac{\sigma(1 - a_s)(\dot{v} + \tan \phi_\mu) + a_s C_o \frac{m-1}{n} (1 + n \sigma/C_o)^{\frac{1}{2}}}{1 - (1 - a_s) \dot{v} \tan \phi_f} \quad . . . \quad (2.10)$$

The results obtained by applying equation (2.10) are shown on Fig. 2.9. It is interesting to note that if one such envelope in the lower normal stress region is tentatively approximated by two straight lines as in the bilinear model, the upper line may have a slope angle close to $\phi_r \approx \phi_\mu$, as found by Patton.

Jennings (1971) discusses the modes of failure in rock with discontinuous joint planes. If a plane of preferentially lower shear strength exists in a material, then the shear failure will tend to select this plane. If the preferential plane contains two or more low-strength discontinuities, then the net shear resistance is the sum of the shear resistances on the discontinuities and on the intact material in between them. If two joint sets exist, then the preferential plane need not coincide with either set and failure can take place by stepping between the joints. Consider

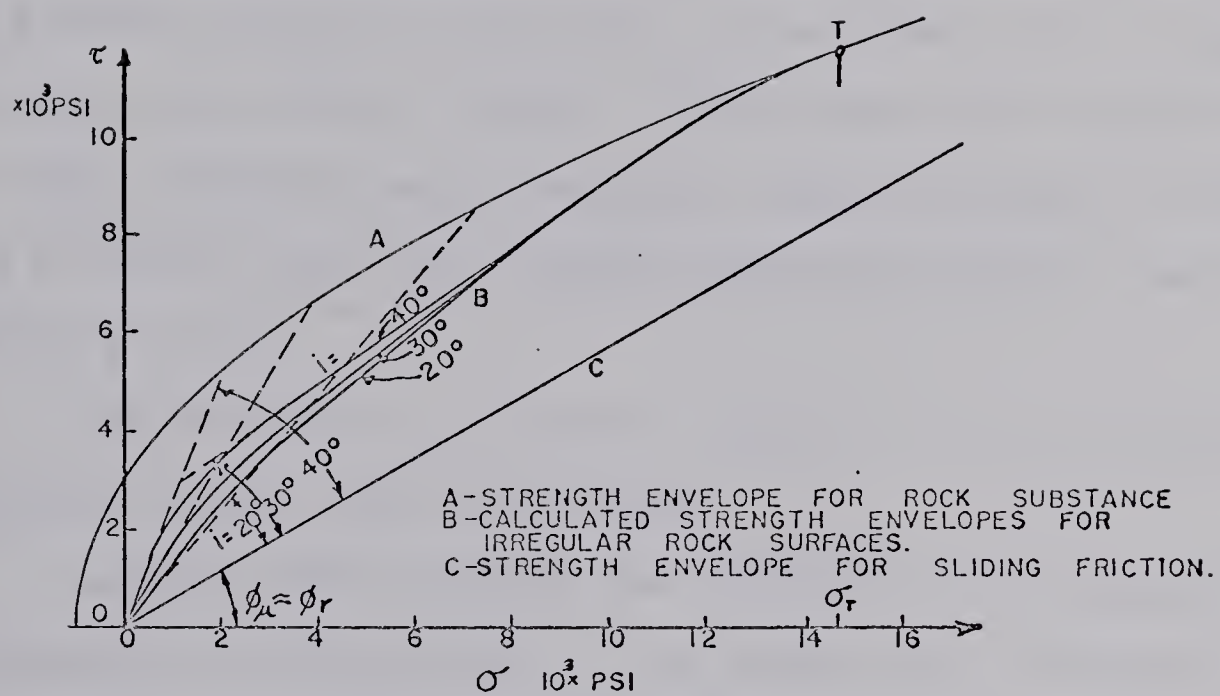


Fig. 2.9 Calculated maximum strength envelopes for shearing along an irregular rock surface with the teeth inclinations of $i=20^\circ, 30^\circ$ and 40° respectively. ($C_0=15,000$ p.s.i., $T_0=-1,000$ p.s.i., $\phi_{\mu}=30^\circ$)

(after LADANYI and ARCHAMBAULT, 1970)

the case where the joints are large and intersect as in Fig. 2.10(a). The shearing displacements will no longer be in the direction of the (mean) preferential plane of failure but will take place in the direction of the α -joints. As shearing takes place in this direction, separation (tension) occurs on the ψ -joints. Consider next the case where the joints are of limited length so that one part of the failure occurs on the joints and another part on intact material, as in Fig. 2.10(b). The assumption is made that the mode of failure will involve a shearing along the extension of the α -joint, this plane extending until it meets the nearest ψ -joint.

The concept of a tension component in the failure mechanism has now been introduced.

Lajtai (1968) studied the influence of a single plane of weakness in direct shear. He showed that the total shear strength is determined by fundamental shear strength (cohesion) and internal friction in solid bridges (the continuous part of the plane of weakness) and by joint friction along the separated parts of the weakness plane. He considered the case when neither of the two frictional resistances is mobilized and postulated that failure will occur when the minimum principal stress exceeds the tensile resistance offered by the solid rock bridges. He developed his theory in the general form of

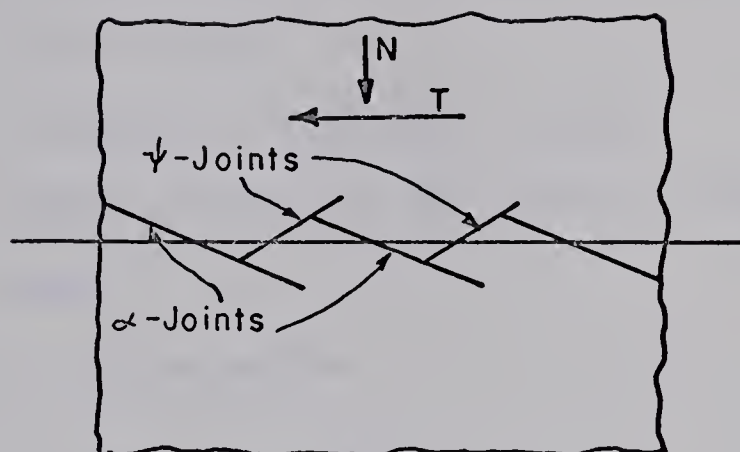


Fig.2.10(a) Shear Failure by Stepping Between α Joints
(the Main Set) and ψ Joints (the Secondary Set)
-Long Joints (after Jennings, 1971)

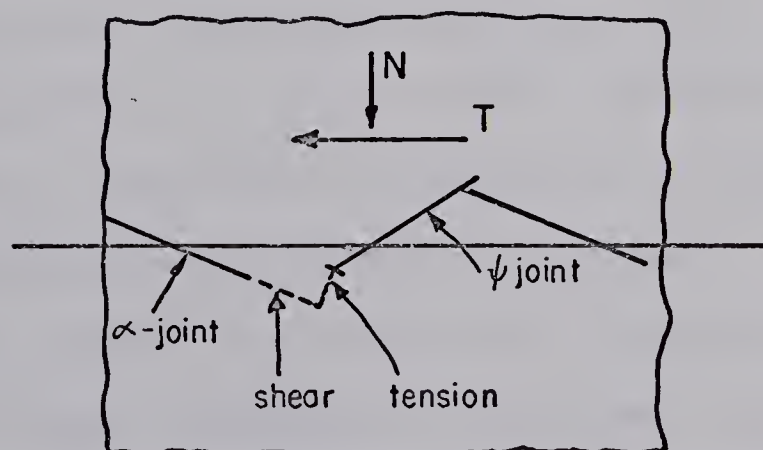


Fig.2.10(b) Stepped Joint Failure - Short Joints
(after Jennings, 1971)

$$\tau_a = f(T_s, \sigma_a) \quad . . . \quad (2.11)$$

where τ_a = maximum shear stress on the plane of weakness in direct shear

T_s = strength in uniaxial tension

σ_a = normal stress on the plane of weakness in direct shear

and arrived at the equation

$$\tau_a = [T_s (T_s - \sigma_a)]^{\frac{1}{2}} \quad . . . \quad (2.12)$$

This defines the direct shear parabola shown in Fig. 2.11. The shear strength is seen to increase with increasing normal stress but at a slower rate than the Mohr-Coulomb criterion. This has the consequence that the parabola intersects the strength envelope for residual sliding resistance. Hence, the direct shear parabola has no meaning when the normal stress exceeds a limiting value. It will still define the state of stress at which tension fractures could appear, but it will have no influence in determining the maximum shear stress that may be applied.

This chapter has dealt with the most fundamental theories of shear strength in fractured rock. It is clear that not all of these theories can be applied simultaneously. A rational analysis based on these theories can only be undertaken when the structural discontinuities existing within the rock mass are detected and described in a quantitative way.

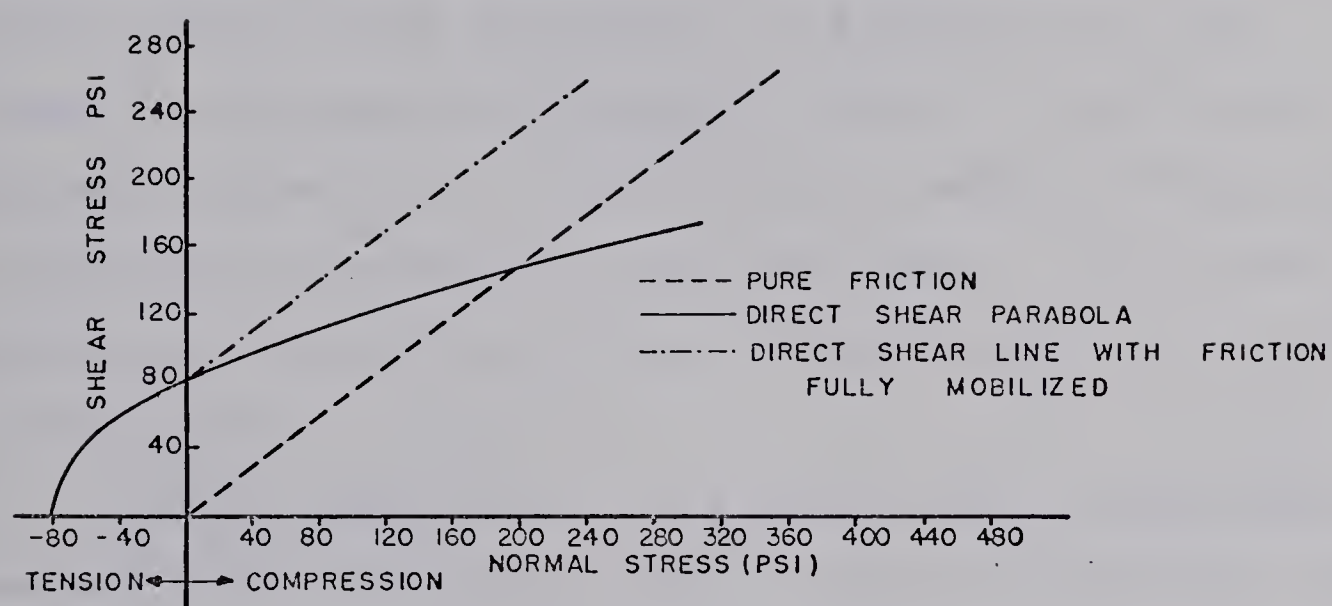


Fig.2.11 A comparison of strength theories.
(after LAJTAI, 1969)

CHAPTER III

SAMPLING PROGRAM

3.1 SAMPLE REQUIREMENTS AND SITE SELECTION

In order to study the strength and deformation characteristics of a fractured rock it was necessary to find a natural material that displayed a uniform geometry with respect to its planes of weakness. Also, it would be of particular interest if a representative number of these planes of weakness were present in each test sample. This would permit the extrapolation of the results to large scale field investigations.

The coal deposits at the Highvale Mine on Lake Wabamun, because of their horizontal bedding planes and regular, vertical and planar joint planes, are an ideal natural material for this study.

It was decided to study the strength and deformation characteristics of seven different configurations with each configuration containing various orientations of planes of weakness. These are shown in Fig. 3.1. The configurations chosen enable the study of strength and deformation characteristics

(I) along the bedding planes parallel, oblique, and normal to joint planes, and

(II) parallel to bedding planes along joint planes,

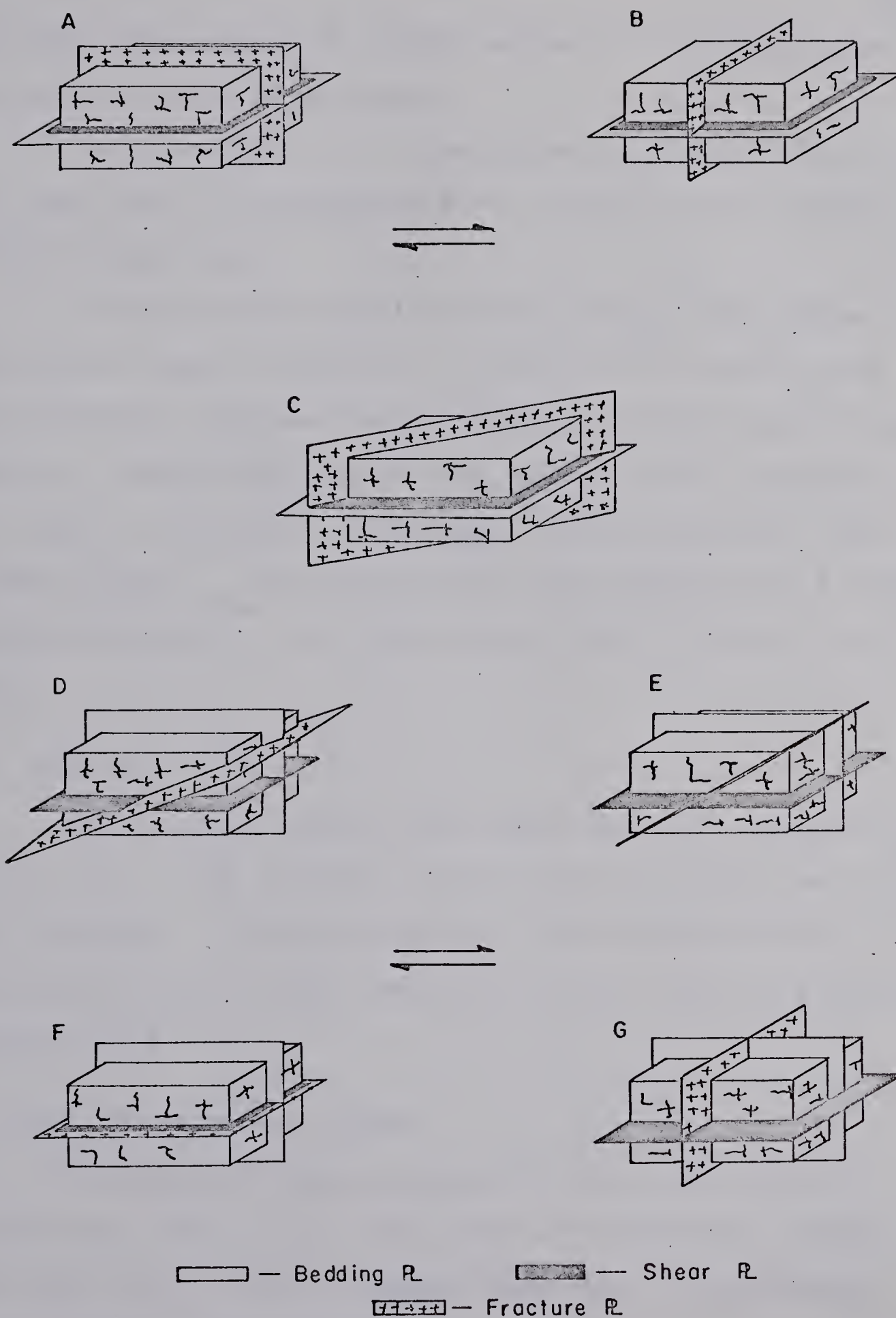


Fig.3.1 Sample Configurations

with the joint planes at varying angles to the shear plane, and normal to the joint planes.

Configurations A to C inclusive are as described in (a) above, and configurations D to G inclusive are as described in (b) above.

It was further established that samples with dimensions of at least 6 inches by 6 inches at the shear plane would contain a representative number of discontinuities per sample. Because the coal has an average joint spacing of $3/4$ inch, a 6 inch by 6 inch sample would contain at least 8 joint planes. The behaviour of these samples would then be representative of the behaviour of the rock mass in the field.

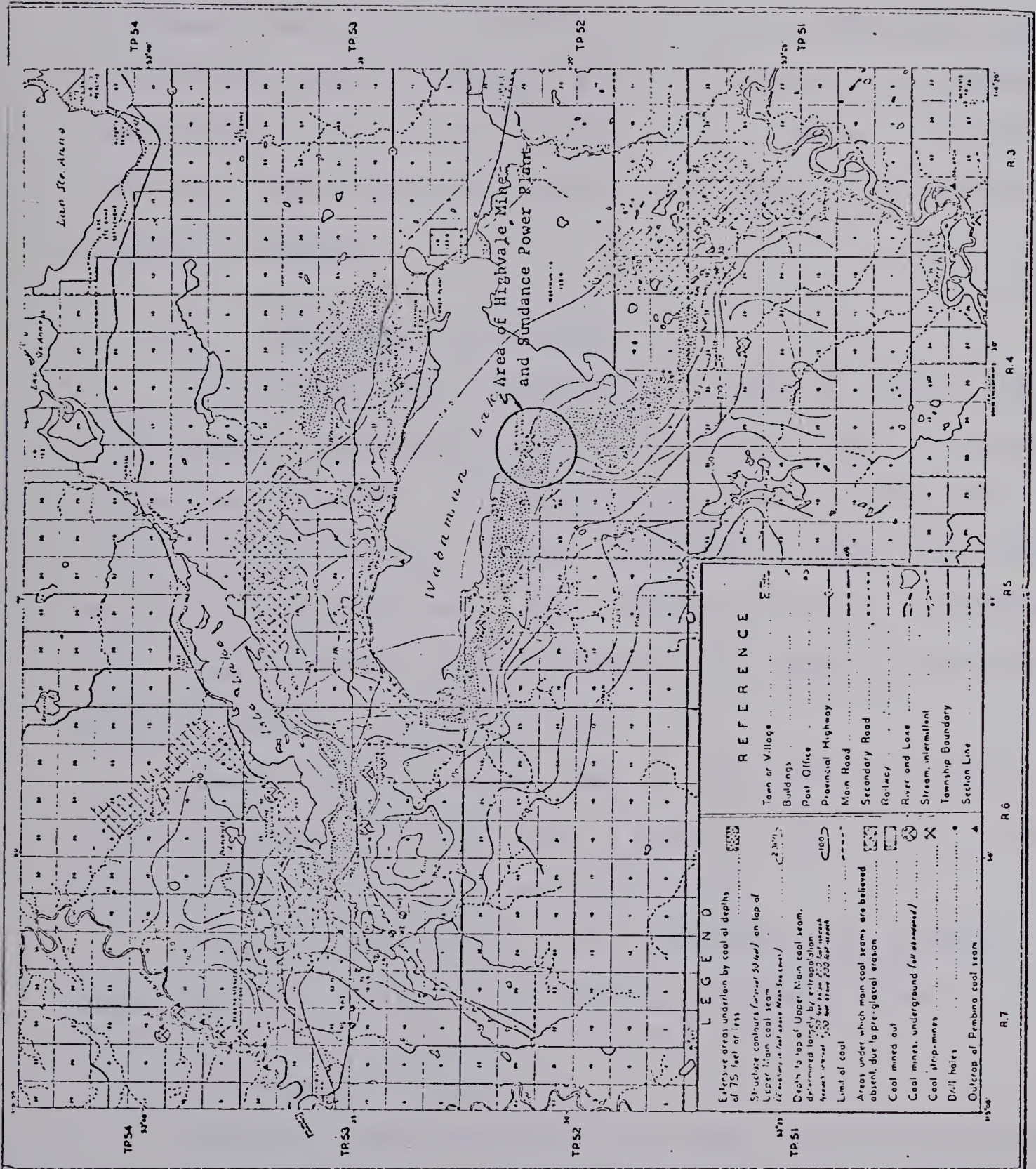
3.2 GEOLOGY

This section outlines the major geologic considerations of the area in the vicinity of the site from which the samples were obtained. A detailed geologic description of the particular location where sampling was performed is given in section 3.3.3.

3.2.1 Location and Access

The Highvale Mine is located on the south shore of Wabamun Lake (Fig. 3.2). The mine is operated by Alberta Coal Ltd. for the use by Calgary Power Ltd. in operating their Sundance Power Plant.

The Wabamun Lake district is west of Edmonton in



Tps. 50-54, Rs. 3-7, W. 5th Mer., and is centered about Wabamun Lake. The Village of Wabamun on the north shore of Wabamun Lake, lies about 45 miles west of Edmonton, and is one mile south of Highway 16 which traverses the Wabamun Lake district in an east-west direction. Wabamun Lake is skirted on the north shore by the main line of the Canadian National Railways.

3.2.2 Topography and Drainage

The Wabamun Lake district is an area of low relief, and belongs physiographically to the plains area of central and eastern Alberta. Elevations are mainly in the range of 2,400 to 2,600 feet but exceed 2,700 feet in the south and west of the district where the Tertiary Paskapoo sandstones form a more resistant bedrock than do the Upper Cretaceous Edmonton Shales to the north and east.

Except where cleared, most of the area is covered with deciduous trees, but spruce grows in some of the muskegs, and scattered pines exist on sandy hills.

Wabamun Lake drains to the southeast via Wabamun Creek which flows into the North Saskatchewan River.

3.2.3 General Geology

Rocks of late Cretaceous and early Tertiary ages constitute the bedrock of the Wabamun Lake district, and consist of sandstones, shales, and coal seams deposited in a freshwater environment. The upper Cretaceous is represented by

strata of the upper part of the Edmonton formation which is the coal bearing formation in the neighbourhood of the City of Edmonton. The lower Tertiary is represented by beds of the Paskapoo formation and consists of a sandstone and shale sequence.

The Edmonton formation in the area is about 1,700 feet thick, but only the upper few hundred feet of the formation are exposed in the Wabamun Lake district. These consist largely of light grey to greenish- or bluish-grey, slightly bentonic shales with scattered zones of clay-ironstone nodules. Interbedded with the shales are thinner siltstone beds and grey, buff-weathering salt-and-pepper textured sandstones, the latter commonly containing abundant small coal fragments. A thick coal-bearing zone has been found near the top of the Edmonton formation at numerous points and it outcrops at several places along the north and south shores of Lake Wabamun. Most coal seams are discontinuous laterally; two seams only a few feet apart may appear to be at the same stratigraphic level, but in places they are found to lens out and others appear to be at slightly different levels. However, the coal bearing unit is continuous in the Wabamun Lake district.

In most places throughout the area the coal bearing unit can be divided into two main seams with a few thinner seams below. The two main seams are each generally about 10 feet thick and are separated by an interval of from a

few inches to 30 feet of shale and sandstone.

A thick mantle of glacial tills, sands and gravels overlies most of the Edmonton and Paskapoo strata around Wabamun Lake. Unconsolidated sands and gravels, known as Saskatchewan gravels, overlie the bedrock and underlie glacial deposits in certain parts of the Wabamun Lake district. The gravels are widely distributed at points of relatively high relief but do not occur at lower parts of old drainage channels. The sands and gravels are absent in a belt a few miles wide along the south shore of Wabamun Lake. The tills are largely clayey to sandy in texture and vary from grey to brown in colour.

3.2.4 Structure

The Cretaceous and Tertiary strata in the Wabamun Lake district have a dip of between 20 and 50 feet per mile towards the southwest. The dip is modified by small anticlines and synclines (termed "rolls" by the local mine operators), with dimensions of a few hundred feet from crest to trough. These rolls are probably near surface features only, produced by ice movement during pleistocene times. Their axes are commonly found to be at right angles to the direction of the ice movement. (Pearson, 1959)

3.3 FIELD INVESTIGATIONS

3.3.1 Location

A map showing the general layout of the mining operation is shown on Fig. 3.3. To minimize interference with the mining operations, all the samples were obtained from the west pit.

3.3.2 Mining Operation

The two main coal seams of the Edmonton formation are presently being mined. In the west pit the number one seam is about 12 feet thick underlying about 20 feet of glacial till. The number two seam is also about 12 feet thick and is separated from the number one seam by a 2 foot thick bed of shale.

Because of the flat-lying nature of the coal seams and their proximity to the surface, a conventional strip mining operation is used. The till is removed by a dragline leaving about a 50 foot wide strip of the number one seam exposed. Light explosive charges are set in boreholes at a depth of 8 feet on half of the exposed seam to loosen the coal thereby facilitating the mining operation. The coal is then loaded into trucks and transported to the Sundance Power Plant. This leaves a bench about 25 feet wide and 12 feet high that is later removed. The same procedure is used on the number two seam.

It was along one of the benches on the number one

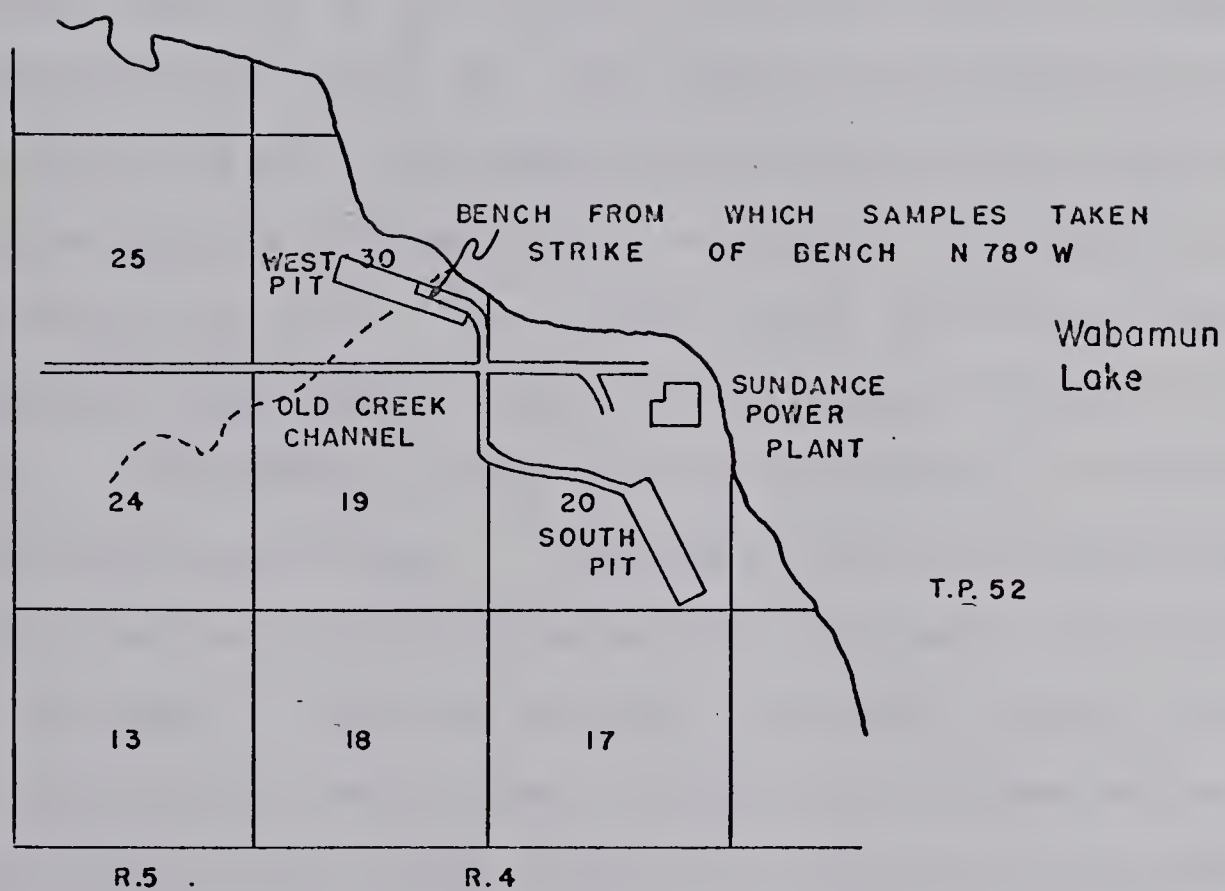


Fig. 3.3 Sampling Area at Highvale Mine

seam in the west pit that most of the samples were obtained for testing. This bench is located on Fig. 3.3. Five samples ('G' configuration) were taken from the top of the number two seam.

3.3.3 Detailed Geology

A detailed structural survey of this bench was carried out and showed the coal seam to have only one set of joints (often referred to as "cleats" in coal) with an average orientation of $N 45^{\circ} E$. The joints were essentially planar, vertical and at right angles to the horizontal bedding planes. A rose diagram displaying the structural observations is shown on Fig. 3.4. The average joint spacing was about $3/4$ inch with most joints being continuous and closed for several feet. The bedding could best be described as consisting of thin horizontal bands. Occasional thin horizontal bands of shale that were discontinuous laterally were found interbedded in the coal. The coal was also fractured between joint planes. These fractures were normal to the joint planes but were neither continuous across joint planes nor planar and presented a very random distribution. For this reason they did not classify as a joint set nor did they present a well-defined plane of weakness. There are, then, only two well-defined planes of weakness, these being the joint planes and the bedding planes.

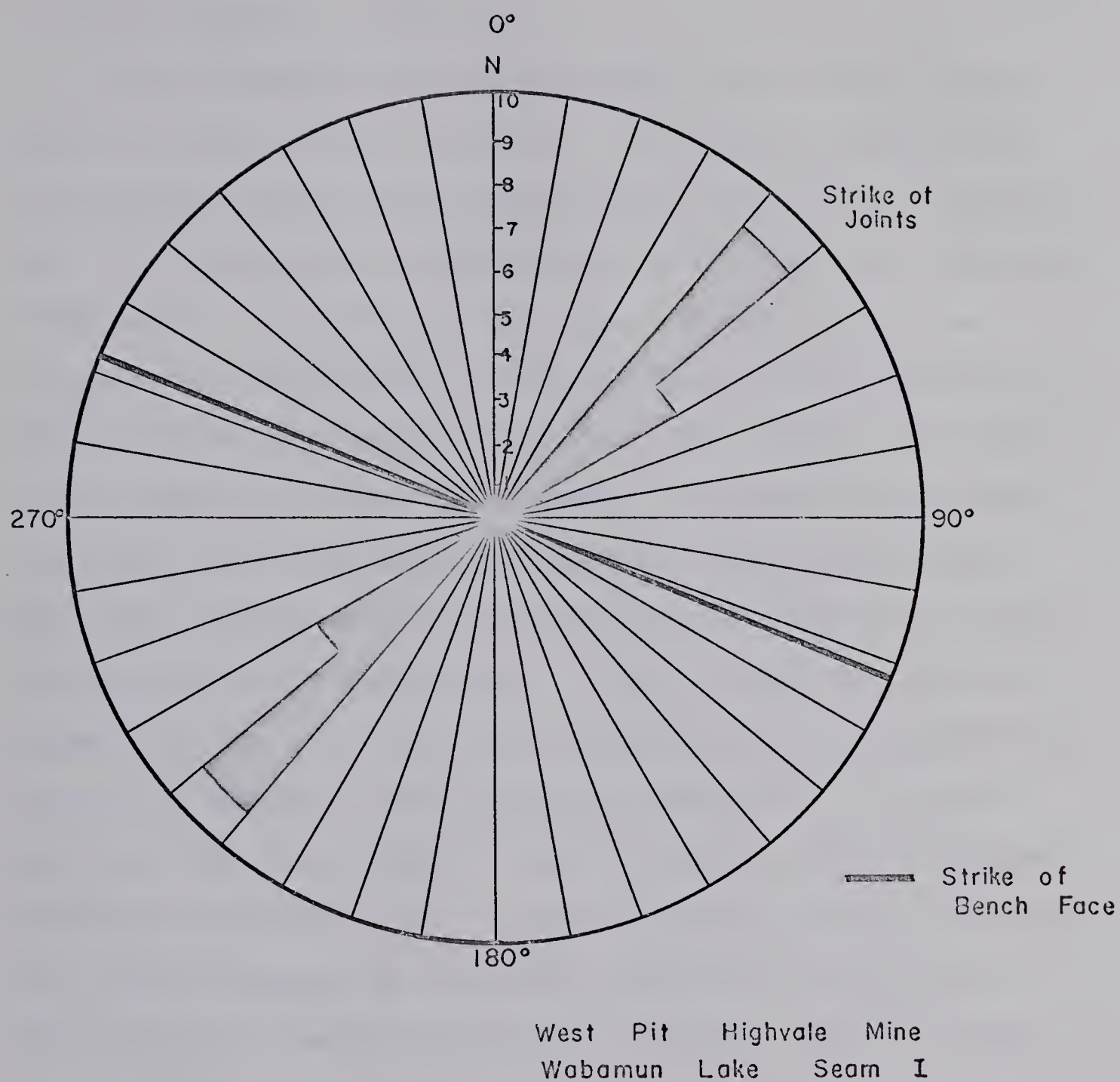


Fig. 3.4 Rose Diagram of Structural Observations

3.3.4 Method of Sampling

All attempts to retrieve intact undisturbed samples from the bench proved fruitless. It was not possible to distinguish between those discontinuities that were continuous in a prospective sampling area and those that were not continuous. A continuous and open discontinuity in a prospective sampling area along the bench would prevent an intact sample from being obtained. The blocks could only be cut along the sides and attempts to separate the block along the base invariably resulted in a shattered sample. Thus, the samples were cut from blocks that had been loosened by the blasting operations. These intact blocks displayed the same structural characteristics but permitted the cutting of samples to the required dimensions. It also minimized the possibility of getting samples that displayed different bulk densities. This was based on the fact that the blocks loosened by the blast would contain fractures with the same relative fracture opening and thus the same porosity. The samples were cut from blocks at the top of the seam to ensure that few, if any, additional fractures had been induced. Because the charge was detonated 8 feet below the top of the seam, no additional fractures would be expected in the coal at the top of the seam as a result of the blasting. The blasting only served to free these blocks along already existing planes of weakness. A careful study of the blast holes exposed along the face of the bench

showed the shatter-zone to extend in a fan-like arrangement only about $1\frac{1}{2}$ feet from the point where the charge was detonated 8 feet down from the top of the seam.

Because of the regular orientation of the joints, the blocks were easily re-oriented to their natural geologic setting.

Following this, the blocks were marked in such a way that the resulting sample would have the proper orientation of bedding planes and joint planes when placed in the shear box. That is, the resulting sample would be one of the desired configurations as presented in section 3.1. The samples were then cut several inches over-size on all sides using a STIHL chain saw (model 041 AV) modified to accommodate a 12-inch diameter circular rock blade. The saw is shown in Fig. 3.5. Because of the guard over the blade, it was only possible to make a 4 inch deep cut at any one time, thus necessitating final trimming in the laboratory. It was found that 6 to 8 intact samples could be obtained by a two man team during each normal working day. The sampling procedure was found to be entirely satisfactory for obtaining intact samples to be used in direct shear testing.

Eight bag samples of coal were taken along the face of the bench at 50 foot intervals to be used for moisture content and specific gravity determinations. Fresh material was obtained by breaking away any of the weathered material along the face.



Fig. 3.5 STIHL Saw Used in Field Sampling

3.3.5 Transportation

After the samples were cut, they were placed on several thicknesses of burlap on the floor of a covered panel truck to minimize the possibility of breakage during transportation to the laboratory.

CHAPTER IV

LABORATORY PROCEDURE

4.1 SAMPLE PREPARATION

4.1.1 Storage

After transporting the test samples to the laboratory, they were stored in a moist room at 40° F. and 100% relative humidity to await trimming.

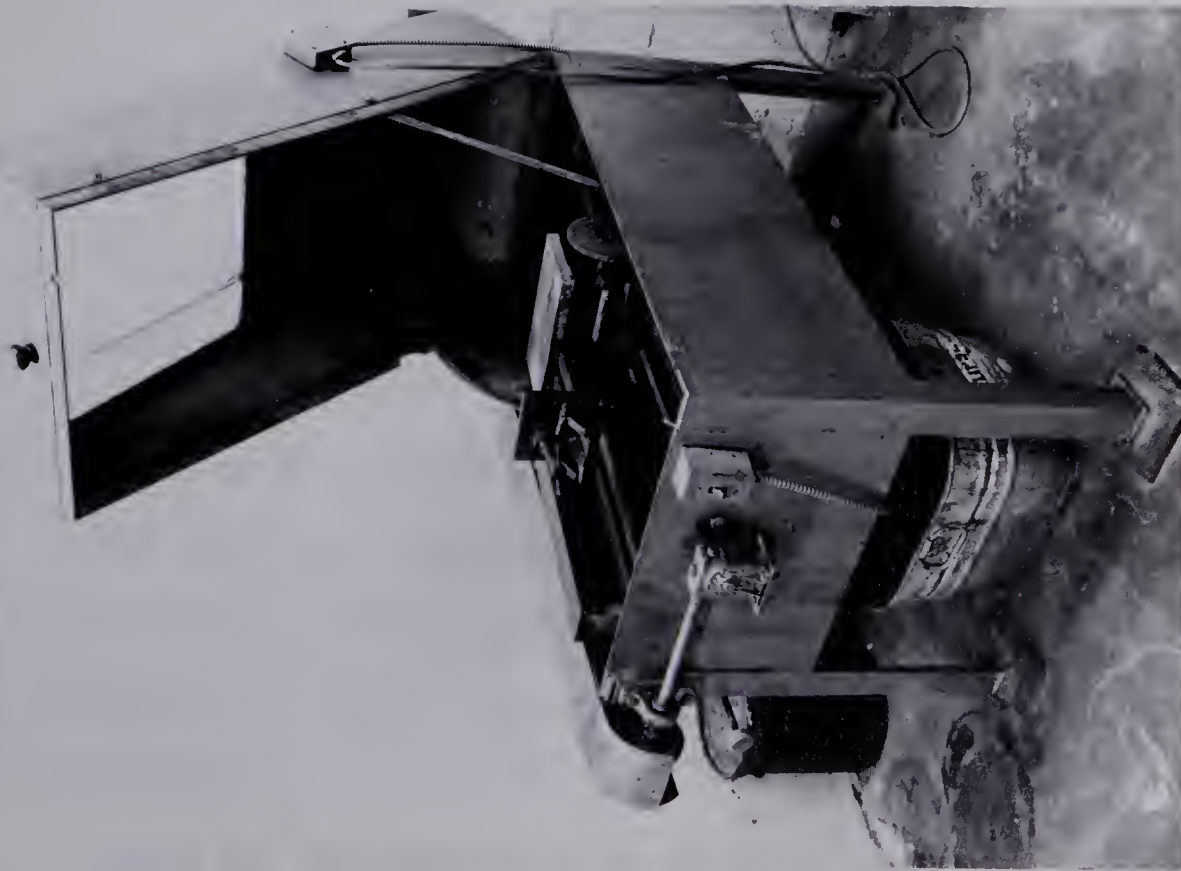
4.1.2 Trimming

The over-sized field samples were cut to about 1/8 inch under-size on all sides using a Northland concrete saw manufactured by Oxford Machine and Welding Co. Ltd. of Edmonton, Alberta, and shown in Fig. 4.1 (a). A cutting fluid of water with 500 c.c. of Esso Kutwell 45 was used. The samples were weighed, the volume calculated, and the samples returned to the moist room to await casting.

4.1.3 Casting

Although good samples of uniform dimensions were obtained by the above methods, it was impossible to prevent small pieces from breaking away along the edges and especially the corners. The samples were thus brought up to final size by casting them in Devcon B plastic steel epoxy. This ensured a snug fit in the shear box and also ensured

a) Northland



b) Mico-Instrument



Fig. 4.1 Saws Used in Laboratory for Cutting Samples

flat horizontal surfaces for seating and loading the samples. A gap of about $\frac{1}{2}$ inch was left in the middle of the sample through which shear was to take place. Samples before and after casting are shown in Fig. 4.2.

The two inch samples, after casting, were pre-cut along the shear plane to enable the determination of the residual angle of friction, ϕ_r . The pre-cut shear plane was made using a Specimen Saw manufactured by Mico Instrument Co., Cambridge, Massachusetts and shown in Fig. 4.1(b). No cutting fluid was used with this saw. This saw permitted more accurate alignment of the small samples thus ensuring the pre-cut shear plane was flush with the interface of the top half and bottom half of the shear box.

The samples, again, were returned to the moist room to await testing.

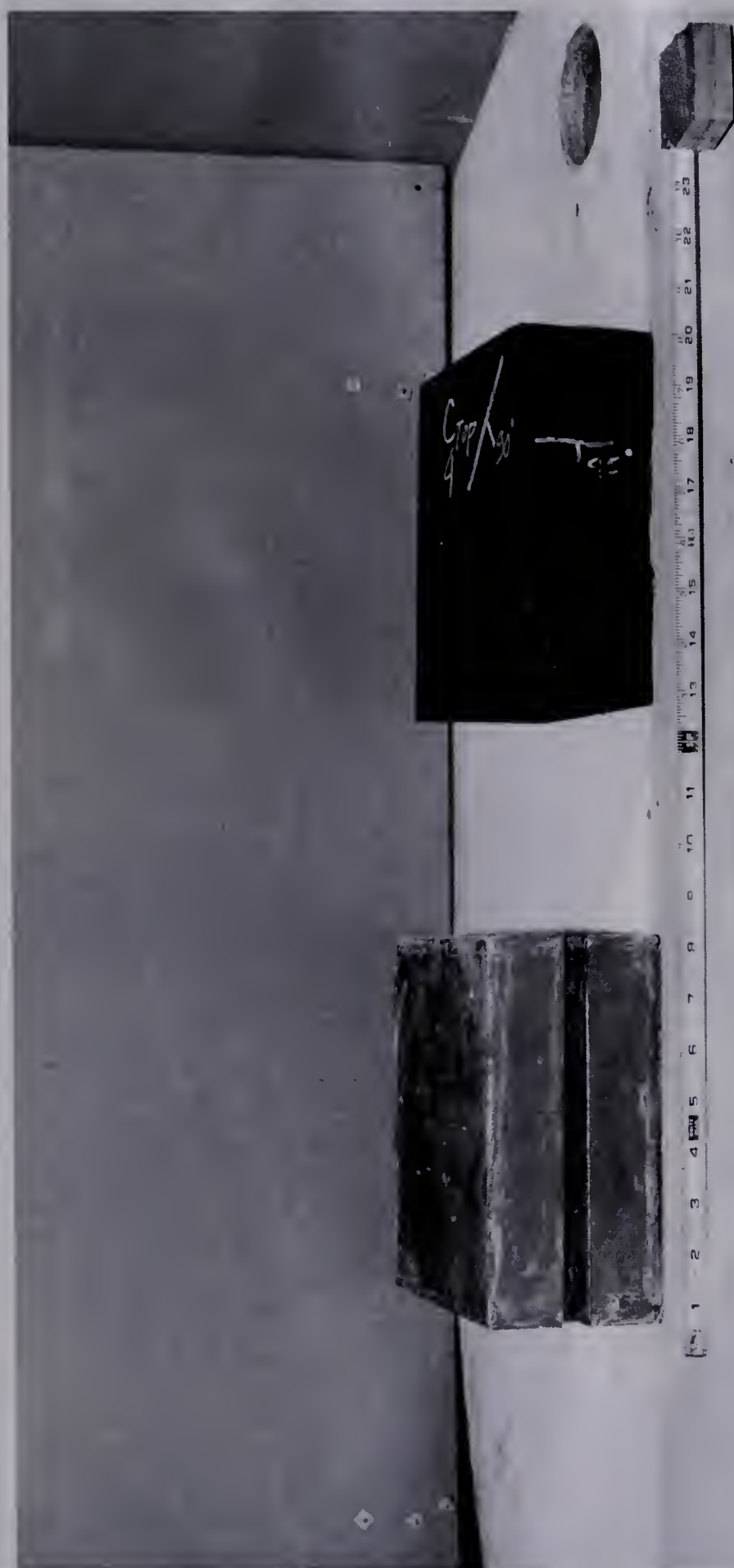
4.2 TESTING PROCEDURE

Fig. 4.3 shows the direct shear testing equipment used. A more detailed description of the equipment is given in the following sections.

4.2.1 Classification Properties

The moisture content of the coal was determined from the bag samples immediately upon returning from the field. Eight samples of about 600 gms. each were oven-dried for 24 hrs. at 105°C .

Three of the oven-dried samples were then used to



b) After

a) Before

Fig. 4.2 Samples Before and After Casting



Fig. 4.3 Layout of Strength Testing Equipment

determine the specific gravity of the coal by the pycnometer method as outlined by Lambe (1967).

Using an average moisture content as determined above, the void ratio (e), porosity (n), and degree of saturation (S) were determined for the samples to be tested in direct shear.

The properties of the coal samples are tabulated and presented in Chapter VI, Table 6.1.

4.2.2 Direct Shear Tests on Pre-cut Samples

A series of 10 tests were run on 2 inch square by $2\frac{1}{2}$ inch thick coal samples with a pre-cut shear plane to determine the residual angle of friction, ϕ_r . The bedding planes in these samples were horizontal and the joint planes were vertical. The exact orientation of the joint planes with respect to the direction of shear was not known. The samples were tested in the modified direct shear box shown in Fig. 4.4. The samples were run wet at a constant strain rate of 0.0266 inches per minute. The shear load was applied by a gear box - chain drive assembly powered by an electric motor. The normal load was kept constant for the duration of each test by a dead weight - lever arm arrangement. A shear displacement of $\frac{1}{2}$ inch was imposed, the direction reversed and a further displacement of one inch imposed, the direction reversed again and the sample displaced $\frac{1}{2}$ inch to realign the two halves of the shear box thus imposing a

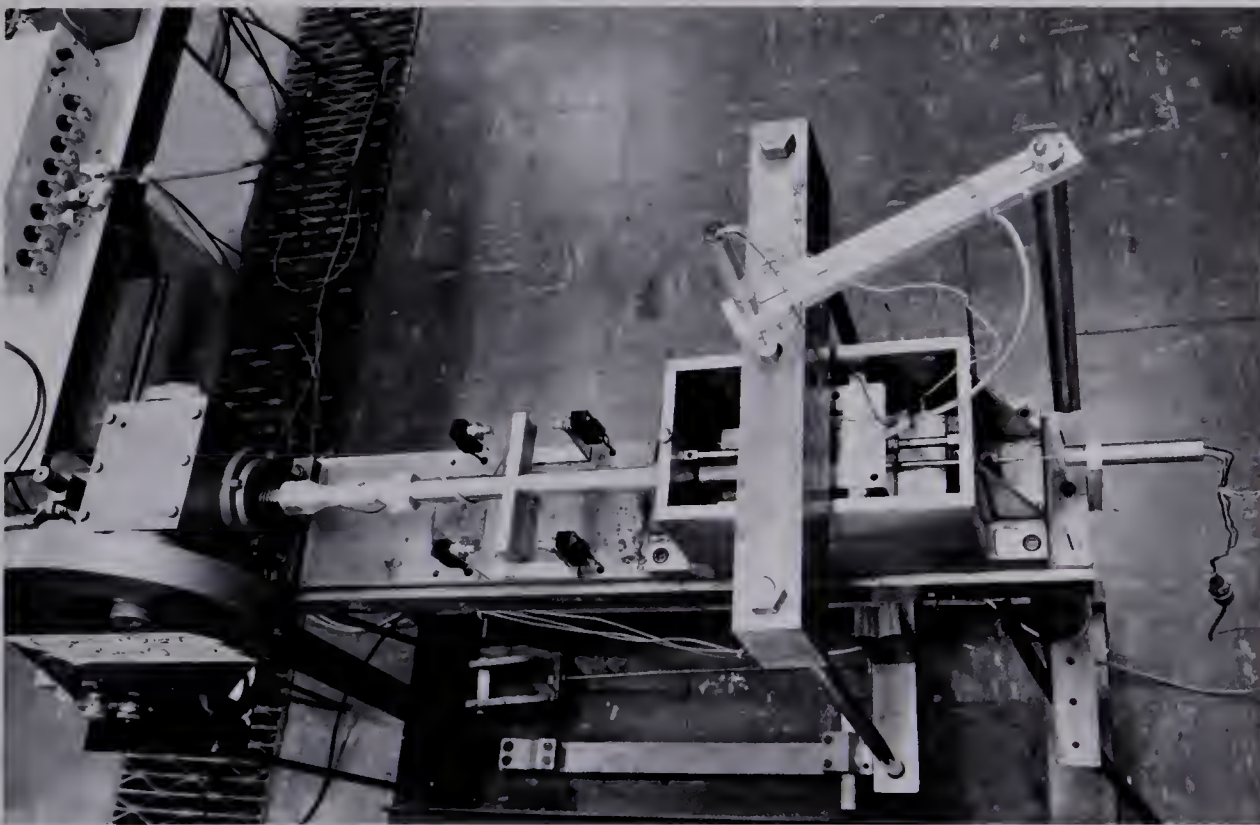


Fig. 4.4 Modified Direct Shear Machine

a total shear displacement of 2 inches. The shear displacement was measured using a linear voltage displacement transducer (LVDT) and the shear load was measured by an 8,000 lb. load cell. An X-Y recorder was used to record the shear load versus shear displacement graphs. The results of the residual tests are given in Chapter VI, section 6.2.

4.2.3 Direct Shear Tests on Intact Samples

All the intact coal samples were tested with the Wykeham-Farrance 10 ton capacity direct shear machine shown in Fig. 4.5. The shear load was applied through a variable gear arrangement powered by an electric motor. The normal load was applied through a loading yoke by a hydraulic ram. The hydraulic system was designed to maintain a constant normal load for the duration of the shear test. However, it was found that the normal load did not remain constant with time and fluctuations on the hydraulic pressure gauge made it impossible to set an accurate normal load. As a result, a load cell was incorporated between the loading yoke and the load cap. Strain gauges on the load cell were connected to a Budd strain indicator. By adjusting the hydraulic pressure control valve to keep a constant Budd reading, it was possible to maintain an accurate and constant normal load.

The apparatus was equipped with a 10 ton capacity proving ring to measure the shear load. Strain gauges

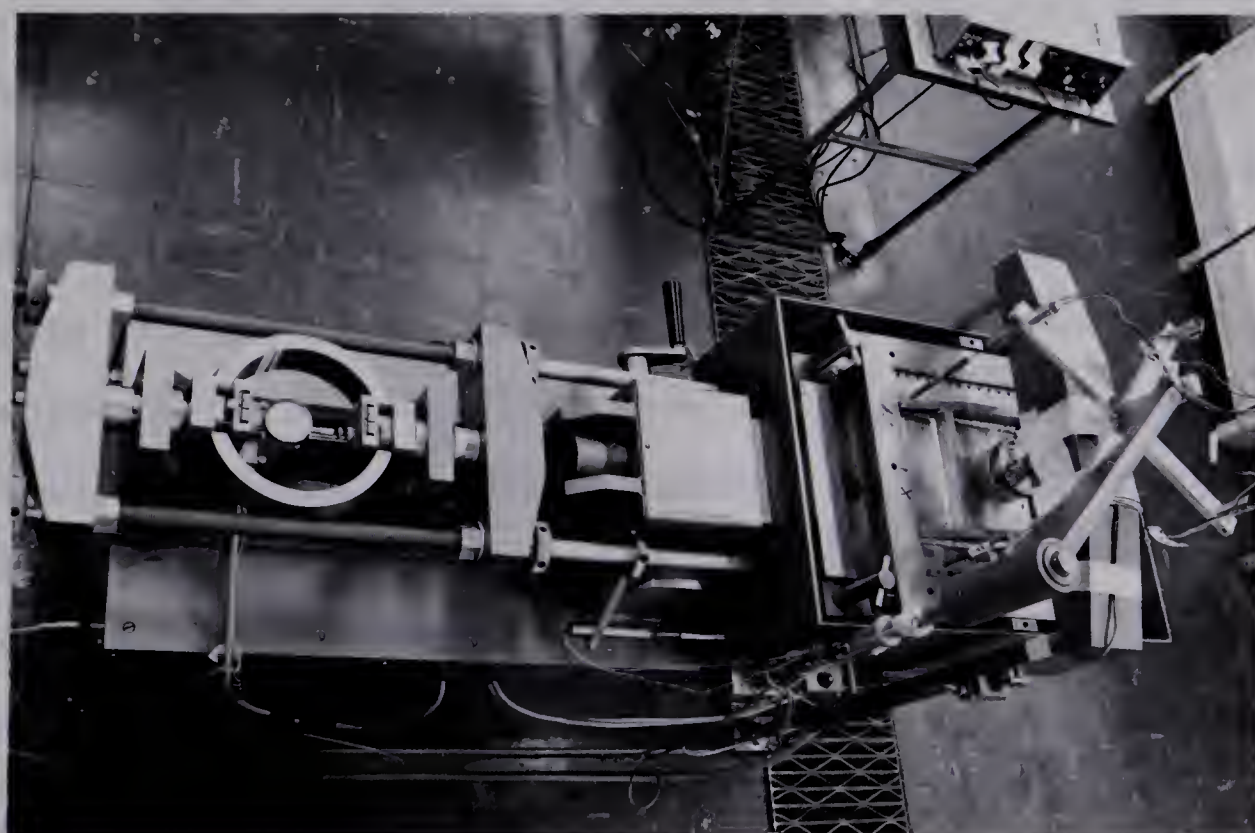


Fig. 4.5 Wykeham-Farrance Direct Shear Machine

were attached to the proving ring and connected to an X-Y recorder. An LVDT was mounted in such a way as to measure the relative displacement between the top half and the bottom half of the shear box and it also was connected to the same X-Y recorder. The resulting shear load versus shear displacement curve was thus plotted as each test progressed.

With the set-up as described, five preliminary tests were run on samples A1, A3, B3, B4, and B5 to establish the behavioural pattern of the coal. For these preliminary tests, the vertical dilation was measured by an LVDT mounted over the centre of the load cap and resting on the loading yoke. The LVDT readings were recorded every minute on a Hewlett-Packard digital recorder. The preliminary tests were run dry at a constant strain rate of 0.03 inches per minute. By reversing the direction of shear, the samples were subjected to a 25% nominal strain (3 inch total displacement); $12\frac{1}{2}\%$ ($1\frac{1}{2}$ inches) in each direction.

The remaining tests on the intact coal samples were run in a similar manner but with several modifications:

(a) Because the remaining samples were all either 6 inches by 6 inches or 8 inches by 8 inches, a spacer arrangement was designed to fit inside the shear box. This spacer arrangement is shown on Fig. 4.6.

(b) All the samples were subjected to a 25% nominal strain in one direction only; that is, the 6 inch by 6 inch

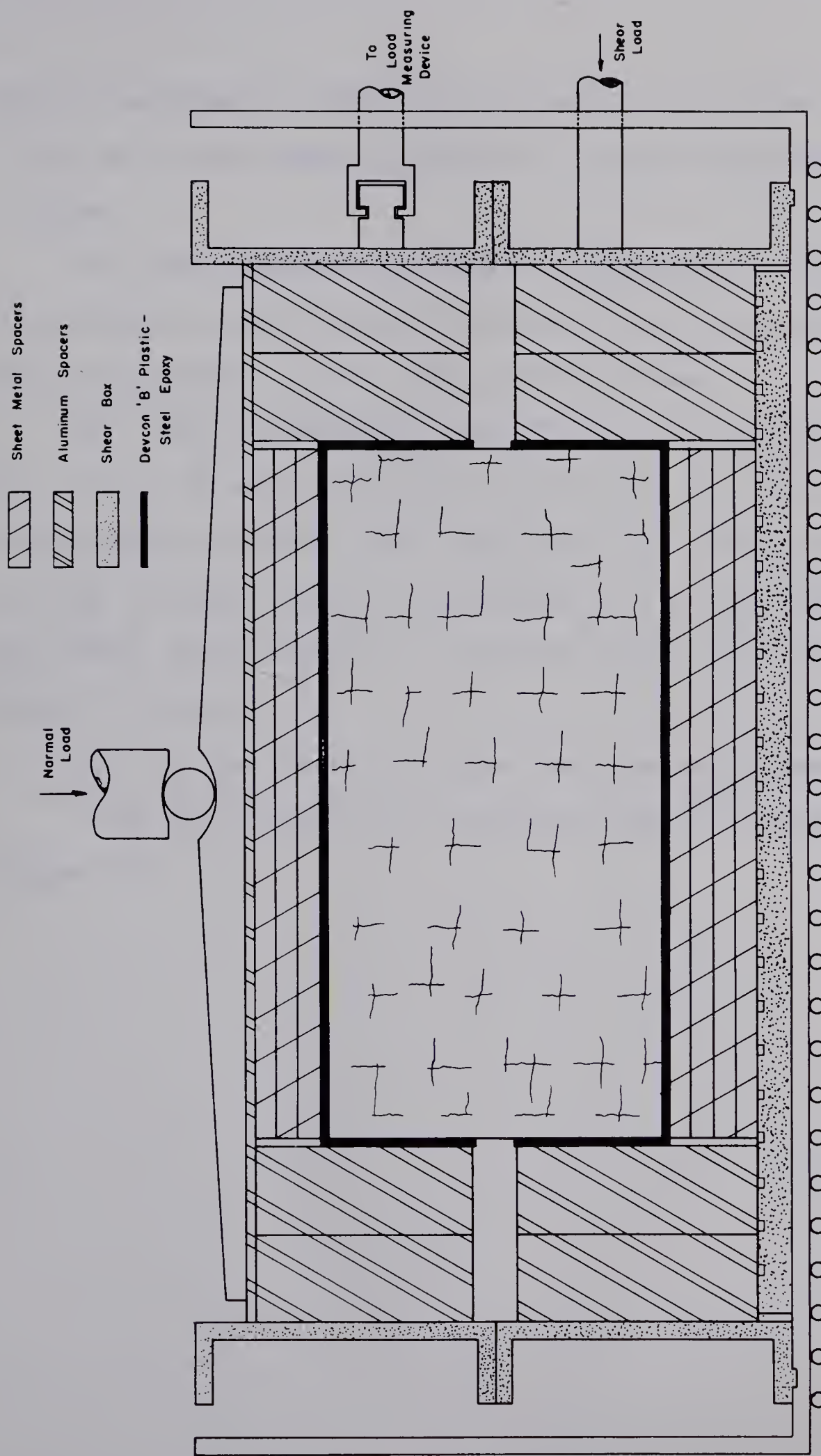


Fig. 4.6 Spacer Arrangement Within Shear Box.

samples underwent a shear displacement of $1\frac{1}{2}$ inches and the 8 inch by 8 inch samples underwent a shear displacement of 2 inches.

(c) The vertical dilation was measured by four LVDT's, one mounted on each corner of the load cap to record the relative movement of the sample during shear.

(d) Threeunjacketed, unconfined, wet compression tests were run on $1\frac{1}{2}$ inch square by 3 inch high coal samples at varying strain rates. The resulting shear strengths were sensibly constant and it was decided to run the remainder of the direct shear tests at a constant strain rate of 0.0096 inches per minute.

(e) All the remaining shear tests were run wet.

The test results are presented and discussed in Chapter VI.

CHAPTER V

FINITE ELEMENT ANALYSIS OF SAMPLE IN DIRECT SHEAR

5.1 THEORETICAL ANALYSIS

The following analysis draws on the theory of linear elasticity to predict stresses and displacements throughout a sample of rock in a direct shear box before peak strength is reached. The analysis provides a method for the evaluation of Young's Modulus for the rock material, information on the state of stress in the sample, and information to be used in the future design of direct shear apparatus.

5.1.1 Theory

When a rigid body displacement is imposed on a linearly elastic body as shown in Fig. 5.1, the applied shear load T will be directly proportional to the imposed displacement δ . The shear load must also be proportional to the shear modulus of the sample material. Thus a relationship of the form

$$T = k' \delta G \quad . . . \quad (5.1)$$

holds, where G = shear modulus, and k' = constant.

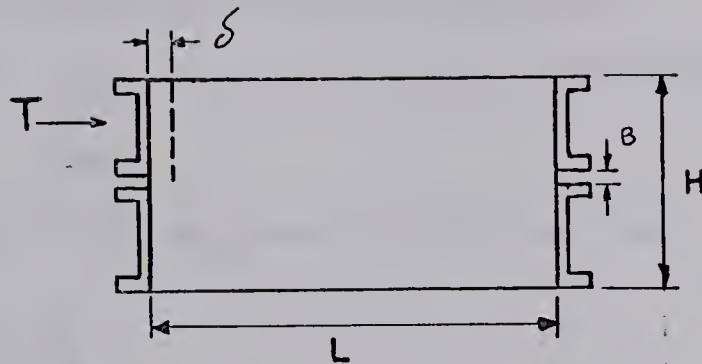


Fig.5.1 Simulation of Sample in Direct Shear

However,

$$G = \frac{E}{2(1+\mu)} \quad . . . \quad (5.2)$$

therefore,

$$T = k \delta E \quad . . . \quad (5.3)$$

where E = Young's Modulus for sample material

μ = Poisson's Ratio

k = constant dependent on μ and the geometry of the test configuration

and T = shear load on the sample per unit width of sample.

As the possible variations in the geometry may be

described in terms of ratios H/L and B/H , then we may write

$$k = f(\mu, H/L, B/H) \quad . . . \quad (5.4)$$

where H = height of the test sample

L = length of the test sample

and B = gap between the top and bottom halves of the shear box.

Equation (5.3) may now be written as

$$k = \frac{T}{E \delta} \quad . . . \quad (5.5)$$

If arbitrary values of E and δ are now adopted, and the elasticity problem is solved subject to the correct boundary conditions, a value of T may be obtained from the solution. Thus k may be evaluated from equation (5.3) for different values of μ , B/H , and H/L .

The results of this investigation provide an obvious method for the determination of Young's Modulus from the direct shear test. If the slope of the linear portion of the shear load versus shear displacement curve is evaluated from test data, a value for T/δ is obtained, and as k is known for that particular test configuration, E is calculated from equation (5.5). Inherent in this procedure is an assumption of Poisson's ratio, μ .

5.1.2 Method of Solution

A finite element technique employing a constant strain

triangle developed by Wilson (1963), was used to solve the elasticity problem. The grid is shown in Fig. 5.2. An arbitrary value of Young's Modulus was input to the computer program, and the ratios of H/L and B/H were varied by simply varying the co-ordinates of the nodal points in the grid, thus keeping the number of elements constant. The program was run three times for each geometrical configuration. The value of μ was changed for each run; the three values being $\mu = 0.2, 0.3$, and 0.45 . The origin of the co-ordinate system was taken at point A.

The boundary conditions may be input either as displacements (u, v) or as forces (F_x, F_y). Now the body is assumed in equilibrium with any normal stress which is applied vertically. Therefore, we only interest ourselves with the changes in stress throughout the body due to a rigid body displacement at the smooth boundary JK. The surfaces AM and GH are assumed to lose contact with the shear box and the upper surface HJ is not constrained. Along the base of the shear box AC, a smooth contact is assumed between the sample and the box and no vertical movement occurs. As the lower half of the shear box is not allowed to move, lateral displacements along the smooth surface CE are zero. The boundary conditions are tabulated in Table 5.1.

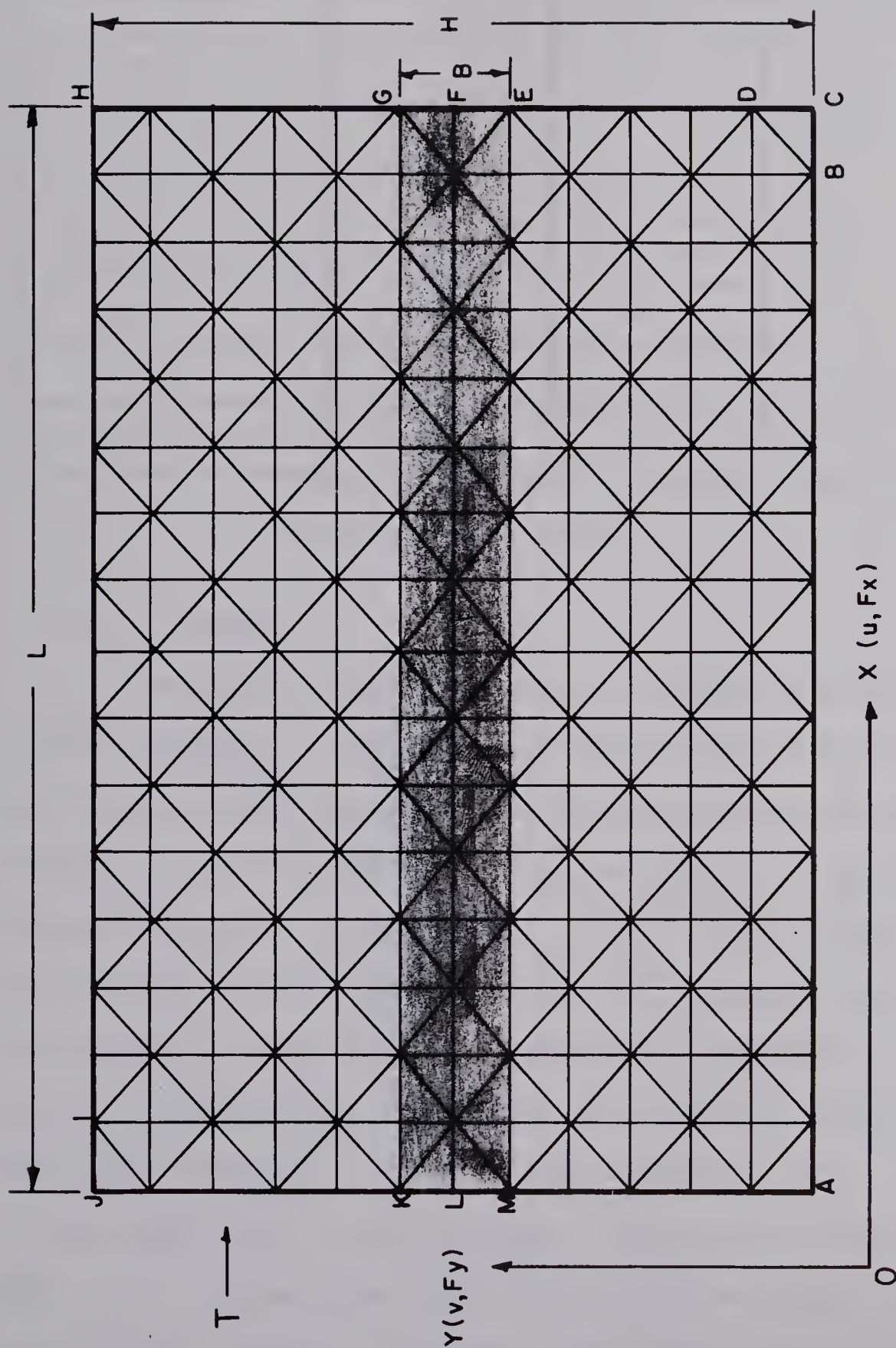


Fig. 5.2 Finite Element Grid

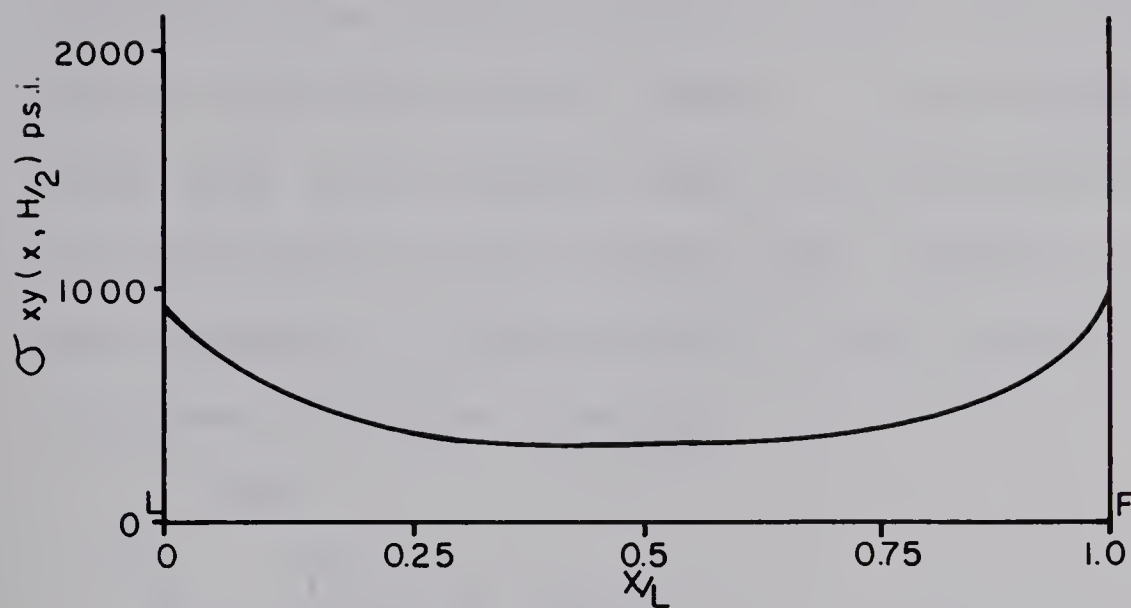
Table 5.1

Surface or Nodal Point	Boundary Conditions			
	u	Fx	v	Fy
AB		0	0	
C	0		0	
DF	0			0
GH		0		0
HI		0		0
JK	0.1			0
LA		0		0

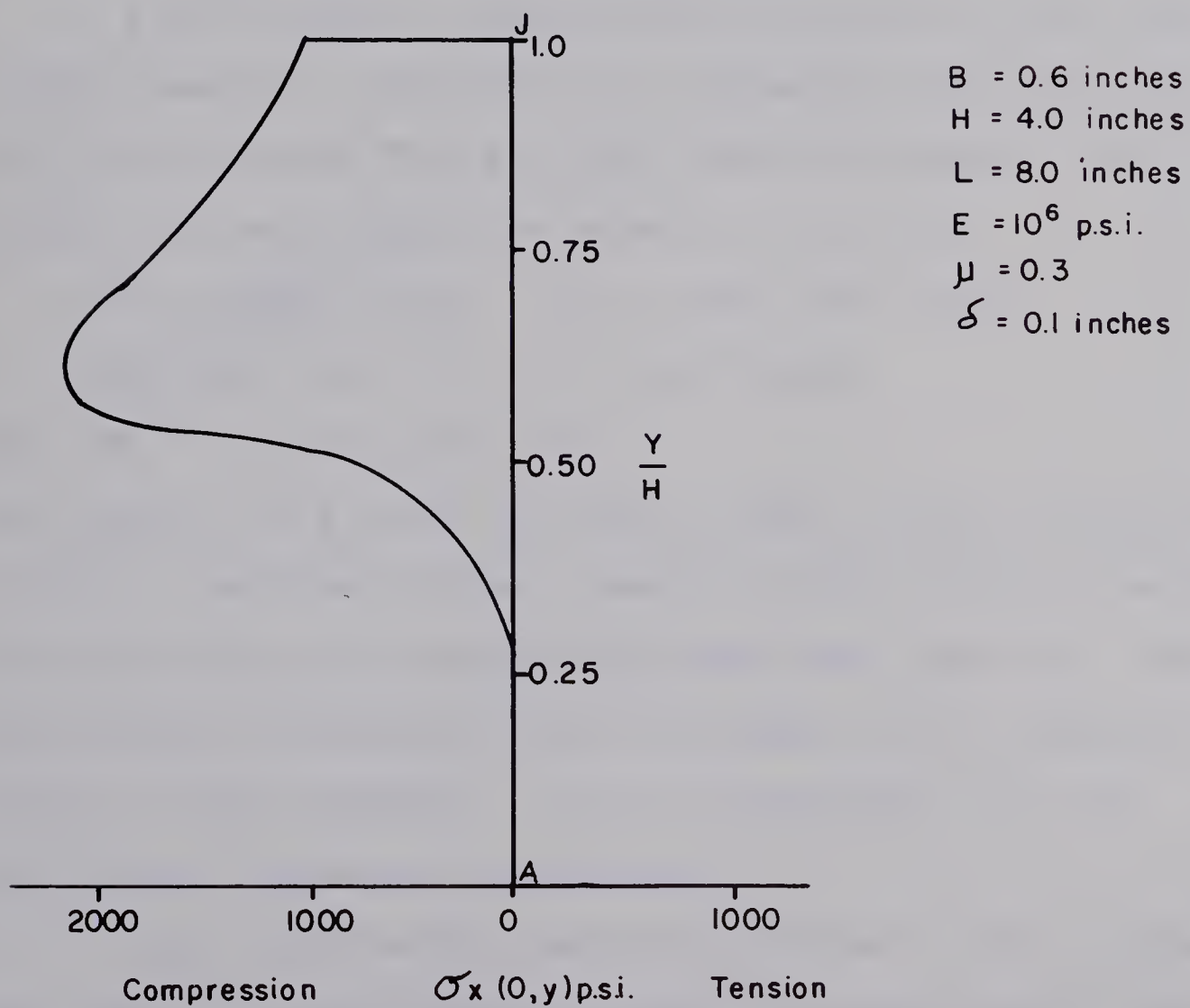
Boundary Conditions

5.1.3 Results

The finite element computer program was run on an IBM 360/67 computer. Nodal displacements and the stresses in each element were listed. The program then evaluated the stresses at each nodal point by averaging the stresses in the elements adjacent to the node. Fig. 5.3(a) shows a typical distribution of the shear stress, σ_{xy} , across the mid-plane of a sample. Fig. 5.3(b) shows the distribution of the lateral stresses, σ_x , evaluated at the nodal points along the left hand boundary. (See LF and AJ, Fig. 5.2). A value of the shear load T was required from the solution. It might be evaluated from the shear stresses along the mid-plane of the sample. However, this was found to be inaccur-



a) Shear Stress Distribution at Mid-Plane



b) Normal Stress Distribution along Left Hand Boundary

Fig. 5.3 Stress Distributions

ate due to the singularities in shear stress existing at the points $L(0, H/2)$ and $F(L, H/2)$. It was decided that the shear load on the sample might be calculated most accurately by integration of the average nodal stresses along the left hand boundary, as the effects of the singularities were less pronounced on these stresses.

Thus

$$T = \int_0^H \sigma_x dy \quad \text{at } x = 0 \quad . . . \quad (5.6)$$

A unit width of sample was considered in the finite element analysis, therefore T as evaluated from equation (5.6) is the shear load per unit width of sample. The values of k were found from equation (5.5) for

$$H/L = 0.250, 0.333, 0.500, 0.667, \text{ and } 0.800;$$

$$B/H = 0, 0.05, 0.10, 0.15, \text{ and } 0.20;$$

$$\text{and } \mu = 0.2, 0.3, \text{ and } 0.45.$$

The results are plotted as shown in Figs. 5.4(a), 5.4(b), and 5.4(c). The results show a smaller sensitivity to the gap ratio B/H , than that which might have been expected. The sensitivity to Poisson's ratio is slight for the smaller values of this parameter but as it approaches 0.5, the sensitivity increases considerably.

Fig. 5.5 shows the variation of shear stress across the sample for the different height to length ratios, H/L . For higher ratios, the shear stress becomes much more uniform over the middle two-thirds of the sample.

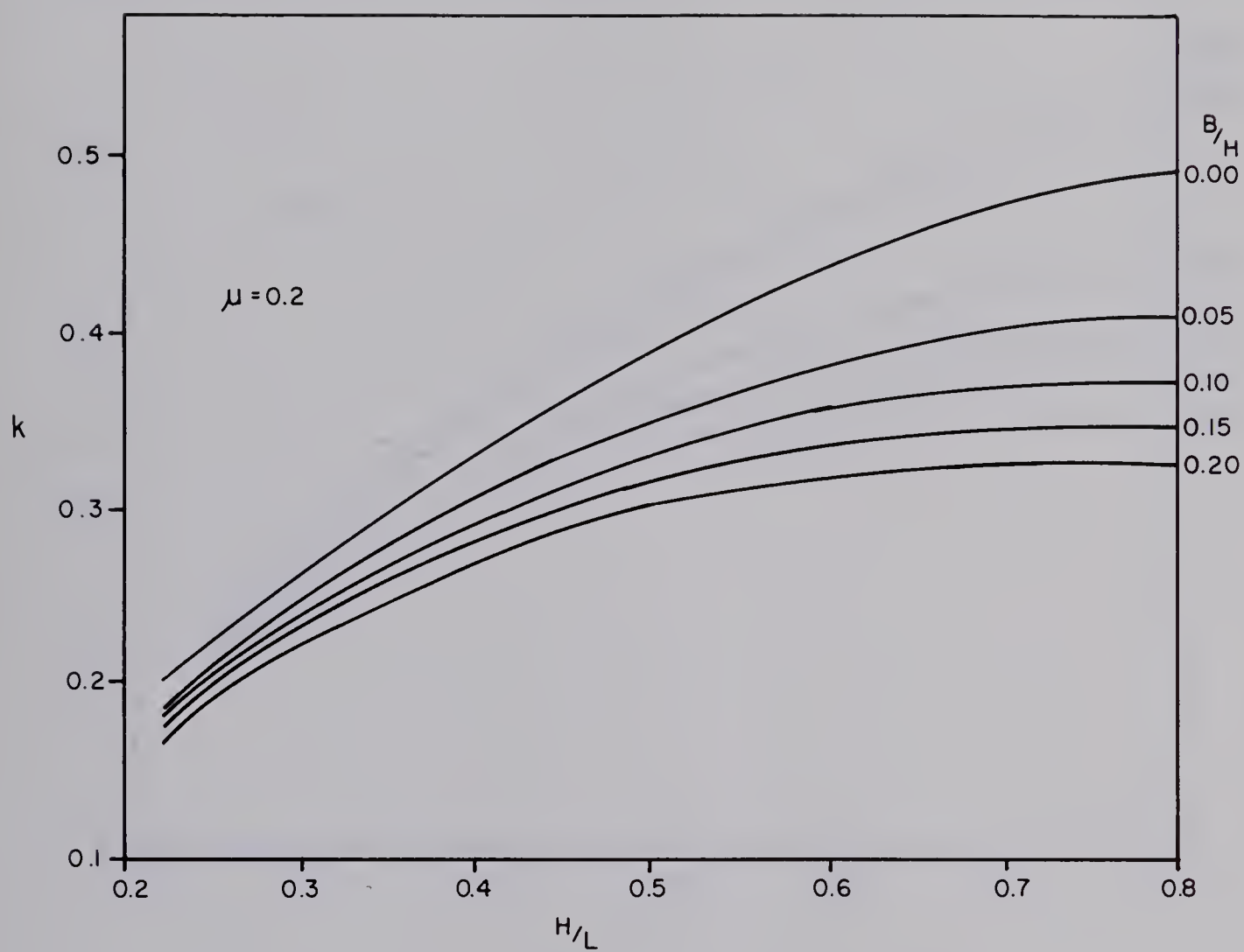


Fig.5.4(a) k values for $\mu = 0.2$

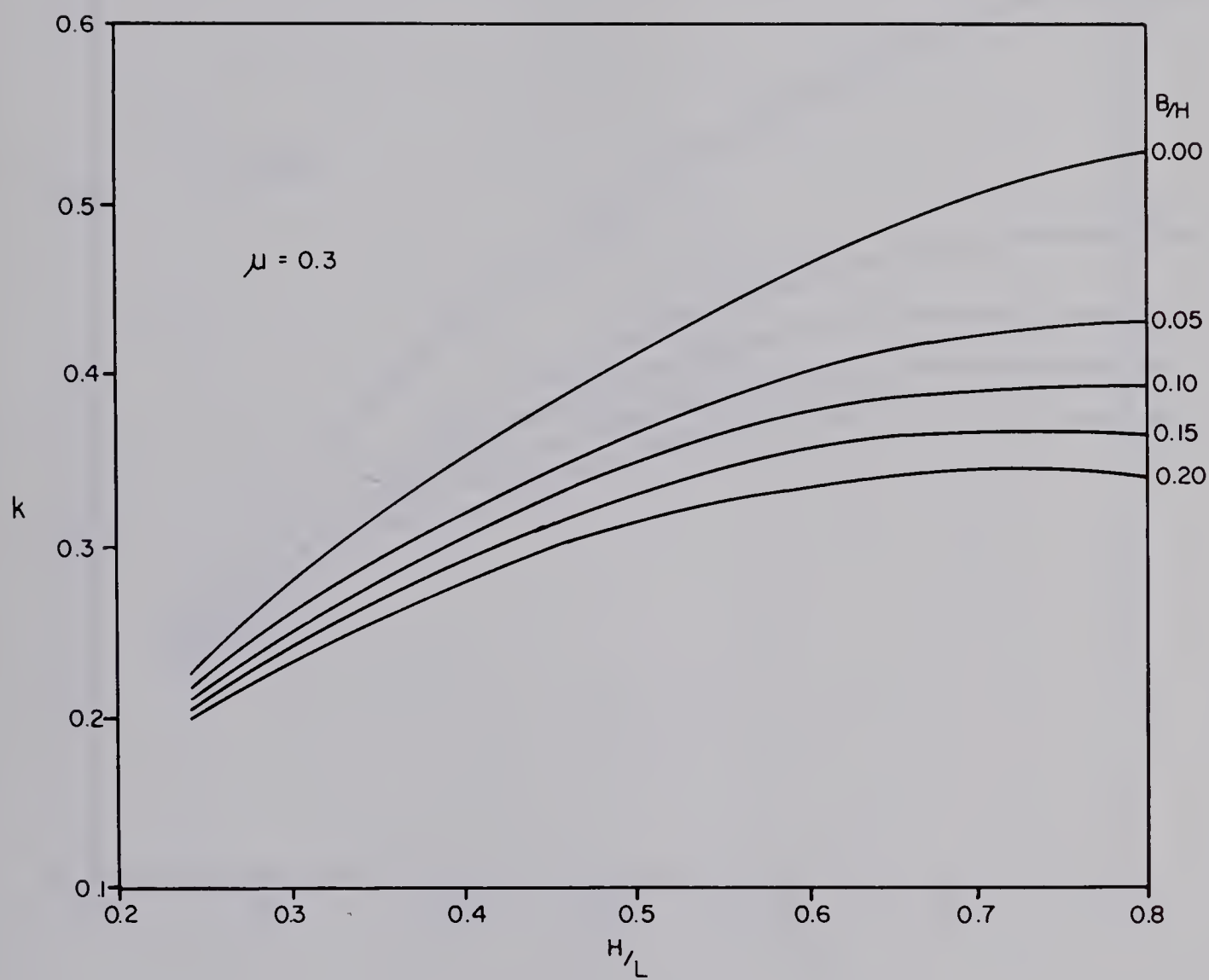


Fig. 5.4 (b) k values for $\mu = 0.3$

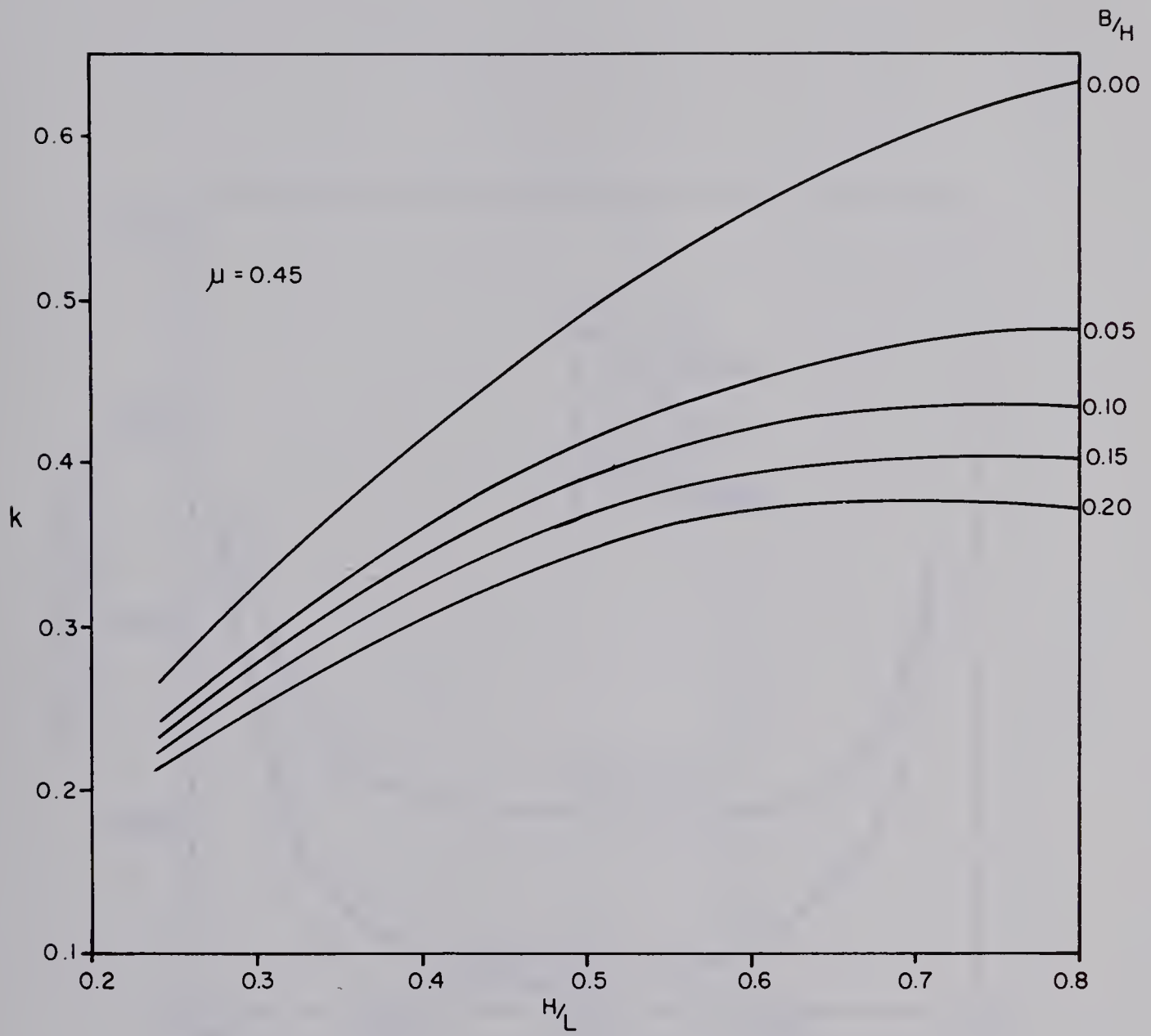


Fig. 5.4 (c) k values for $\mu = 0.45$

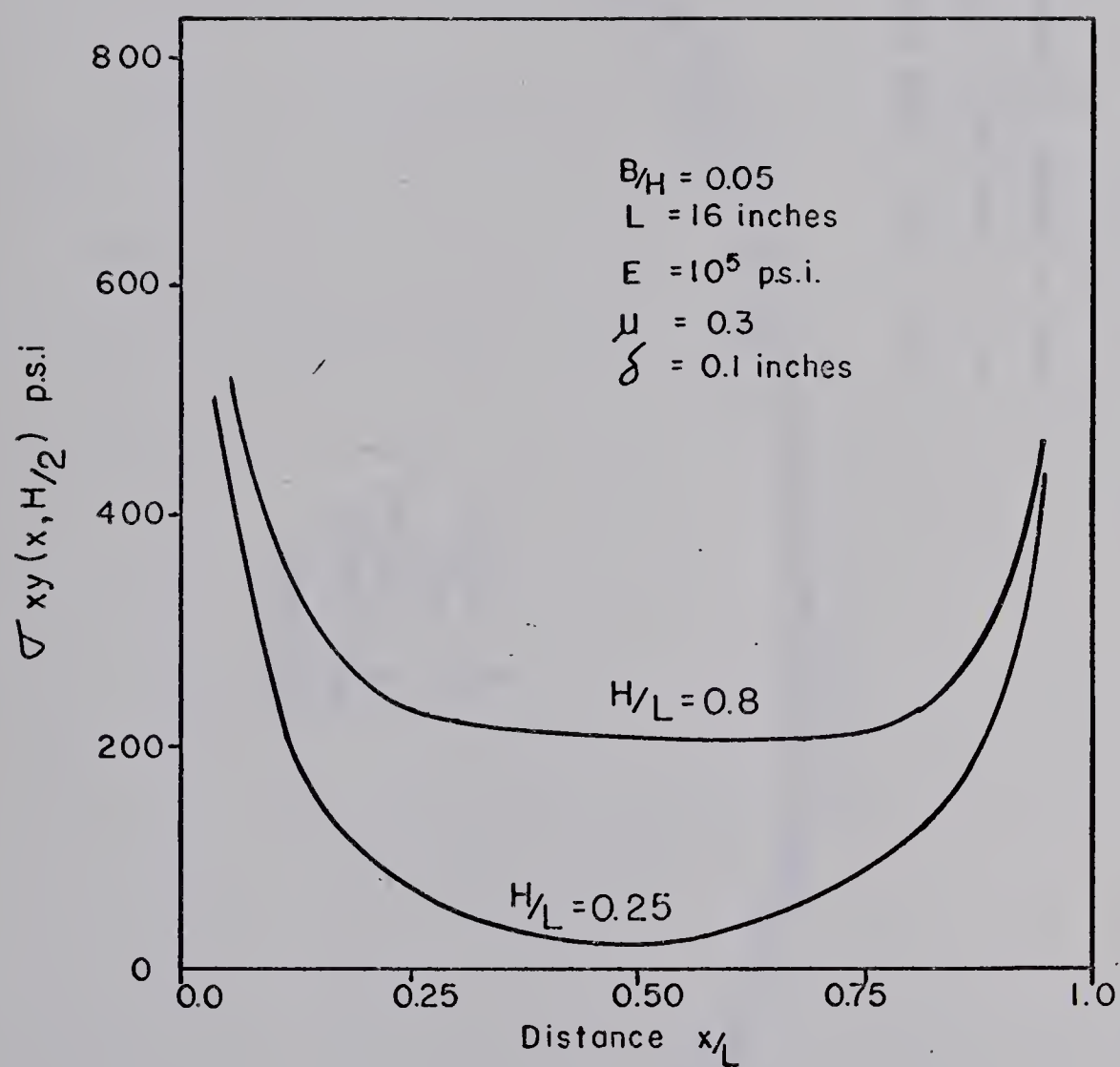


Fig. 5.5 Shear Stress Distribution along the Mid-Plane for Different H/L Ratios.

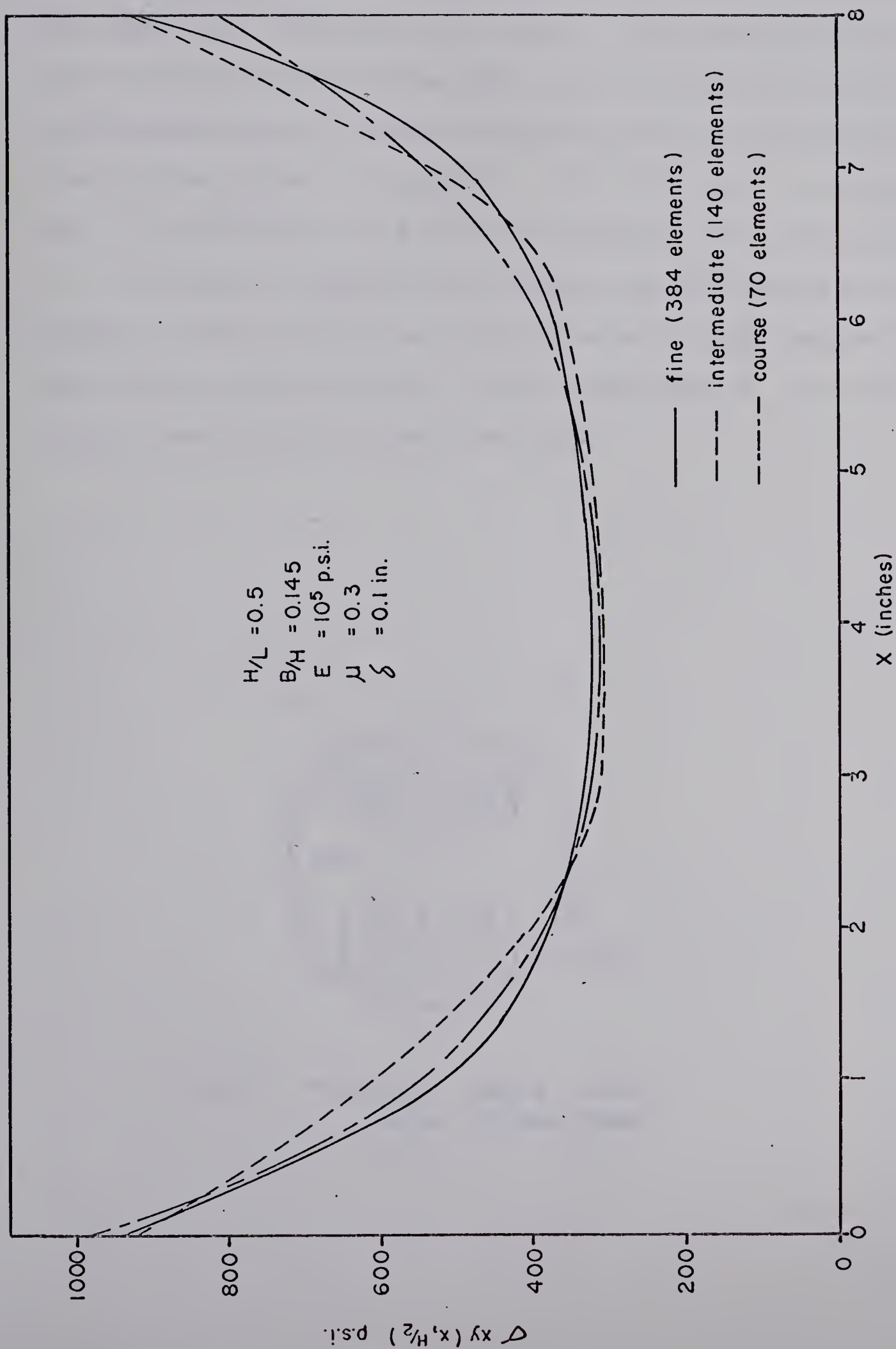


Fig. 5.6 Sensitivity of Shear Stress to Grid Size

Fig. 5.6 shows the variation of the shear stress across the sample for different grid sizes. The results do not vary significantly for the three grid sizes investigated and it was established that no further accuracy could be obtained by increasing the number of elements. The fine grid is shown on Fig. 5.2 and it was the grid used throughout the analysis.

A similar analysis was carried out by Goodman et al (1968) to determine E from an NX bore hole plate bearing device. The device is shown in Fig. 5.7 as consisting of two steel plates forced apart in the bore hole.

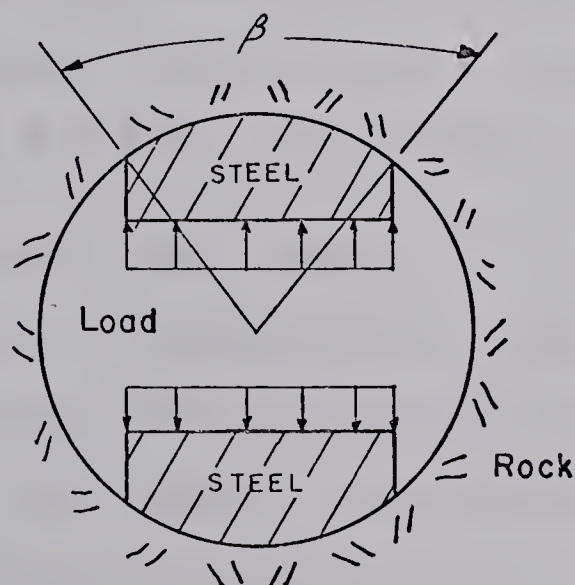


Fig. 5.7 NX Plate Bearing Device.
(after GOODMAN, 1968)

The diametral deformation was measured for increments in load applied. The solution to this problem was obtained using a complex variable method by imposing a constant displacement boundary condition. The following equation:

$$E = \frac{\Delta Q}{\Delta \bar{u}_d / d} K(\mu, \beta) \quad . . . \quad (5.7)$$

was derived where ΔQ = increment of pressure

$\Delta \bar{u}_d$ = average diametral displacement

d = diameter of bore hole

K = constant derived from the solution

and dependent upon Poisson's Ratio

μ and the geometry expressed by β .

This expression is similar in form to equation (5.5) where E is derived from the direct shear tests. A comparison of terms shows T to be the counterpart of ΔQ , $\Delta \bar{u}_d$ the counterpart of δ , and $d \times K$ the counterpart of k .

5.2 APPLICATION TO TEST SAMPLES

The method of interpretation derived for the direct shear tests was applied to the intact coal samples tested in direct shear. The results and discussion for all of the tests are presented in section 6.3.1.

5.3 GENERAL APPLICATION OF METHOD

During the manufacture of testing equipment, it is difficult to assemble the various parts in such a way that no yielding will occur when loads are applied. In designing

direct shear boxes for field tests, it would be possible, in a practical sense, to reinforce the shear box in such a way that a "hard" system was obtained thus ensuring that any displacement measured was displacement within the sample alone. This may be done by using stiff structural sections or by pre-stressing the shear box components before assembling them. In the latter case, when the pre-stressing is released after the sections are connected, a stress would be locked into the system in such a way as to oppose the reaction load applied by the sample during testing.

After the apparatus has been built, a check must be made to ensure that the boundary conditions specified in section 5.1.2 satisfy the testing configuration. If the boundary conditions differ, they must be changed in the computer program and a new series of k values generated. The effects of varying boundary conditions is presently under investigation. Noonan and Nixon (1972). If the E values then, could be determined from the direct shear test, the need for jacking tests or plate loading tests would be minimized thus cutting the cost of field investigations by a considerable amount.

This method also presents a convenient check on already existing direct shear data. It is the author's contention that many direct shear tests have been carried out with "soft" systems, thus casting some doubt on the validity of the reported shear displacements prior to failure. The author

is not aware of any published work where the reported shear displacements have been corrected for the compliance of the testing apparatus. For example, Goodman (1970) has defined the slope of the shear stress versus shear displacement curve up to peak as the shear stiffness of the material and quotes values of shear stiffness determined in this manner.

However, no mention is made that these shear displacements reported had been corrected for the compliance of the testing apparatus.

CHAPTER VI

RESULTS AND DISCUSSION

6.1 CLASSIFICATION PROPERTIES

Proximate coal analyses and brief petrographic descriptions indicate the coal to have a subbituminous B classification and to be bright and banded in nature. (Pearson, 1959).

The results of the eight moisture content determinations ranged from 21.3% to 26.9% giving an overall average of 24.2%.

The specific gravity was found to be 1.58 for the three samples analysed.

Using the average moisture content of 24.2% and a specific gravity of 1.58, the void ratio (e), porosity (n), and degree of saturation (S) were determined and are tabulated in Table 6.1.

All the samples, except the G series were taken from the top of the number one seam and display sensibly constant characteristics. The G series, taken from the top of the number two seam have a lower porosity and higher degree of saturation. The lower porosity can be explained by the fact that porosity decreases with depth. The increase in overburden pressure at depth prevents the material from opening along discontinuities. The G series may be considered to be

Table 6.1

Sample	e	n	S(%)
A4	0.417	0.295	92.2
B2	0.484	0.326	79.0
C2	0.413	0.292	92.4
C3	0.365	0.267	105.2
C4	0.406	0.289	94.0
C5	0.450	0.310	85.4
E1	0.447	0.309	86.1
E2	0.445	0.308	86.2
E3	0.454	0.312	84.4
E4	0.443	0.307	87.7
E5	0.451	0.311	84.8
F1	0.438	0.304	87.2
F2	0.433	0.302	88.6
F3	0.427	0.299	89.6
F4	0.420	0.296	91.5
F5	0.430	0.301	99.1
G1	0.392	0.282	97.1
G2	0.381	0.276	100.2
G3	0.379	0.275	101.3
G4	0.370	0.270	103.9
G5	0.340	0.254	111.4

Classification Properties

fully saturated. These samples were taken below the water table as it existed in the field.

Because the calculations were based on an average moisture content, the values given in Table 6.1 should not be taken as absolute values. They only serve as evidence for the uniformity of the test samples.

6.2 DIRECT SHEAR TESTS ON PRE-CUT SAMPLES

The shear loads measured in these tests were corrected for the frictional resistance provided by the apparatus. The frictional resistance was found to vary with shear displacement and was more pronounced at low normal loads. Typical curves, corrected for the friction of the apparatus, are presented in Fig. 6.1.

As can be seen from Fig. 6.1, a sensibly constant value of shear load was reached under the imposed displacement.

The shear stress was plotted against the normal stress as shown in Fig. 6.2. The shear stress plotted is the value obtained at a shear displacement of 2 inches. The slope of this line was taken as the residual angle of friction, ϕ_r , for the coal, and has a value of 30° .

At very high loads the failure envelopes for most rocks become relatively flat. But in such cases one cannot say that the internal friction is zero. The horizontal envelope no longer reflects the frictional resistance but merely reflects the fact that the maximum internal strength

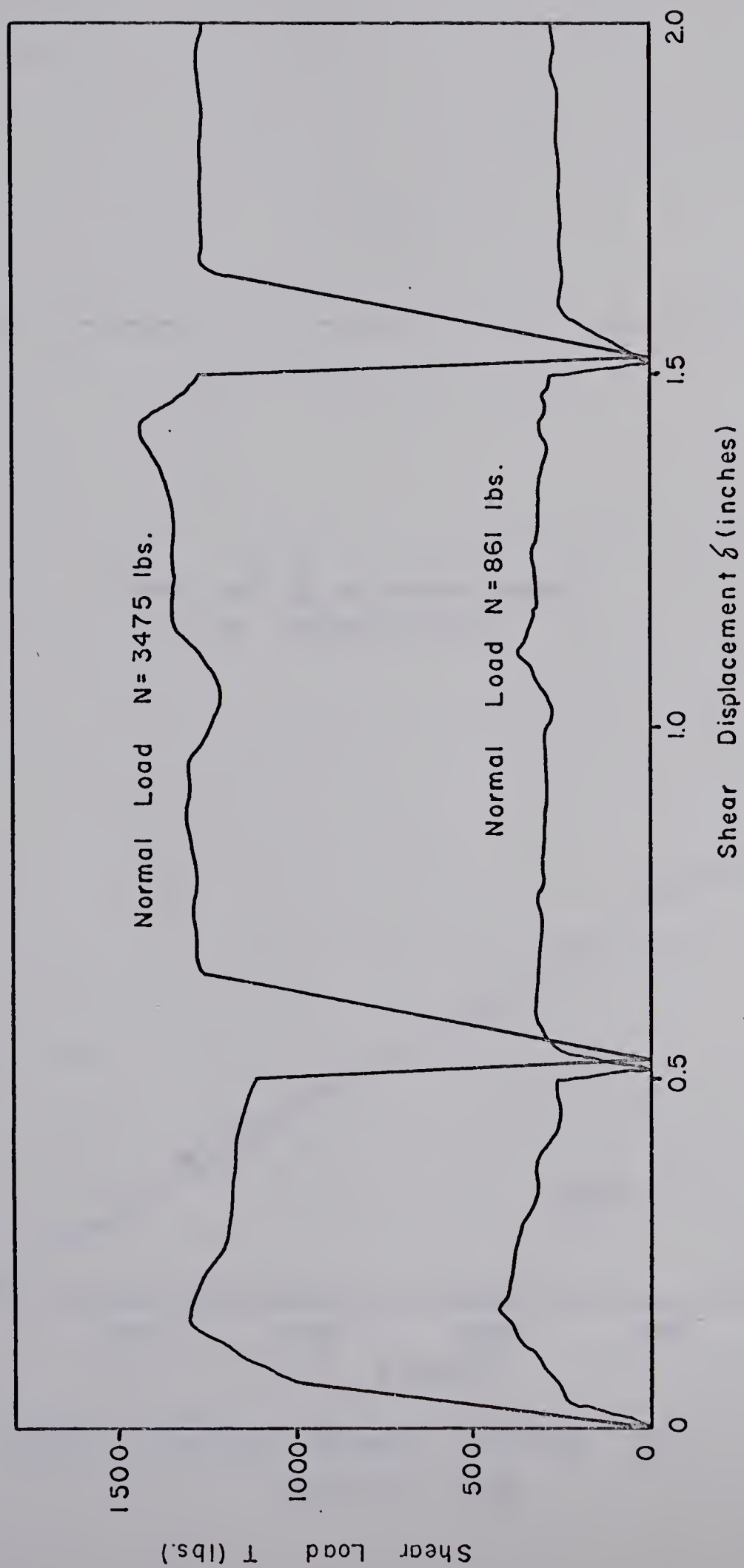


Fig.6.1 Shear Load Vs. Shear Displacement
for Pre-cut Plane

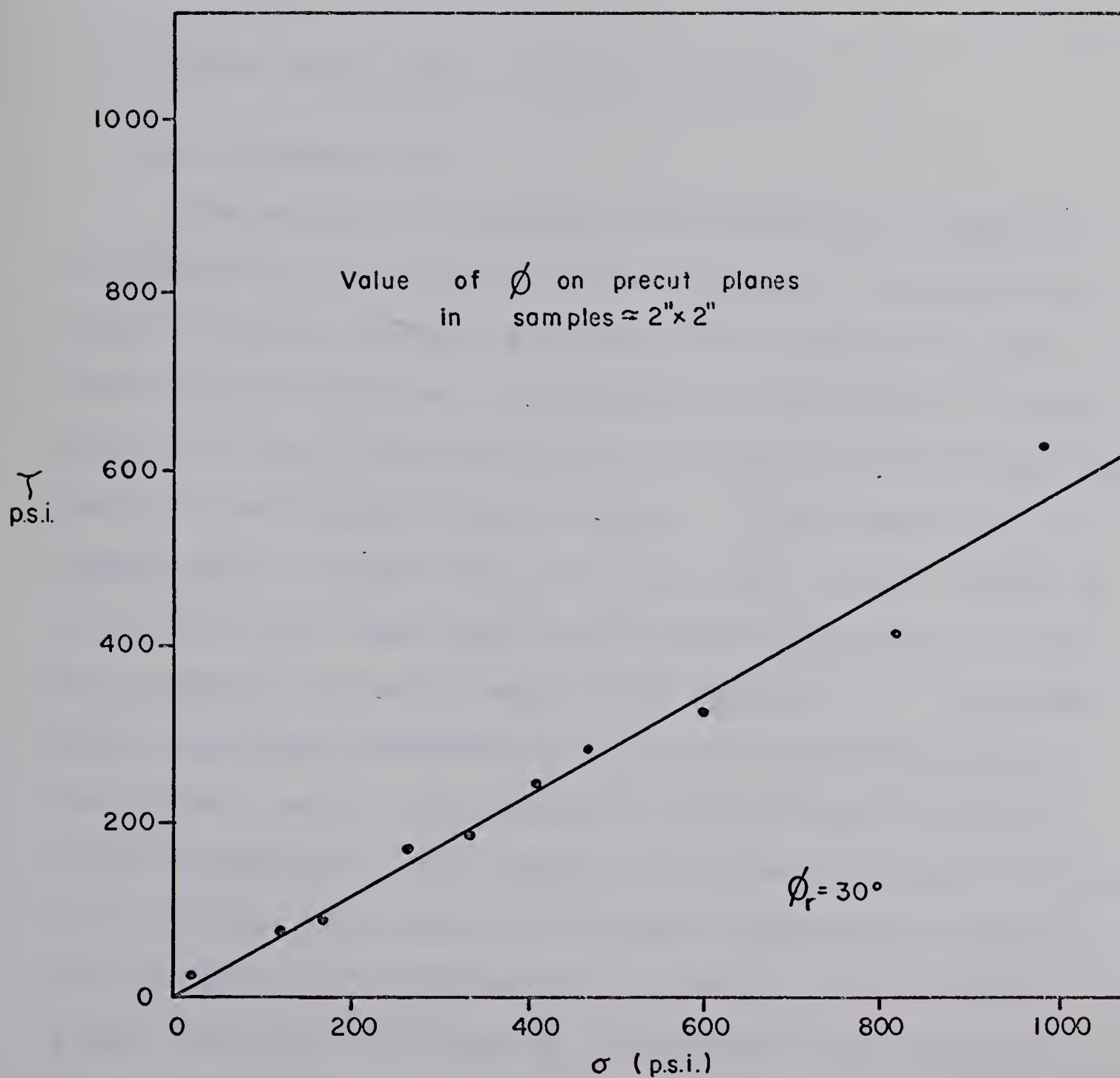


Fig. 6.2 Residual Strength Envelope for
Pre-cut Plane

available has been exceeded. (Patton, 1966). By considering the data points on Fig. 6.2, a case may be made for the fact that this envelope is starting to curve above a normal load of about 600 psi. However, for the stress range involved in the testing program, the straight line, as shown, is valid.

6.3 DIRECT SHEAR TESTS ON INTACT SAMPLES

6.3.1 Before Peak

The method of interpretation developed in Chapter V was applied to the tests on intact samples to determine the value of Young's Modulus for the coal at different normal loads and for different orientations of the planes of weakness. For the interpretation to be valid, the material must behave in a linearly elastic manner. Test sample A3 was subjected to a shear load of 10 tons and a normal stress of 100 psi and the shear load versus shear displacement graph was plotted as shown on page A-3 of Appendix A. The shear displacement was reversed and the unloading graph plotted. The normal load was then reduced to 50 psi and the sample taken to failure. The loading and unloading graphs are seen to be similar over most of the shear displacement imposed. The similarity in slopes of the linear portions of these graphs indicates that most of the imposed displacement is recoverable, and therefore the consideration of coal as a linearly elastic material is a reasonable assumption. It

is of interest to interpret the results within this framework.

The apparatus used in testing the coal samples was such that the top half and the lower half of the shear box were in contact at the shear plane. However, as can be seen in Fig. 4.6, the existence of the box spacers and epoxy on the samples in effect constitute a gap at the shear plane. The values of B , H , and L , and thus B/H and H/L are therefore specified for each sample. A value of $\mu = 0.3$ was chosen as reasonable for this particular material and hence k was determined for each sample from Fig. 5.4(b). Using this k and the values of T and δ from the linear portion of the shear load versus shear displacement curves as shown in Appendix A, the value of E for each test was derived from equation 5.5. It is important to emphasize that the value of T must be the shear load per unit width of sample. Thus, the values of T taken from the load-displacement graphs were divided by the sample width. The values of δ from the load-displacement graphs were also corrected for the displacement that resulted from compliance of the testing apparatus. To do this, a sample of steel with similar dimensions as the coal samples was placed in the shear box and the resulting load-displacement graph recorded. The procedure was repeated over a range of normal loads to ensure that the measured compliance was reproduceable. The steel was considered to be infinitely stiff as compared with the coal. The results of this investigation showed the compliance of the testing

apparatus to be 2.2×10^{-6} inches of shear displacement per pound of shear load applied. This indicates that the testing apparatus constitutes a relatively "hard" system because of the small compliance. The shear load measured over the linear portion of the shear load versus shear displacement graph for each test sample was then multiplied by 2.2×10^{-6} inches to determine the amount of shear displacement resulting from the compliance of the system. This shear displacement, when subtracted from the shear displacement recorded for the test samples, gave the shear displacement within the coal sample alone. The test results are tabulated in Table 6.2. The calculated E values are plotted against normal stress in Fig. 6.3 for each test configuration shown in Fig. 3.1.

Bieniawski (1968) presents a complete load-deformation curve recorded automatically during laboratory testing of coal specimens 2-ft. cube in size in uniaxial compression. This curve is shown in Fig. 6.4.

Two values of Young's Modulus were determined as shown on Fig. 6.4 and have the values of 16.7×10^3 and 33.4×10^3 psi. These values are in the same range as those determined in this study from the direct shear tests and shown on Fig. 6.3. Bieniawski quotes values of Young's Modulus determined from in-situ compression tests on 5-ft. cubes ranging from 420×10^3 to 720×10^3 psi. He attributes the variation to changes in temperature and humidity that affected the coal to such a degree that it cracked and

Table 6.2

Test	Bulk Density (lbs./ft. ³)	σ (psi)	B/H	H/L	k	T (per unit width) (lbs./in.)	δ (in.)	E (x10 ³ psi)
A1	86.5	52	0.135	0.314	0.252	709.2	0.102	27.6
A2		14	0.188	0.444	0.298	119.7	0.053	7.6
A3		51.8	0.114	0.373	0.289	915.6	0.096	33.0
A4		30	0.132	0.492	0.332	252.4	0.027	28.2
B1	82.5	70	0.167	0.539	0.335	400.8	0.033	36.3
B2		30	0.157	0.572	0.347	208.7	0.022	27.3
B3		51.6	0.114	0.373	0.289	529.4	0.092	19.9
B4		36.1	0.135	0.313	0.252	528.5	0.078	26.9
B5		20.6	0.139	0.304	0.247	449.2	0.081	22.5
C1	86.5	20	0.119	0.544	0.354	269.6	0.016	47.6
C2		40	0.139	0.462	0.320	333.3	0.034	30.6
C3		60	0.159	0.569	0.345	437.4	0.031	40.9
C4		80	0.233	0.388	0.268	504.3	0.034	55.3
C5		100	0.132	0.392	0.293	503.5	0.031	55.4
D1		70	0.158	0.659	0.358	675.9	0.052	36.3
D2		20	0.190	0.401	0.283	273.3	0.028	34.6
D3		90	0.197	0.524	0.322	625.2	0.033	58.8
D4		35	0.148	0.392	0.289	501.3	0.034	51.0
D5		50	0.179	0.499	0.321	416.1	0.039	33.2
E1	84.7	70	0.164	0.659	0.354	493.4	0.029	48.1
E2	84.8	80	0.115	0.558	0.358	669.7	0.034	55.0
E3	84.3	35	0.163	0.511	0.329	367.4	0.032	34.9
E4	85.3	50	0.139	0.460	0.320	664.2	0.047	44.2
E5	84.4	90	0.185	0.415	0.289	832.3	0.034	84.7
F1	85.2	20	0.168	0.535	0.333	701.8	0.068	31.0
F2	85.6	40	0.235	0.389	0.268	559.3	0.057	36.6
F3	85.6	60	0.137	0.468	0.325	750.0	0.037	62.4
F4	86.4	80	0.163	0.395	0.298	770.1	0.037	69.8
F5	85.6	100	0.180	0.575	0.338	453.2	0.042	31.9
G1	87.9	90	0.143	0.601	0.359	782.6	0.040	54.5
G2	88.7	20	0.152	0.510	0.333	503.6	0.041	36.9
G3	88.9	35	0.189	0.406	0.283	400.0	0.026	54.4
G4	89.4	70	0.184	0.585	0.338	503.9	0.030	49.7
G5	91.3	50	0.183	0.423	0.293	470.7	0.042	38.3

Results of Finite Element Application to Test Samples

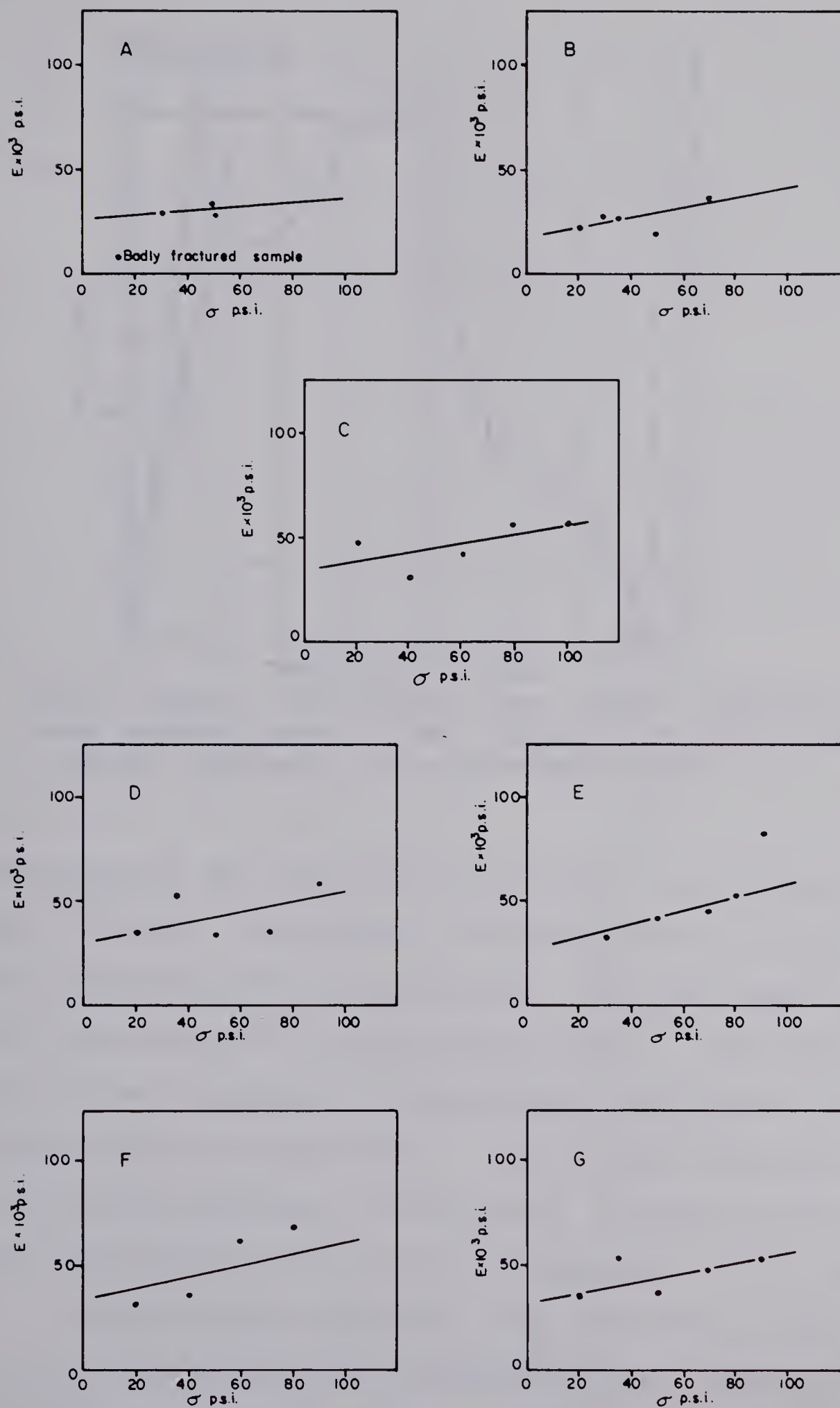


Fig.6.3 Calculated Values of Young's Modulus

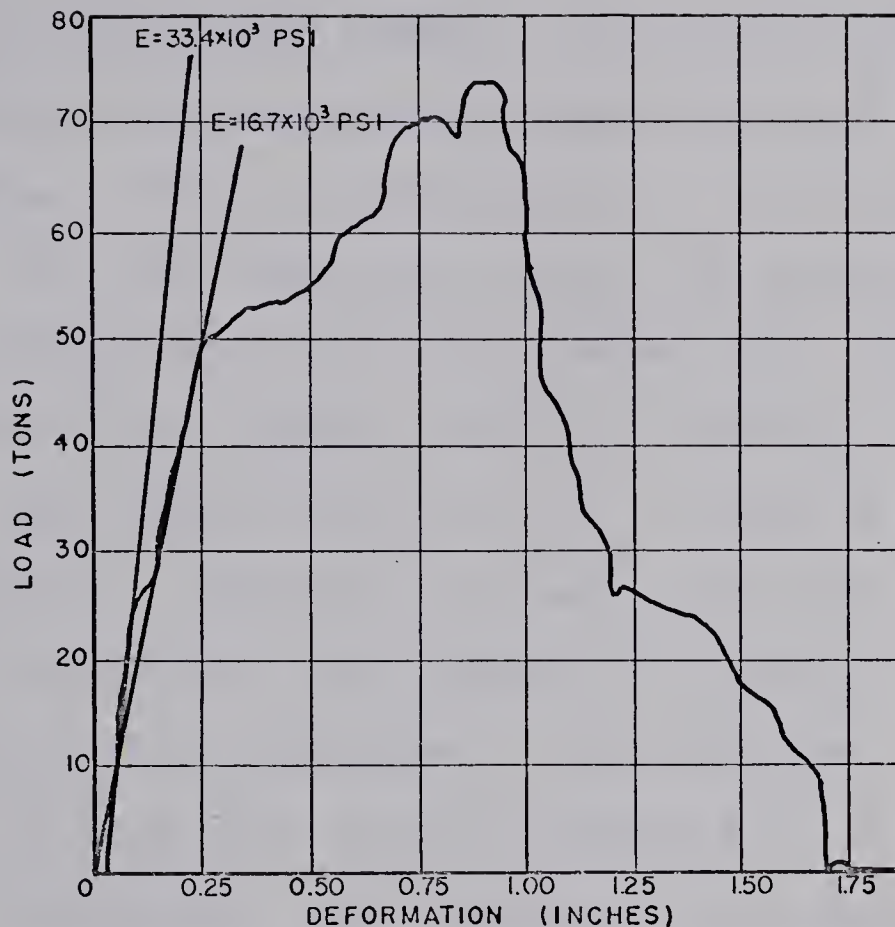


Fig.6.4 Complete load-deformation curve recorded automatically during laboratory testing of coal specimens 2-ft. cube in size in uniaxial compression. (after BIENIAWSKI, 1968)

disintegrated when the moisture content, upon removal from the mine, changed. Bieniawski was dealing with coal extracted from underground mining operations. The coal used in this study was extracted from an open pit mine. Therefore the coal had been subjected to temperature and humidity changes before removal from the mine. Any further variations incurred during sampling, transporting, or preparing the samples would not significantly affect its behaviour in the laboratory.

As can be seen from Fig. 6.3, the trend is for E to increase with an increase in normal stress. This is similar to E increasing with depth in the field as has been determined

by Ward and Burland (1968). In effect, an increase in normal pressure causes existing discontinuities within the sample to close. This is reflected by a corresponding increase in E.

The bulk densities for all the samples do not vary considerably and no definite relationship exists between the values of bulk density and Young's Modulus.

The results shown on Fig. 6.3 may be grouped into two categories. Category I is made up of test configurations A to C inclusive, and category II is made up of test configurations D to G inclusive. The lines for category I generally lie below the lines for category II in the normal stress range considered. This indicates that when shear is taking place along the bedding planes the values of Young's Modulus are less than the values obtained when shear is taking place with the bedding planes vertical and oriented in the direction of the applied shear load. Because the bedding planes are planes of weakness, the results are as expected and will be seen to be consistent with the results and discussion given for peak behaviour in the following section 6.3.2. Any variation in orientation of the joint planes does not affect the value of Young's Modulus. This, again, is consistent with the results and discussion given in section 6.3.2 for the same reasons presented in that section.

The closing of the joint is dependent upon the normal stress, and closed joints lead to a stiffer specimen. For A, B, C, and G the joints are not closed by the normal stress

and the E values are seen to be less dependent upon the normal stress for these configurations.

6.3.2 Peak

The shear load versus shear displacement curves for all the tests on intact samples are presented in Appendix A.

For each test, the maximum shear stress recorded was plotted against the normal stress for that particular test in order to define the shear strength parameters ϕ and c , where ϕ is the internal friction angle and c is the cohesion intercept or shear strength recorded under no normal load. The Mohr-Coulomb failure criterion

$$\tau = c + \sigma \tan \phi \quad . . . \quad (6.1)$$

was used where τ = shear stress along shear plane

σ = normal stress on shear plane.

The shear stress versus normal stress graphs are plotted on Figs. 6.5 and 6.6 and the values of ϕ and c determined from these graphs are tabulated in Table 6.3. Investigations of these results showed that they could best be explained by grouping them into two categories.

The dashed line shown for test configuration A is the line that best fits the experimental data. However, the test indicated as being badly fractured, does not reflect the strength of the material because all continuity in the zone of shear was lost during sample preparation. Also,

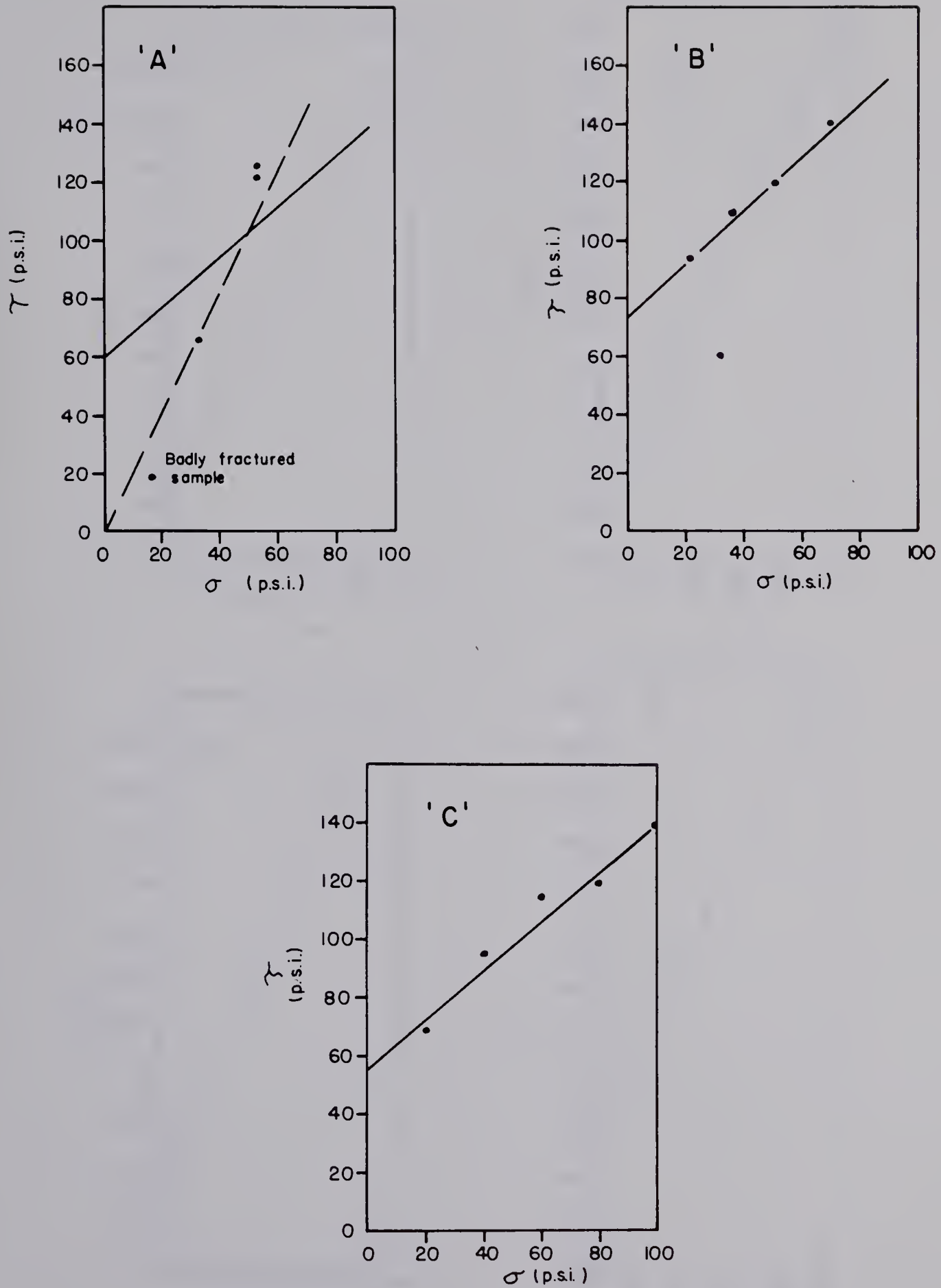


Fig. 6.5 Strength Envelopes at Peak
Category I

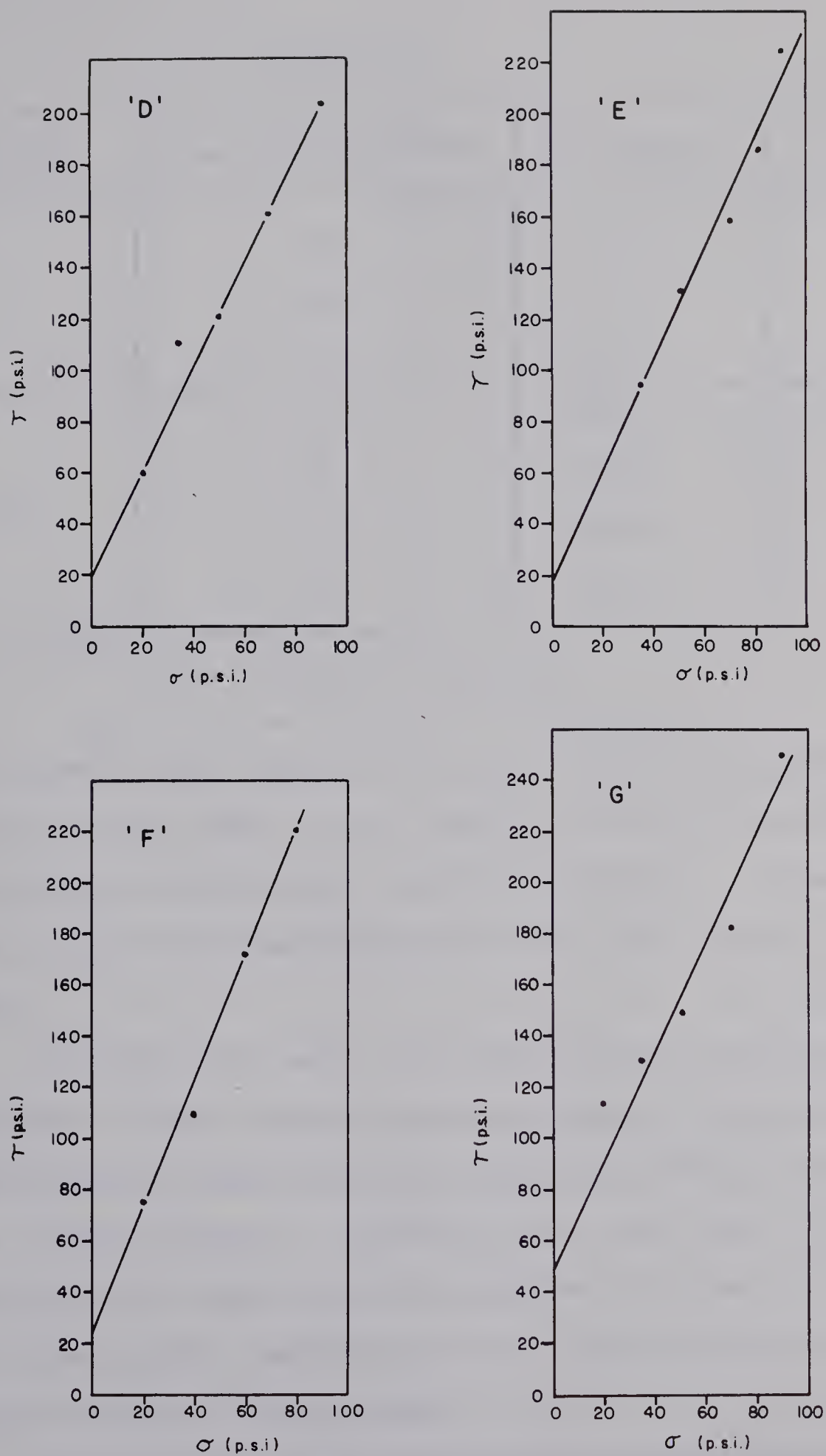


Fig.6.6 Strength Envelopes at
Peak- Category II

Table 6.3

Category	Test Configuration	ϕ (degrees)	c (psi)
I	A	41.5	60
	B	41.7	76
	C	40.5	56
II	D	64.0	20
	E	65.5	17
	F	67.8	25
	G	65.0	50

Shear Strength Parameters

some value of the cohesion intercept would be expected. The solid line, then, is the best fit line for the valid data points assuming some cohesion intercept. It will be shown in the following discussion that this line is indeed valid.

Category I is made up of test configurations A to C inclusive. These samples share the common component of bedding planes being horizontal and shear taking place along these bedding planes. As can be seen from Fig. 6.7, test configurations B and C can be generated from test configuration A by rotating the sample about the Y axis keeping the direction of applied shear load constant.

Category II is made up of test configurations D to G inclusive. These samples share the common component of

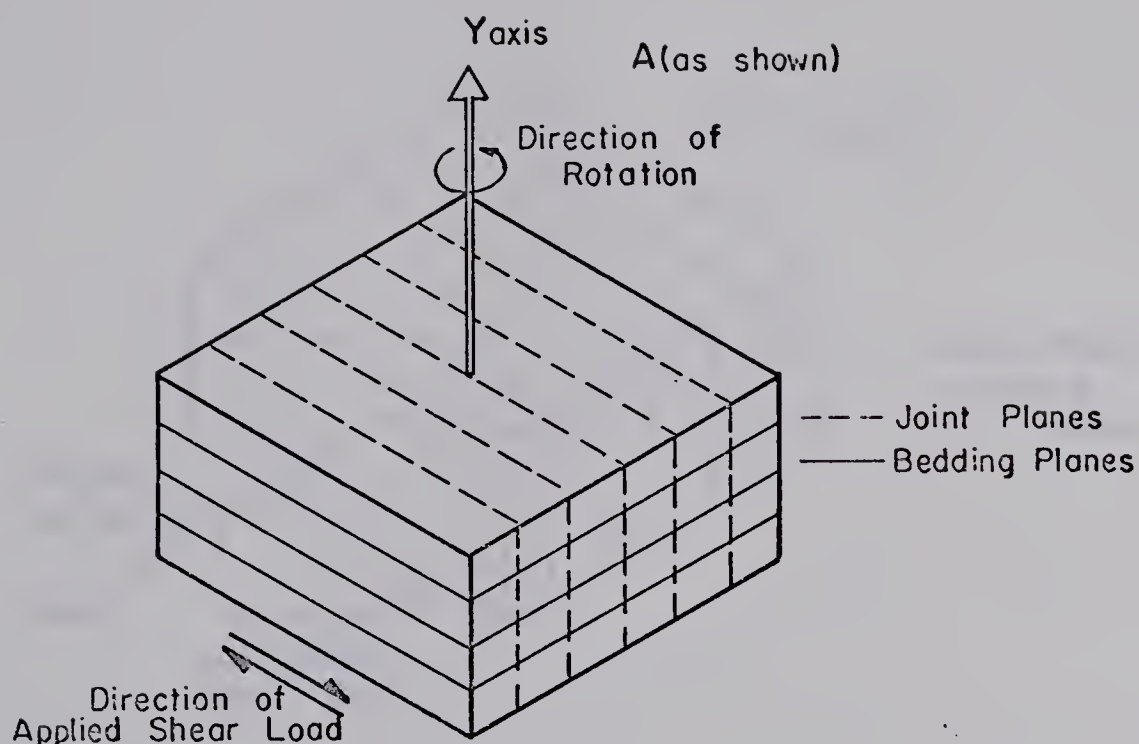


Fig. 6.7 Test Samples in Category I

bedding planes being vertical and oriented in the direction of the applied shear load. As can be seen from Fig. 6.8, test configurations D, E, and G can be generated from test configuration F by rotating the sample about the X axis keeping the direction of applied shear load constant.

Consideration is given to A and F as shown in Figs. 6.7 and 6.8. Before dealing with the complications demonstrated in these figures, it is necessary to think in simpler terms. If the only planes of weakness present in the sample are assumed to be bedding planes, it is clear that the shear strength of A will be less than the shear strength of F,

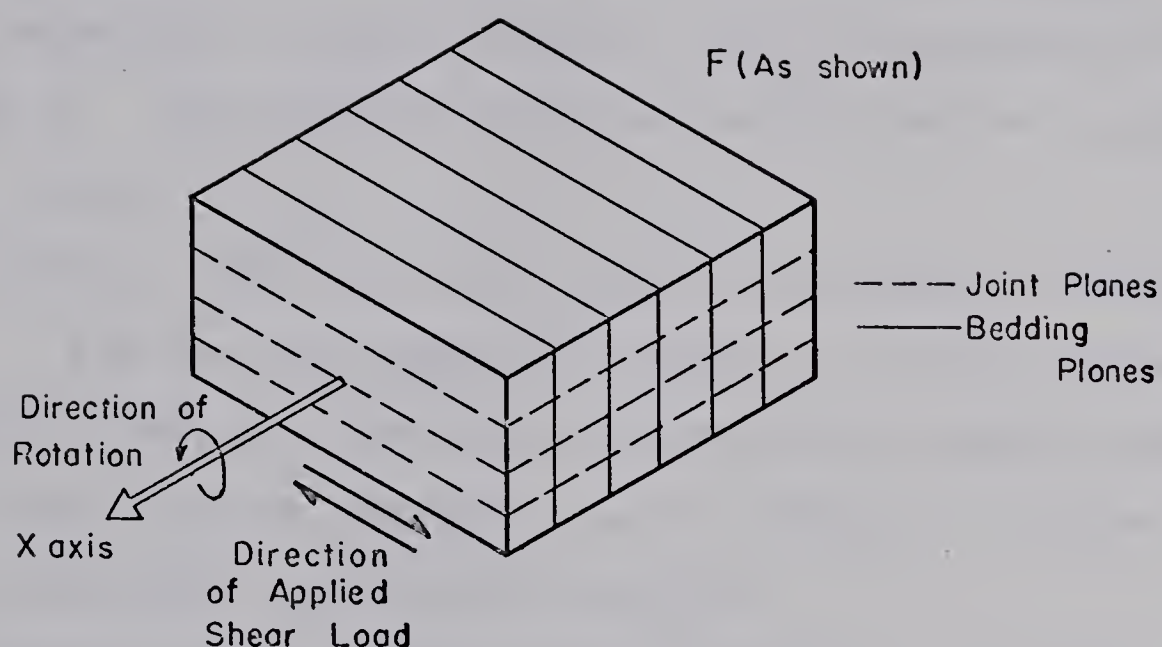


Fig. 6.8 Test Samples in Category II

because in A shear is taking place along the plane of weakness. Hobbs (1964) tested 2 inch long by 1 inch diameter cylindrical coal samples in triaxial compression. These samples contained mutually orthogonal planes of bedding, cleat and cross-cleat. He found that the Pentremawr anthracite and Linby coal cylinders compressed perpendicular to the bedding planes were stronger at all confining pressures than those loaded parallel to the bedding planes.

The bedding planes are not continuously open discontinuities, therefore some cohesion intercept for A would be expected. Also, a greater cohesion intercept would be

expected for F because shear is not taking place along a plane of weakness. Because of the strength anisotropy of the material, a smaller ϕ angle would be expected for A than for F. The strength envelopes would then be as shown in Fig. 6.9.

This is consistent with results presented by Hobbs (1964). For the Pentremawr coal tested he found a cohesion intercept of 400 psi when testing parallel to bedding and 700 psi when testing perpendicular to bedding. He does not, however, give any comparative ϕ values.

Donath (1961) tested Longwood shale in triaxial compression and found ϕ to be in the range of 20° when testing parallel to bedding and in the range of 30° when testing perpendicular to bedding. Donath does not give any comparative c values for Longwood shale but describes the material as having "well developed bedding plane fissility produced by the parallel arrangement of mica flakes and elongated quartz particles. The rock tends to break easily along bedding planes."

If the planes of weakness defined by the joint planes are now introduced, the sample configurations used in this testing program will be obtained. For category I the joint planes are vertical. The strength envelopes for A, B, and C, would be expected to be similar to each other and also similar to that envelope shown for A in Fig. 6.9. The results as tabulated in Table 6.3 show that the ϕ angle is

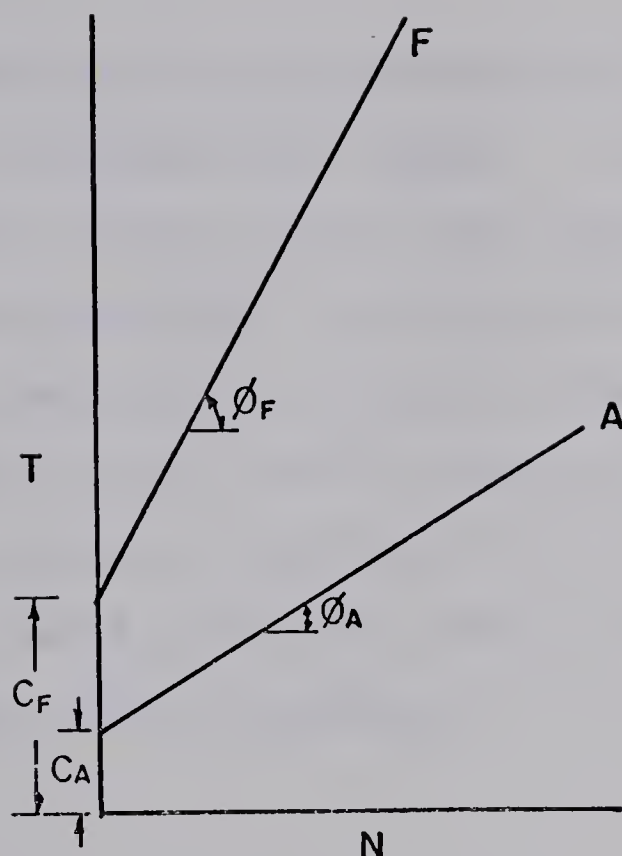


Fig. 6.9 Predicted Strength Envelopes with Bedding Planes Only in Sample.

about 41° for these samples. The cohesion intercept is seen to vary between 56 psi and 76 psi. This variation in c , although small, may reflect a lower value of cohesion at some preferred orientation. The tests are not extensive enough to determine this preferred orientation if, in fact, it exists. In general, however, the test results are seen to behave as predicted. The results for the A test configuration are not conclusive. Based on the preceeding discussion, the strength envelope shown on Fig. 6.5(a) is the most reasonable for the data obtained.

In category II, the joint planes are oriented at varying angles to the direction of the applied shear load. These

joint planes are open discontinuities but they are not continuous throughout the sample. The degree of continuity of the joint planes is less than that of the bedding planes. If test configurations A and F as shown in Figs. 6.7 and 6.8 are again compared, the cohesion intercept for F would be expected to be less than the cohesion intercept for A. The strength envelopes would then be as shown on Fig. 6.10 as opposed to those previously shown in Fig. 6.9 where bedding was the only plane of weakness.

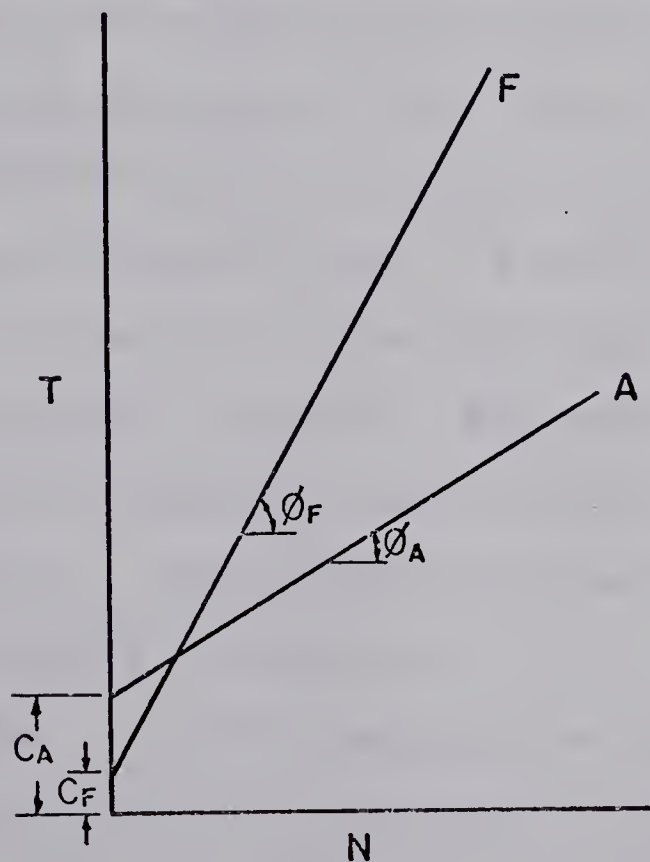


Fig. 6.10 Predicted Strength Envelopes with Joint Planes and Bedding Planes in Sample.

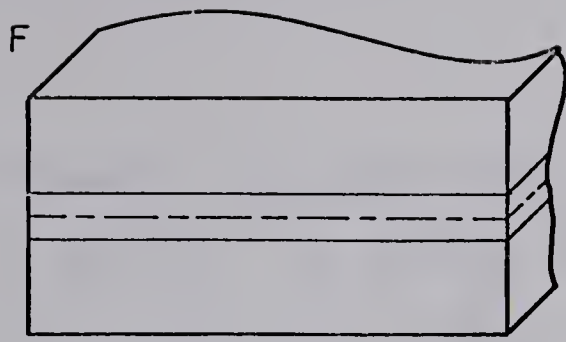
By varying the angle of inclination of the joint plane with the direction of the applied shear load, the areal extent of the joint plane with respect to the shear plane would vary as shown in Fig. 6.11.

Only a small variation in the cohesion intercept would be expected for D, E, and F because of the small variation in the areal extent of the joint planes. However, the cohesion for G would be expected to be higher. The joints in G are vertical having an areal extent of 0% and thus should not affect the value of C.

Because the bedding planes are always vertical and oriented in the direction of the applied shear load, no variation in the ϕ angle for the tests in category II would be expected and it would be similar to the ϕ angle for test configuration F shown on Figs. 6.9 and 6.10. The results as tabulated in Table 6.3 show that the ϕ angle varies within a range of from 64° to 67.8° . The cohesion for tests D, E, and F is in the range of 17 psi to 25 psi and the cohesion for G is 50 psi. These results are seen to be consistent with the preceeding discussion.

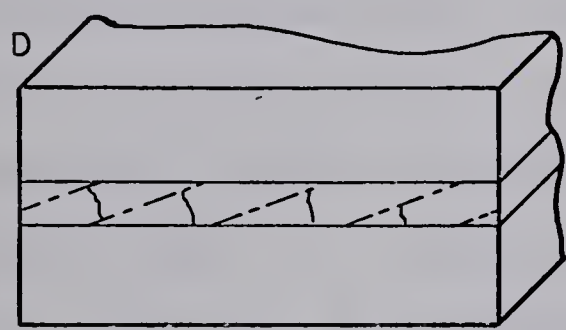
In order to further explain the consistent value of ϕ for the two categories regardless of the orientation of the joint planes, the shear displacement and vertical dilation at peak are considered. These values are shown on the graphs presented in Appendix A. The average dilation at peak is very small. This clearly indicates that there was little

Aeral Extent of Joint Plane
with Respect to Shear Plane



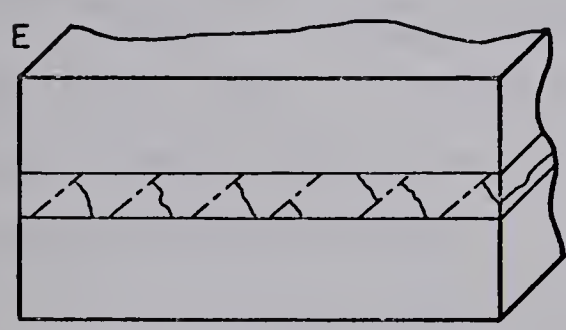
100 %

25



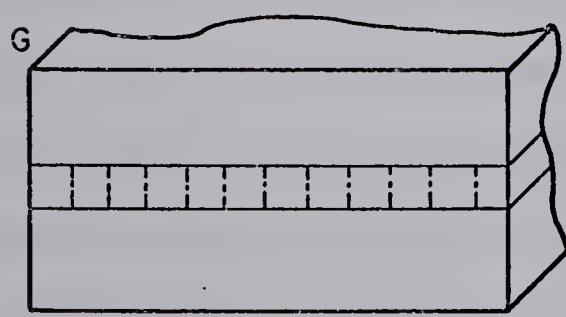
94.5 %

20



75.7 %

17



0%

50

----- Joint Plane

NOTE — The aeral extent is the percentage of
the shear surface made up of the
joint plane.

Fig. 6.11 Percentage of the Shear Surface Composed
of the Joint Plane

movement along the discontinuities up to peak. For example, in test E2, the average dilation at peak was 0.005 inches for a shear displacement of 0.163 inches. If the sample had moved along the joint plane inclined at 40° , the vertical dilation measured for a shear displacement of 0.163 inches would have been 0.137 inches. This is several orders of magnitude greater than the measured dilation. Thus, the peak ϕ angle is a function of the sample material only and not a function of the geometry of the discontinuities. This is only the case when the open discontinuities are not continuous throughout the sample. When they are continuous as is the case for models such as those used by Patton (1966) and Ladanyi and Archambault (1970), then the orientation of these discontinuities plays a dominant role at peak.

The method used in loading the sample is shown on Fig. 4.6. The shear load is applied along the left hand boundary on the upper half of the sample and along the right hand boundary on the lower half of the sample. The normal load is applied at the centroid of the top surface of the sample and distributed evenly over the sample by the rigid loading cap. Because a gap exists at the shear plane and because the sample does not fit perfectly into the shear box, the sample will rotate a small amount as the shear load increases. The rotation will take place about a horizontal line on the top surface of the sample passing through the centroid and normal to the direction of the applied shear load.

The sense of rotation will be such that the left side moves upward and the right side moves downward. When the results are plotted as shown on the figures given in Appendix A, the dilation curves have a trumpet-like shape up to failure that reflects the rotation of the sample. The upper line of the trumpet curve is in all cases the dilation measured on the left side of the sample and the lower line of the trumpet curve is in all cases the dilation measured on the right side of the sample.

6.3.3 After Peak

After the peak strength of the material is overcome, the shear surface becomes a continuous and open discontinuity through the sample. The geometry of this surface is dependent upon the orientation of the planes of weakness within the sample. Figs. 6.12 and 6.13 show a representative sample from each test configuration after having been sheared. A, B, C, F, and G are seen to have a relatively planar shear surface. In all cases the planes of weakness are either horizontal or vertical. When the planes of weakness are vertical, no shear displacement can be mobilized along these planes. (Patton, 1966). When the planes of weakness are horizontal, they are in the direction of the applied shear load and thus shear will occur along these planes. Therefore, for all of the above mentioned test configurations with the exception of G, the shear will take place along the

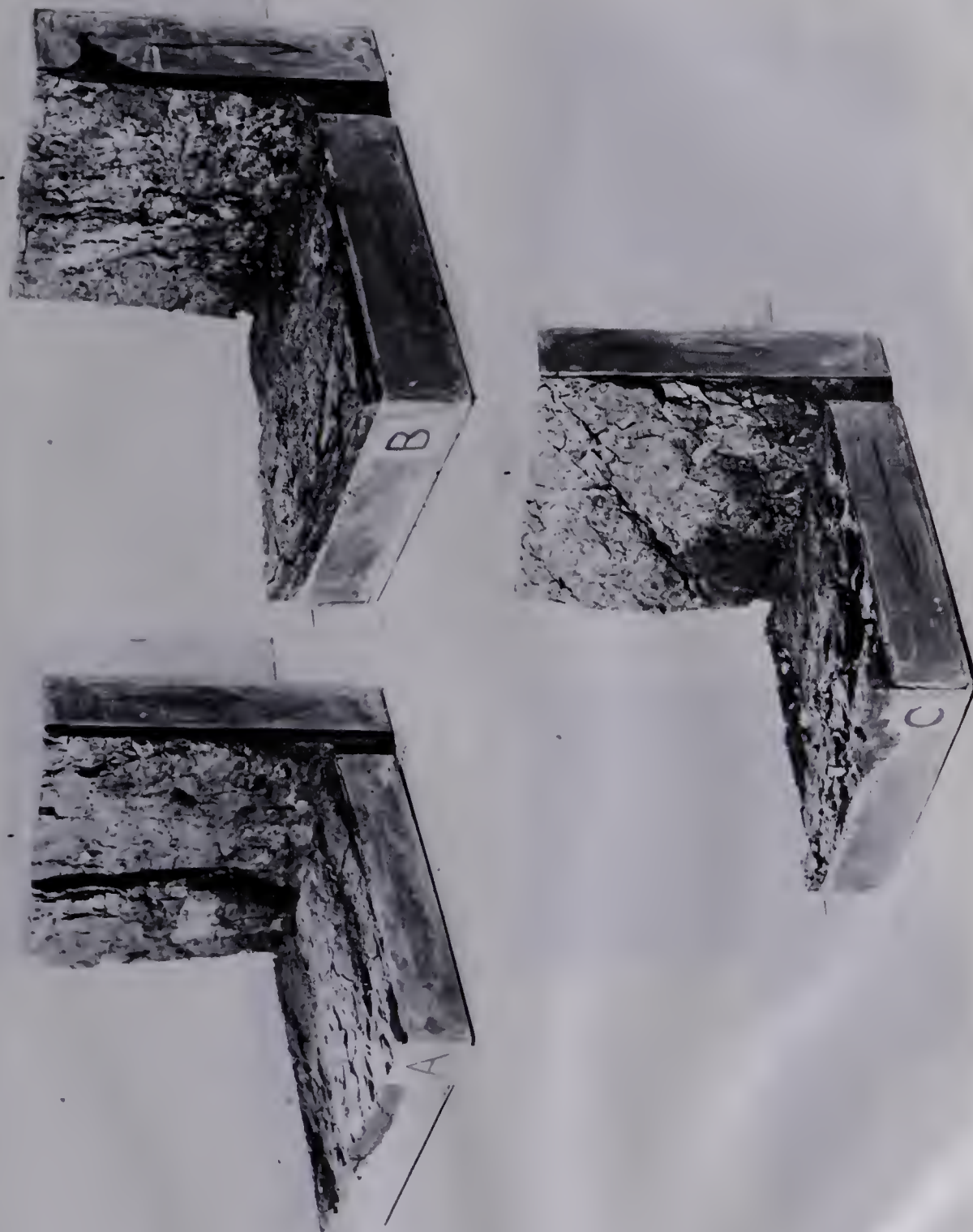


Fig. 6.12 Representative Samples from Category I After Testing

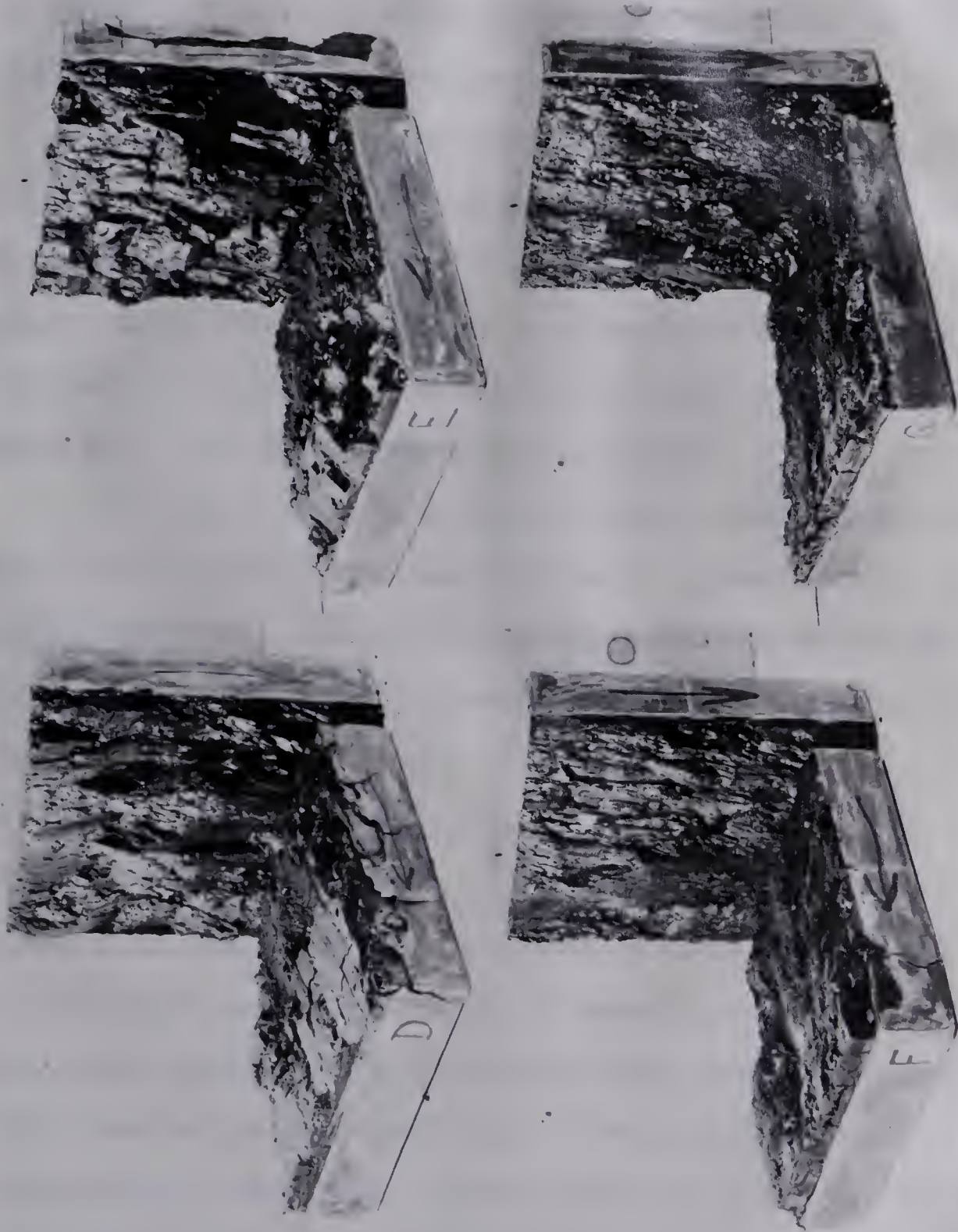


Fig. 6.13 Representative Samples from Category II After Testing

horizontal plane of weakness. In G, both planes of weakness are vertical. Shear will take place along a horizontal plane but in this case the horizontal plane does not constitute a plane of weakness.

Test configurations D and E have the joint planes at angles of 20° and 40° respectively to the direction of the applied shear load. The displacement may take place along these planes because $\phi_r + i$ is less than 90° (Patton, 1966). The bedding planes are vertical and thus no shear displacement will take place along these planes.

For each test sample, the shear load was recorded as the shear displacement was imposed. These graphs are given in Appendix A. The Mohr-Coulomb equation defining the failure criterion after peak may now be written as (Patton, 1966).

$$\tau = \sigma \tan(\phi_r + i) \quad . . . \quad (6.2)$$

where i is the inclination of the shear surface with respect to the direction of the applied shear load. Now, because the shear surface is a continuous and open discontinuity, the cohesion term is omitted. The normal stress, σ , is constant for each test and the shear stress, τ , is seen to vary with $\tan(\phi_r + i)$. Because ϕ_r is a constant for the material, the shear stress, then, varies with changes in i . From these tests, ϕ_r for the material can be obtained if some method of determining i is adopted.

The shear stress and normal stress at all values of shear displacement are known. The value of $\tan(\phi_r + i)$ and thus $\phi_r + i$ can be evaluated for any value of shear displacement. The values of $\phi_r + i$ are plotted on the figures in Appendix B for each test sample.

For all values of shear displacement, the vertical movement of the sample was measured at each corner of the loading cap. Thus, for any increment of shear displacement, dx , the corresponding increments of vertical movement, dy , are known. The values of dy/dx then give four $\tan i$ values from which four values of i can be determined. For example, in test E2 over the range of shear displacement from 0.63 inches to 0.80 inches the increment of shear displacement, dx , is 0.17 inches. The four increments of vertical dilation, dy , over this range of shear displacement are +0.061, -0.046, +0.095, and +0.136 inches resulting in four i values of $+2.2^\circ$, -15.1° , $+29.2^\circ$, and $+38.7^\circ$. These values of i are shown on the figures in Appendix B for each test. The value of ϕ_r as determined from the tests on samples with pre-cut shear planes is also plotted on each of the figures in Appendix B. Given this data, it remains to compare the theoretical relationship of $\phi_r + i$ with the independently determined parameters ϕ_r and i .

The maximum, minimum, and average values of i recorded at a specified shear displacement were subtracted from the value of $\phi_r + i$ recorded at that specified shear displacement.

The results are shown on the figures in Appendix B for each test sample.

According to Patton, the maximum value of i should govern the behaviour of the test sample. When this value of i is subtracted from $\phi_r + i$, the resulting ϕ_r value should lie on the ϕ_r line determined independently. An investigation of the results show that this is not generally the case. Neither the average nor the minimum values of i when subtracted from $\phi_r + i$ give a resulting ϕ_r value corresponding to the independently determined value of ϕ_r . In general, however, the correlation is much better for test configurations A, B, C, G, and F where the shear surface is relatively planar. No fault lies with Patton's theory, so the question then arises: is the calculated i the controlling value for the sample at that point in time?

In Patton's laboratory study, he dealt with artificially prepared samples having rigidly controlled geometry along the shear surface. The samples in this study consisted of a natural rock material taken through peak and thus no rigid control was imposed on the formation of the shear surface. Because the two halves of the sample are rigid bodies moving over each other on an irregular surface, the values of i calculated at the corners of the sample need not be the i that is being mobilized within the sample. The two halves of the sample at one corner that registers the maximum value of i may, in fact, not be in contact at the shear

surface. Because of the irregularities on the shear surface, some rotation of the upper rigid body about these irregularities would be expected (Goodman, 1970), and the calculated i would reflect this rotation. If there was no rotation of the upper half of the sample, the vertical dilation measured at each corner of the load cap would be the same at any point in time. The vertical dilations shown on the figures in Appendix A indicate that this is not the case and, in fact, the upper half of the sample is rotating. This rotation is more pronounced on test configurations D and E because they have the most irregular shear surfaces. Better results are obtained for the remainder of the test configurations where the shear surfaces are relatively planar.

At the completion of shear displacement, the values of $\phi_r + i$ obtained in test configuration D and E are seen to be consistently higher than the value of ϕ_r determined independently even though the value of i is small. This indicates the possibility of buttressing and interlock of the irregularities during shear displacement. This is reflected by an increase in the friction angle with no increase in i . When buttressing or interlock takes place, the mobilized ϕ increases to overcome the resistance. For test configurations A, B, C, F, and G, there is less possibility of buttressing and interlock. Again the value of i is small at the completion of shear displacement but the value of $\phi_r + i$ is seen to be closer to the ϕ_r line. Occasionally the value of $\phi_r + i$ is

seen to fall below the ϕ_r line. This can be explained by the presence of gouge or rounded particles on the shear surface (Patton, 1966), or by the rotation of individual blocks of coal at the shear surface. (Ladanyi, 1972).

The value of i is seen generally to decrease with an increase in normal stress for all the test configurations. No significant changes in $\phi_r + i$ are recorded for this increase in normal stress. This suggests that the increase in normal stress serves to decrease the amount of rotation of the upper half of the sample which is reflected by a decrease in i .

CHAPTER VII

CONCLUSIONS

On the basis of the investigation undertaken, it is concluded that:

1. A satisfactory method of field sampling and laboratory preparation has been achieved to obtain fractured rock samples for testing in direct shear.
2. A testing apparatus has been assembled that enables the maximum compilation of experimental data from direct shear tests.
3. The shear strength of fractured rock is anisotropic and dependent upon the orientation of discontinuities within the sample. The shear strength parameters ϕ and c are affected in different ways.

(a) When a continuously open discontinuity is present at the shear surface, the cohesion intercept, c , is zero and ϕ depends upon the frictional sliding resistance of the material, ϕ_r , and the inclination of the shear surface, i , to the direction of the applied shear load. ϕ_r for the coal tested is 30° .

(b) When discontinuities are present that are not continuously open at the shear surface:

- (i) ϕ is dependent only upon the peak shearing resistance presented by the unfractured material. ϕ has a smaller value when shear takes place along discontinuities (bedding planes) within the unfractured material (about 41° for the coal tested) and larger values when shear takes place with the discontinuities within the unfractured material vertical and oriented in the direction of the applied shear load, (about 66° for the coal tested).
- (ii) The cohesion intercept, c , reflects the degree of continuity of the fractures at the zone of shear within the sample and increases or decreases with a corresponding increase or decrease in the continuity. The cohesion intercept, c , varied between 17 psi and 76 psi for the coal tested.

4. A method for determining Young's Modulus from direct shear tests has been developed and applied successfully. E increases with an increase in normal stress. When a continuously open discontinuity is present at the shear surface, the material is no longer an elastic continuum and quoting values of E may be erroneous. E increases or decreases with a corresponding increase or decrease in ϕ . The average E for the coal tested was in the range of 50×10^3 psi and varied about 20×10^3 psi over the normal stress range of 20 psi

to 100 psi.

5. The combination of very irregular geometry at the shear surface on a small scale rendered the measuring system incapable of accurately recording the i value mobilized during shear.

6. Very little movement occurs along discontinuities prior to peak when the discontinuities are not continuously open.

7. Theories governing the peak strength derived from models with continuously open discontinuities can only be applied to a natural rock mass when the discontinuities within the rock mass are continuously open and their geometry can be completely specified.

Theories governing the peak strength derived from models with discontinuities that are not continuously open can only be applied to a natural rock mass when the discontinuities within the rock mass are not continuously open and the degree of continuity of the discontinuities can be completely specified.

LIST OF REFERENCES

LIST OF REFERENCES

- Bieniawski, Z.T., 1968, "In Situ Strength and Deformation Characteristics of Coal", Engineering Geology, Vol.2, No. 5, pp. 325 - 340.
- Donath, F.A., 1961, "Experimental Study of Shear Failure in Anisotropic Rocks", Geological Society of America Bulletin, Vol.72. pp. 985 - 990.
- Goodman, R.E., Van, T.K., Heuze, F.E., 1968, "The Measurement of Rock Deformability in Bore Holes", 10th Symposium on Rock Mechanics, University of Texas, Austin, Texas.
- Goodman, R.E., 1970, "The Deformability of Joints", Determination of the In Situ Modulus of Deformation of Rock, ASTM STP 477, American Society for Testing and Materials, pp. 174 - 196.
- Hobbs, D.W., 1964, "The Strngth and Stress-Strain Characteristics of Coal in Triaxial Compression", Journal of Geology, Vol.72, No.2, pp. 214 - 231.
- Jennings, J.E., 1971, "An Approach to the Stability of Rock Slopes Based on the Theory of Limiting Equilibrium with a Material Exhibiting Anisotropic Shear Strength", Notes Presented at a Course on the Analysis and Design of Rock Slopes, University of Alberta, Edmonton, Alberta.
- Ladanyi, B., Archambault, G., 1970, "Simulation of Shear Behaviour of a Jointed Rock Mass", 11th Symposium on Rock Mechanics, University of California, Berkeley, California, pp. 105 - 125.
- Ladanyi, B., Archambault, G., 1972, "Évaluation de la Résistance au Cisaillement d'un Massif Rocheux Fragmenté," Préparé pour présentation au 24^e Congrès Géologique International, Montreal.
- Lambe, T.W., 1967, Soil Testing for Engineers, John Wiley & Sons, Inc., New York, pp. 15-21.
- Latjai, E.Z., 1969, "Shear Strength of Weakness Planes in Rock", International Journal of Rock Mechanics and Mining Sciences, Vol.6, No.5, pp. 499 - 515.

- Noonan, D.K.J., Nixon, J.F., 1972, "Evaluation of Young's Modulus from Direct Shear Tests", (in preparation).
- Patton, F.D., 1966, "Multiple Modes of Shear Failure in Rock and Related Materials", PhD Thesis, University of Illinois, Urbana, Illinois.
- Pearson, G.R., 1959, "Coal Reserves for Strip Mining, Wabamun Lake District Alberta", Research Council of Alberta, Geological Division, Preliminary Report 59 - 1.
- Piteau, D.R., 1970, "Geological Factors Significant to the Stability of Slopes Cut in Rock", Proceedings of the Symposium on the Theoretical Background to the Planning of Open Pit Mines with Special Reference to Slope Stability, Johannesburg, Republic of South Africa, pp. 33 - 53.
- Ward, W.H., Burland, J.B., 1968, "Assessment of the Deformation Properties of Jointed Rock in the Mass", Proceedings of the International Symposium on Rock Mechanics, Madrid, pp. 35 - 44.
- Wilson, E.L., 1963, "Finite Element Analysis of Two-Dimensional Structures", SESM Report No.63 - 2, University of California, Berkeley.

Appendix A

EXPERIMENTAL SHEAR LOAD VERSUS SHEAR DISPLACEMENT GRAPHS

APPENDIX A

EXPLANATORY NOTES

The shear load versus shear displacement curves from all the tests on intact samples are given in this appendix. The following notes are included to assist in the interpretation of the results.

1. The shear load was applied and the vertical dilation measured by LVDT's at the corners of the sample as shown in Fig. A.1. The LVDT numbers correspond to the channels on the Hewlett-Packard digital recorder.

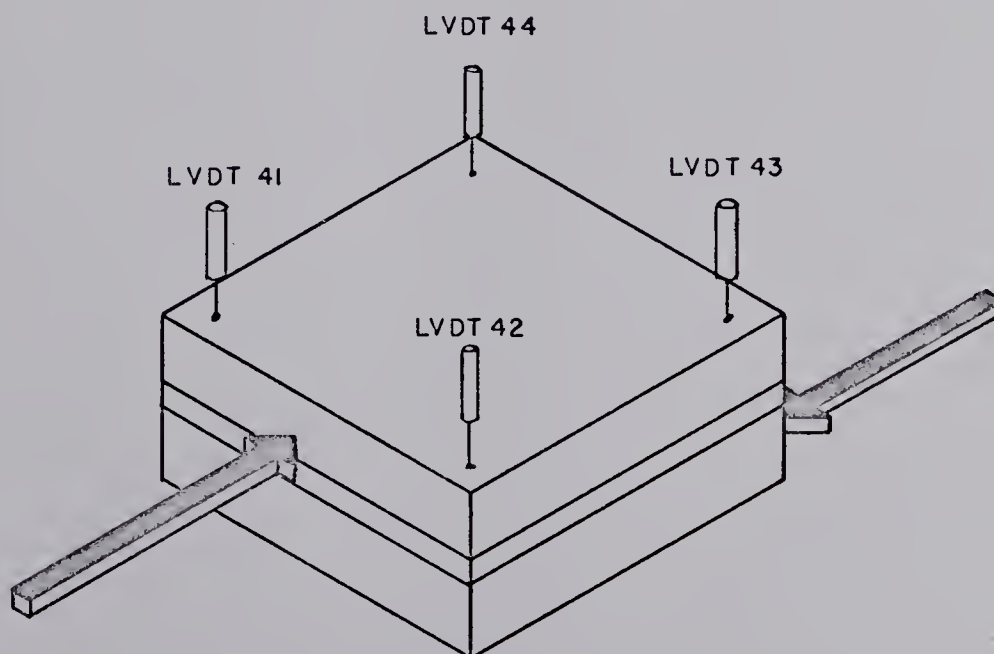


Fig. A.1 Vertical Dilation Measuring Device.

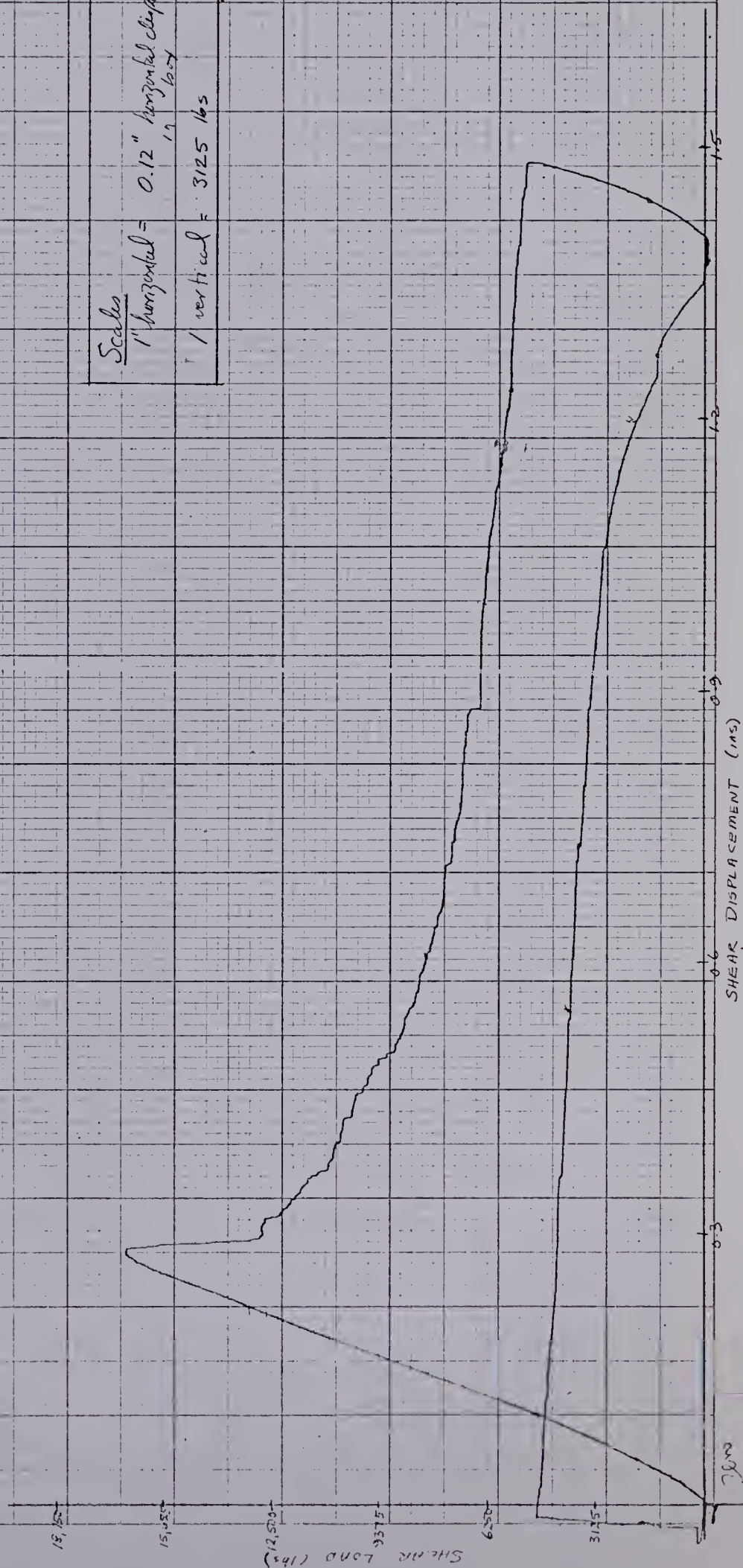
2. Because the exact shear load was not known before the tests were run, occasionally it was found necessary to change the attenuation (i.e. scale) on the X-Y recorder. Thus, some graphs show two curves before peak. The scale as shown corresponds in all cases to the curve that contains the peak point.

p. A-1

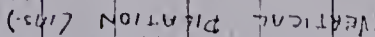
SAMPLE A1

Shear Rate = 0.03 in/min
Area of shear Plane = 138.4 in²
Normal Stress = 520 psi

Scales
1" horizontal = 0.12" horizontal displacement
1" vertical = 3125 lbs



NOTE THIS SAMPLE WAS
BADLY FRACTURED
BEFORE SHEAR

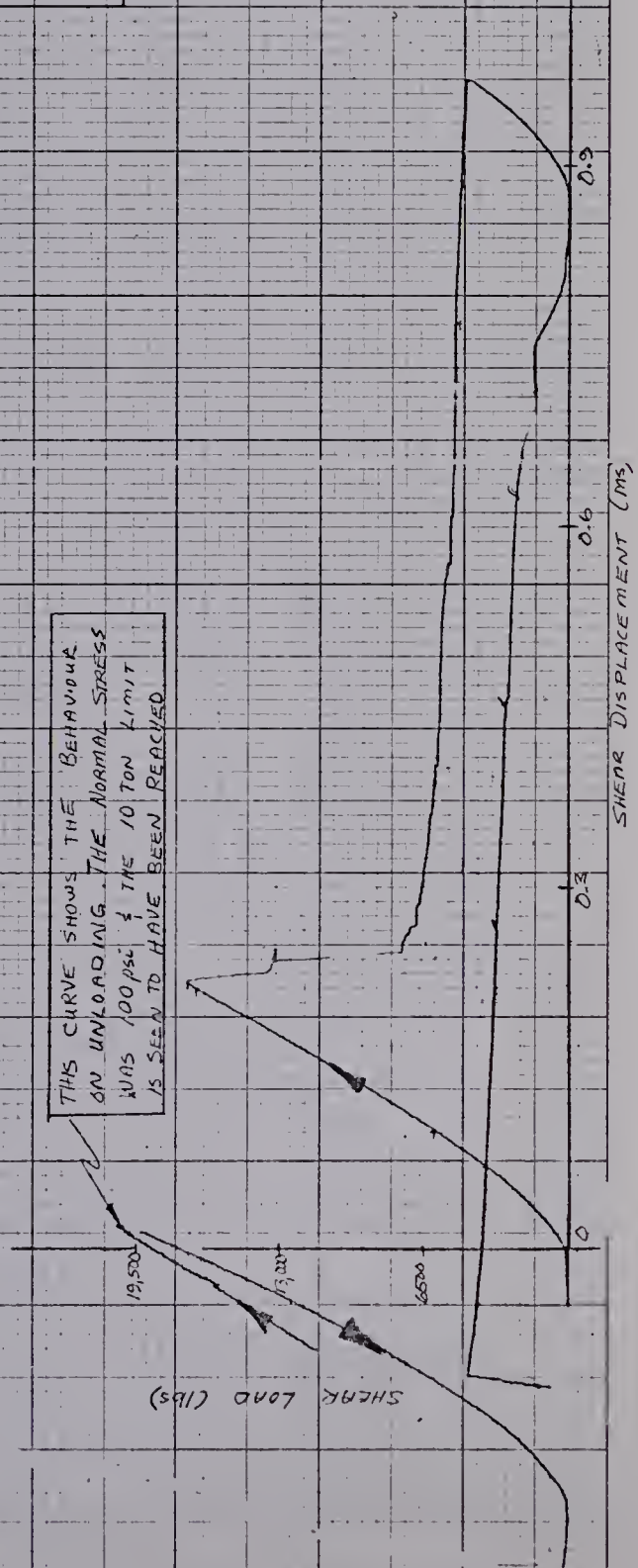


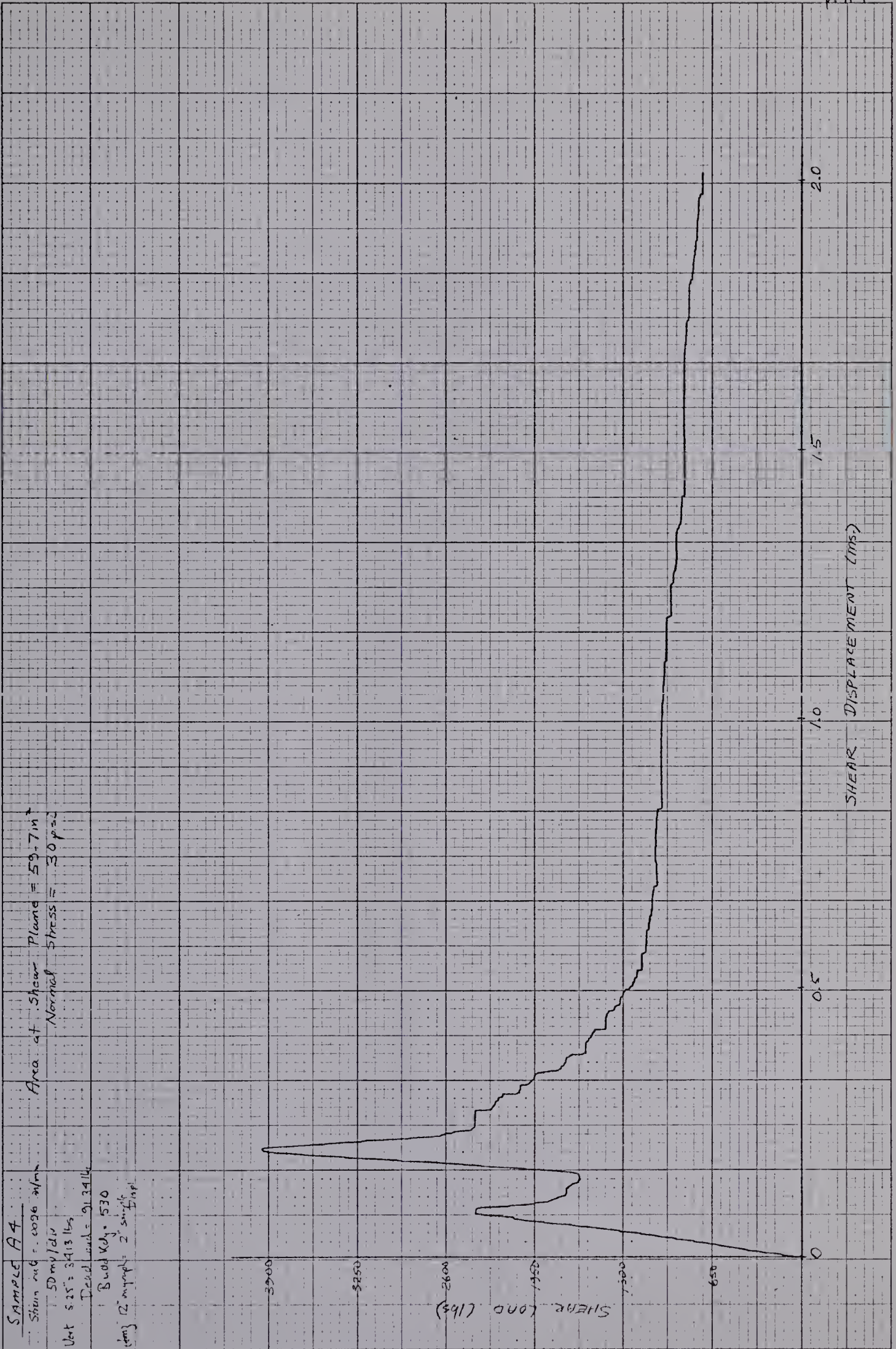
SAMPLE A3

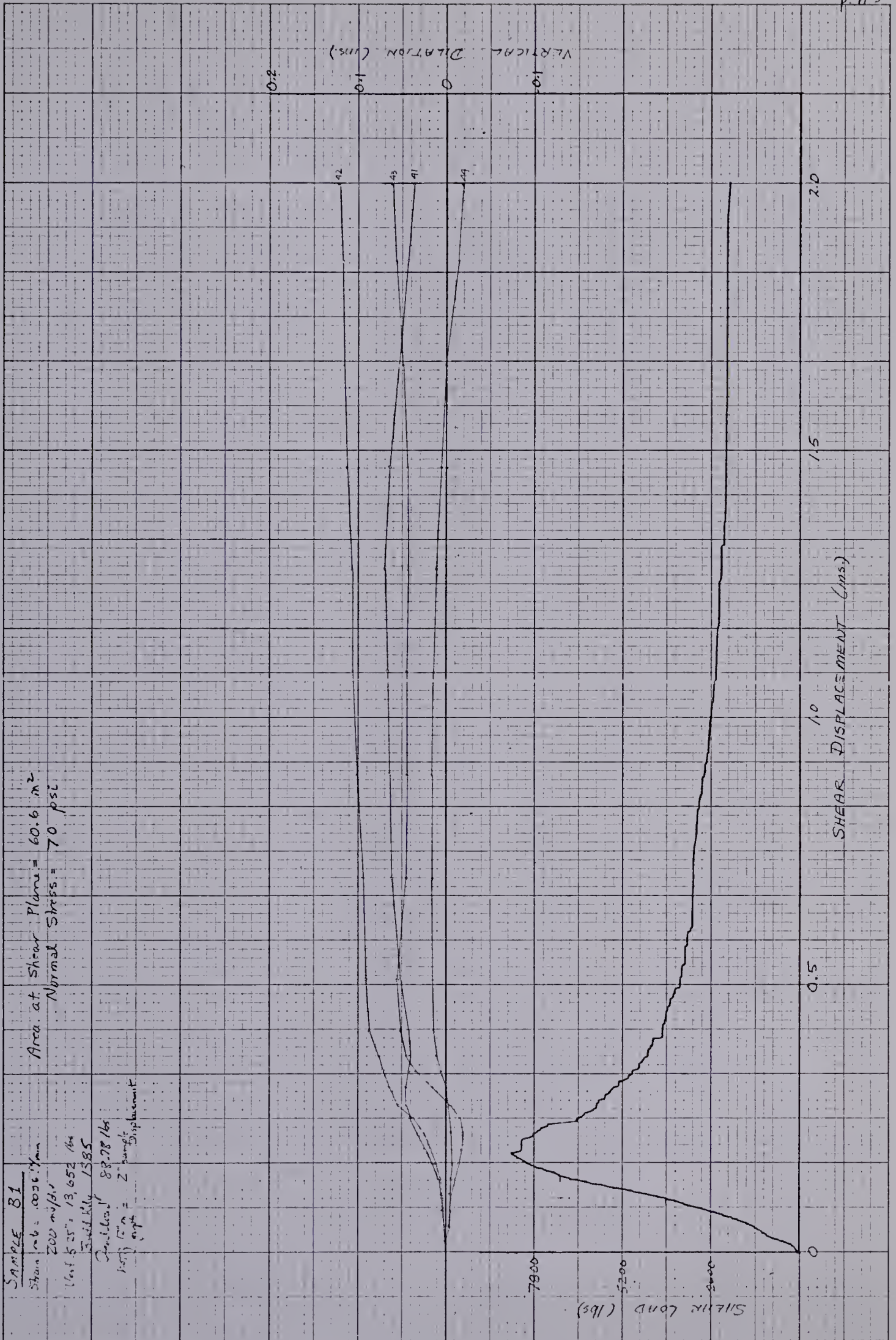
Strain Rate = 0.03 in/min
at Shear Plane = 138.9 in²
Normal Stress = 51.8 psi

Scales
1" horizontal = 0.12" horizontal displacement in box
1" vertical = 6500 lbs

THIS CURVE SHOWS THE BEHAVIOUR ON UNLOADING THE NORMAL STRESS WAS 100 psi & THE 10 TON LIMIT IS SEEN TO HAVE BEEN REACHED







SAMPLE B2

Strain rate = .005"/min
 100 mV/div
 Unit 525, 6826 lbs
 Bolt 1/2" - 5/16"
 Bolt Load 87.00 Ks
 Displacement 2" sample

Area of Shear Plane = 60.6 in²
 Normal Stress = 30 psi

VERTICAL
 DIRECTION (in.)

0
 1.0
 2.0

1.0
 2.0
 3.0

2.0

1.5

1.0

0.5

0

SHEAR DISPLACEMENT (in)

SHEAR LOAD (lbs)

3000

2000

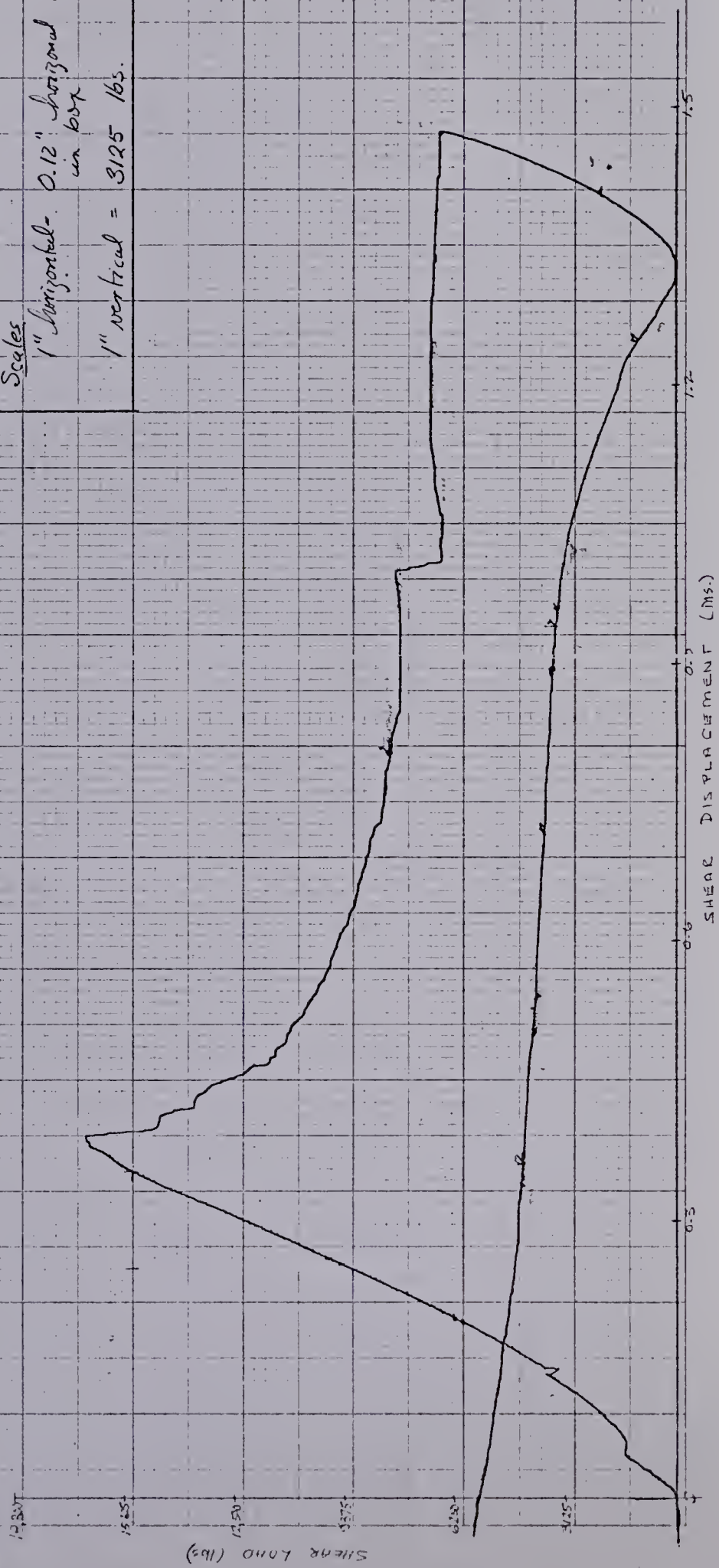
1000

0

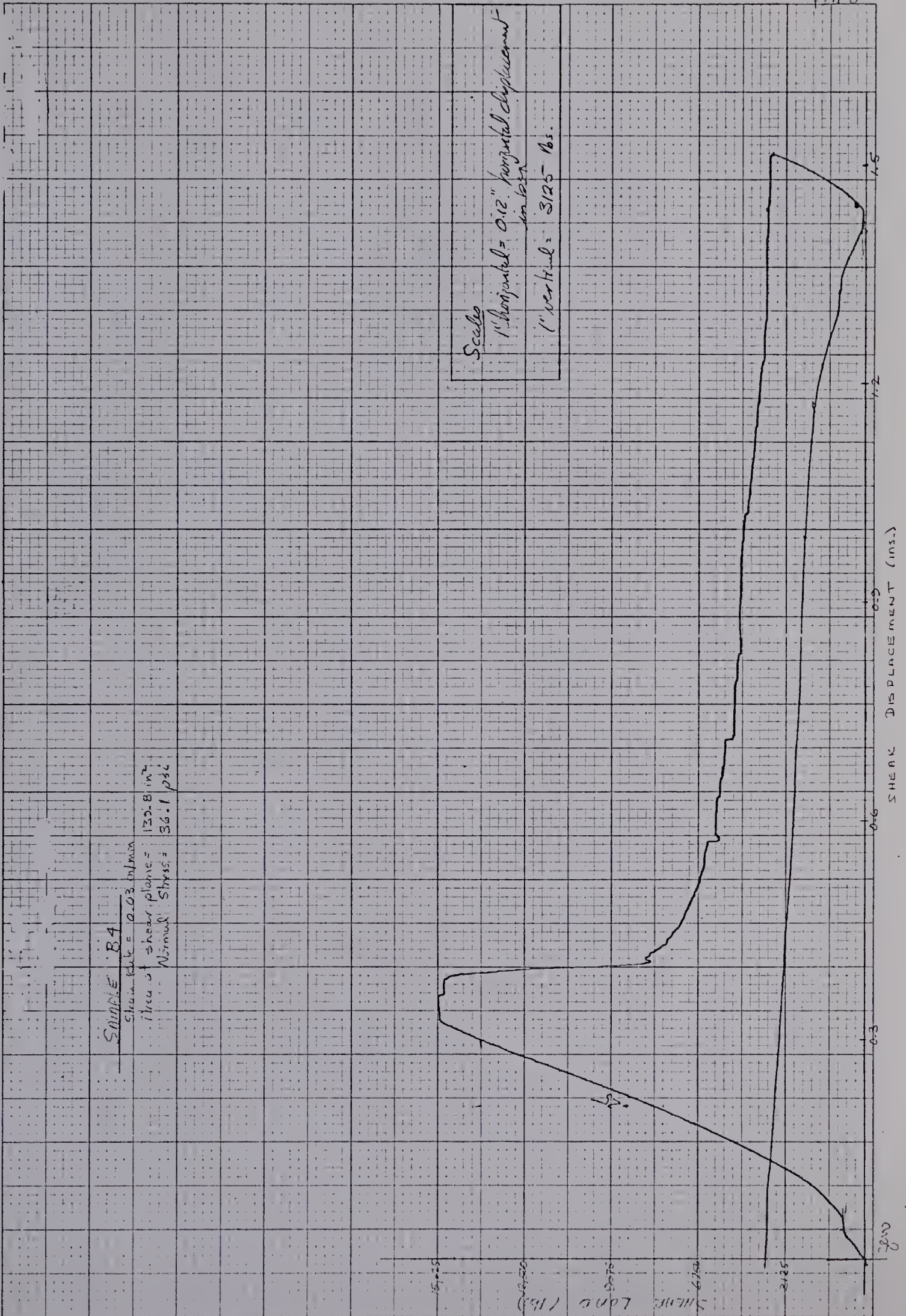
SAMPLE B3

Strain Rate = 0.03 in/min
Area at Shear Plane = 133.4 in²
Normal stress = 51.6 psi

Scales
1" horizontal = 0.12" horizontal displacement
in box
1" vertical = 3125 lbs.



P. A-3

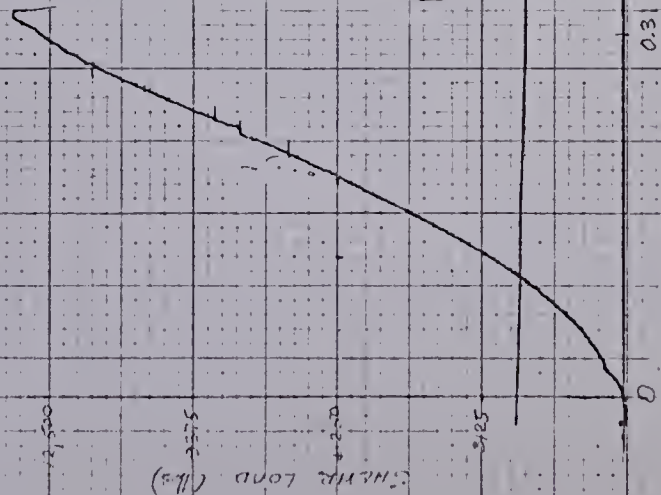


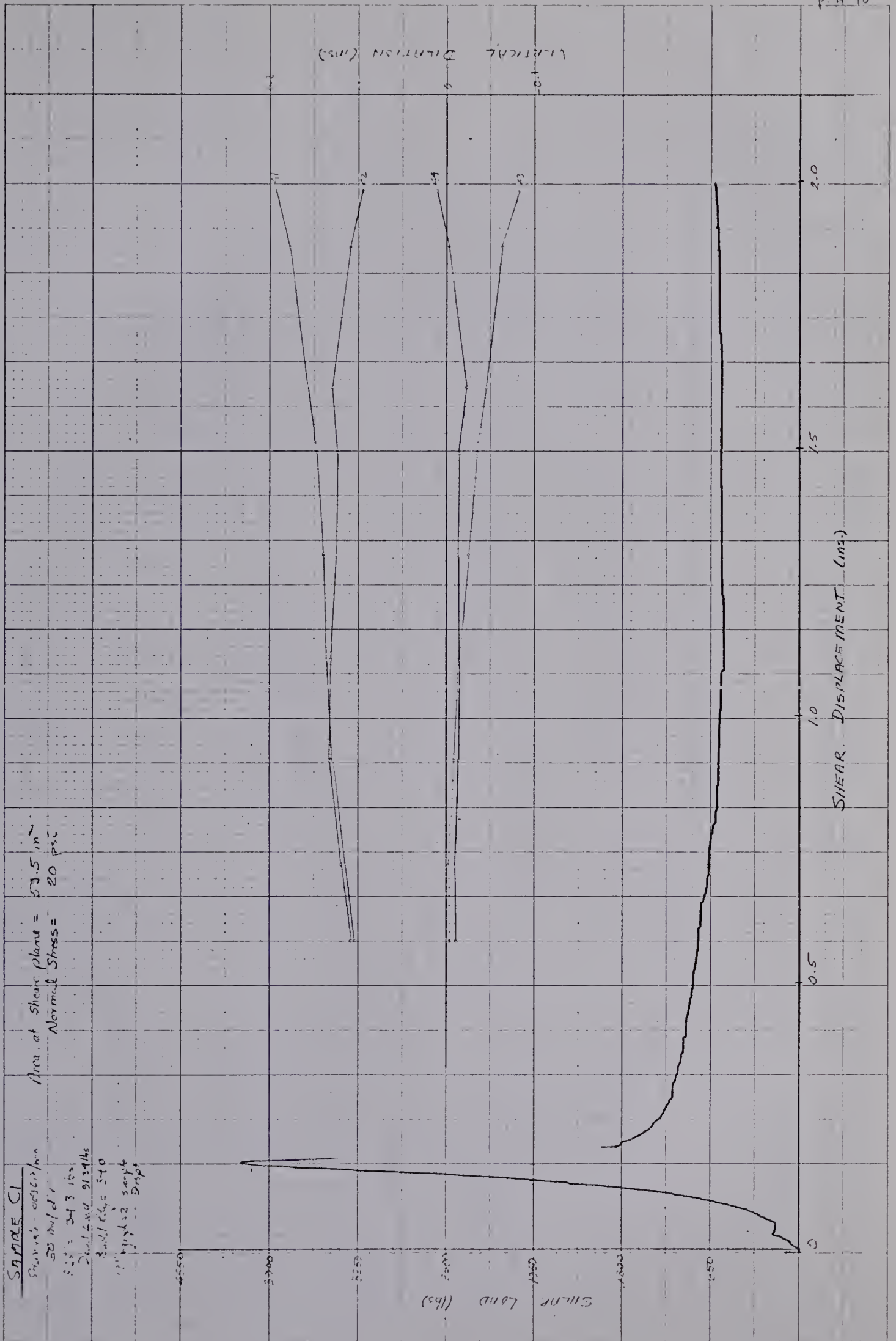
SAMPLE B5

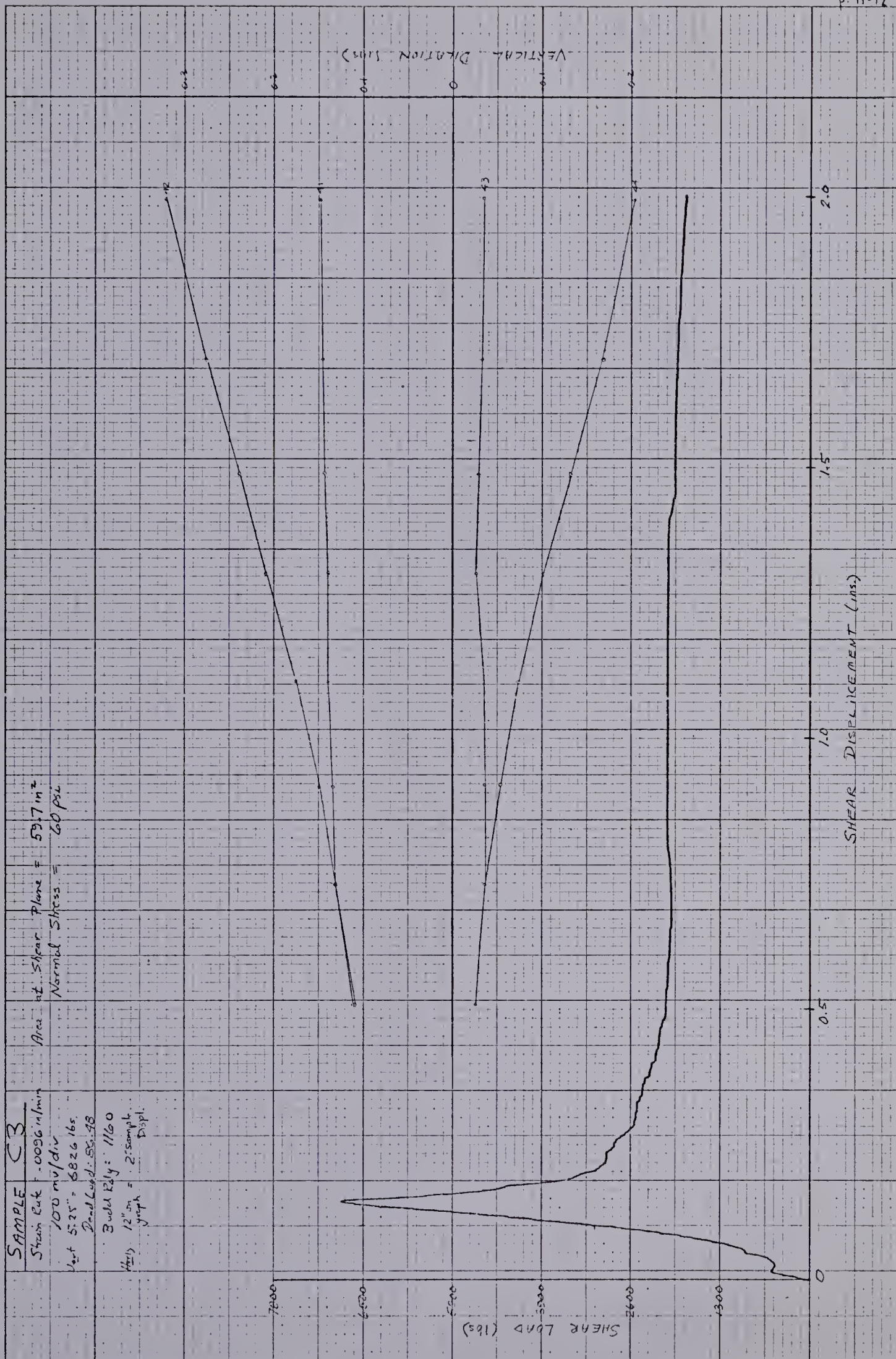
Strain Rate = 0.03 in/min.
Area of Shear Plane = 139.8 in²
Normal Stress = 20.6 psi

Scale

1" horizontal = 0.12 horiz. displ. in box
1" vertical = 3125 lbs.

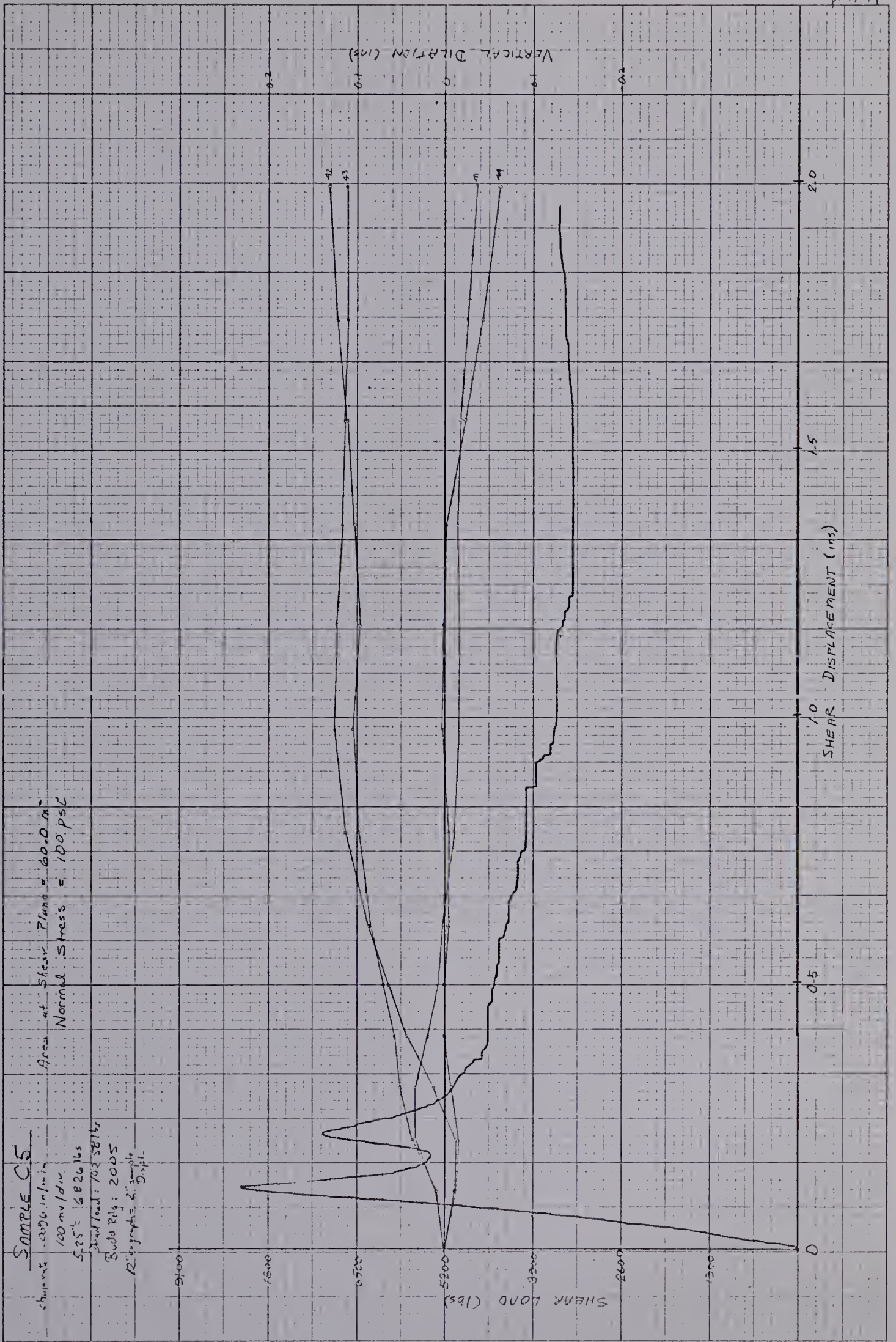


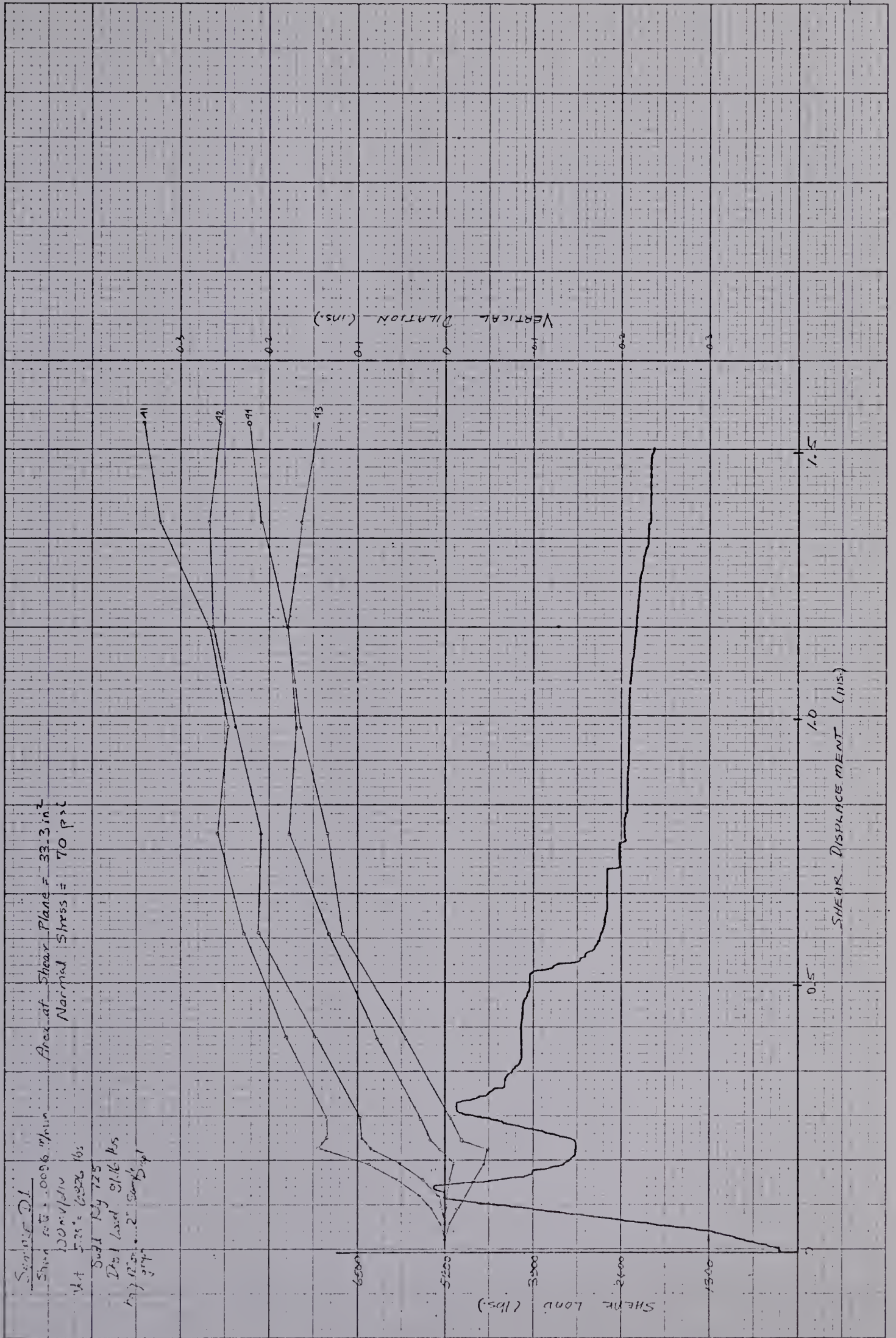


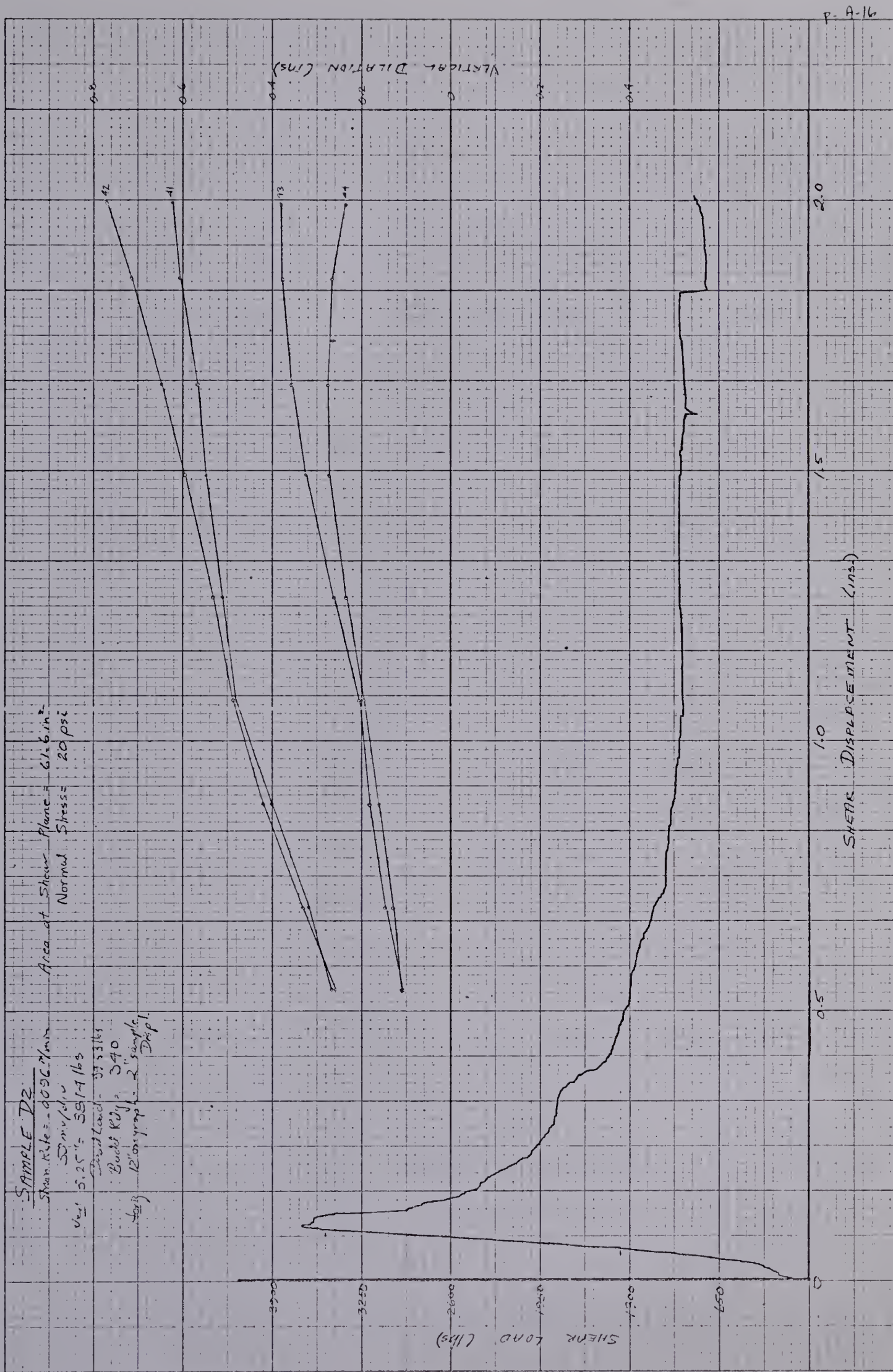


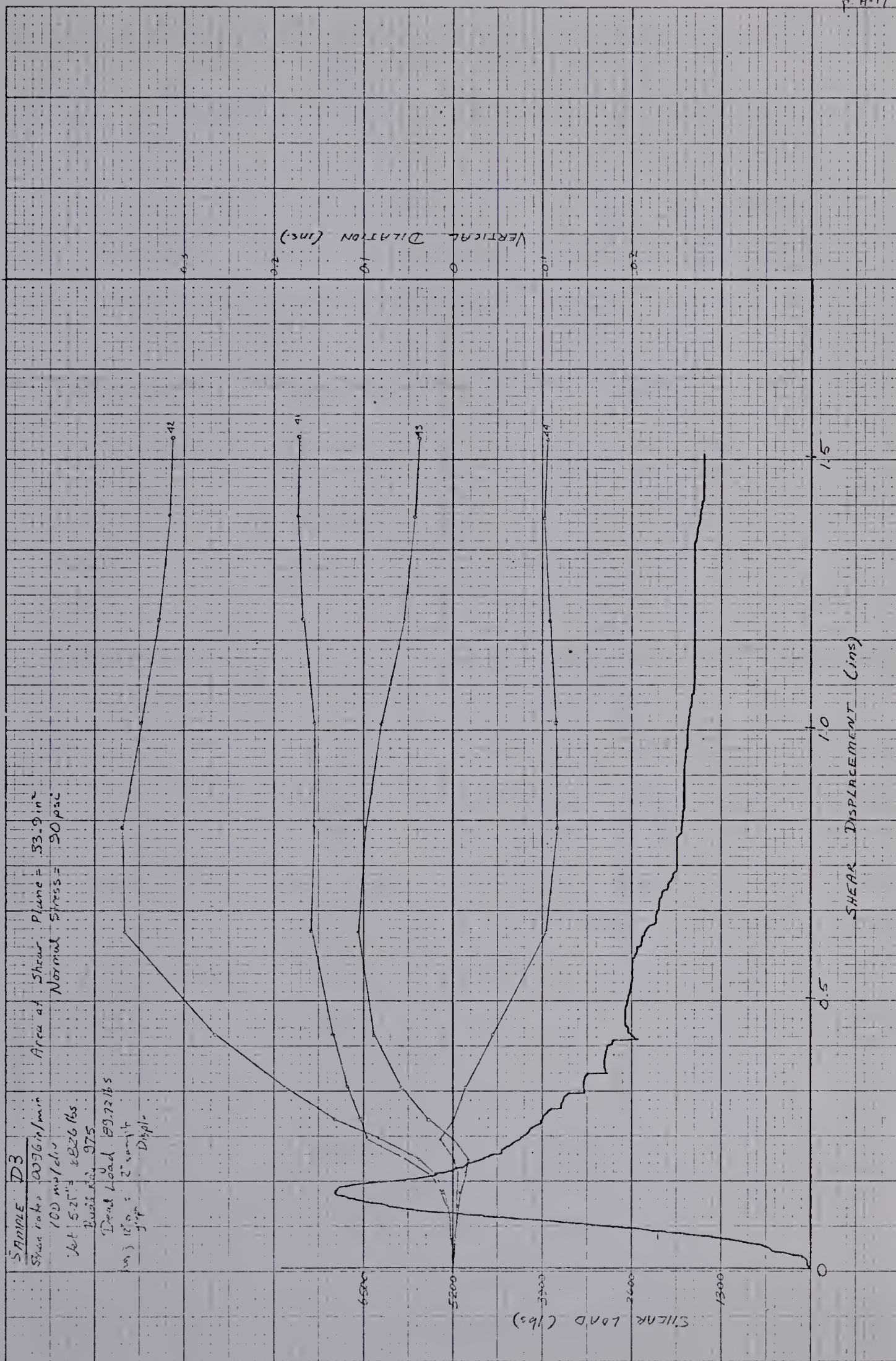
SAMPLE C3
 Strain Rate: 0.0096 in/min
 100 mv/div
 Vert 5:25" = 6826 lbs.
 Dead Load: 55.48
 Buckle Rly: 1160
 After 12" = 2" sample
 graph = Displ.

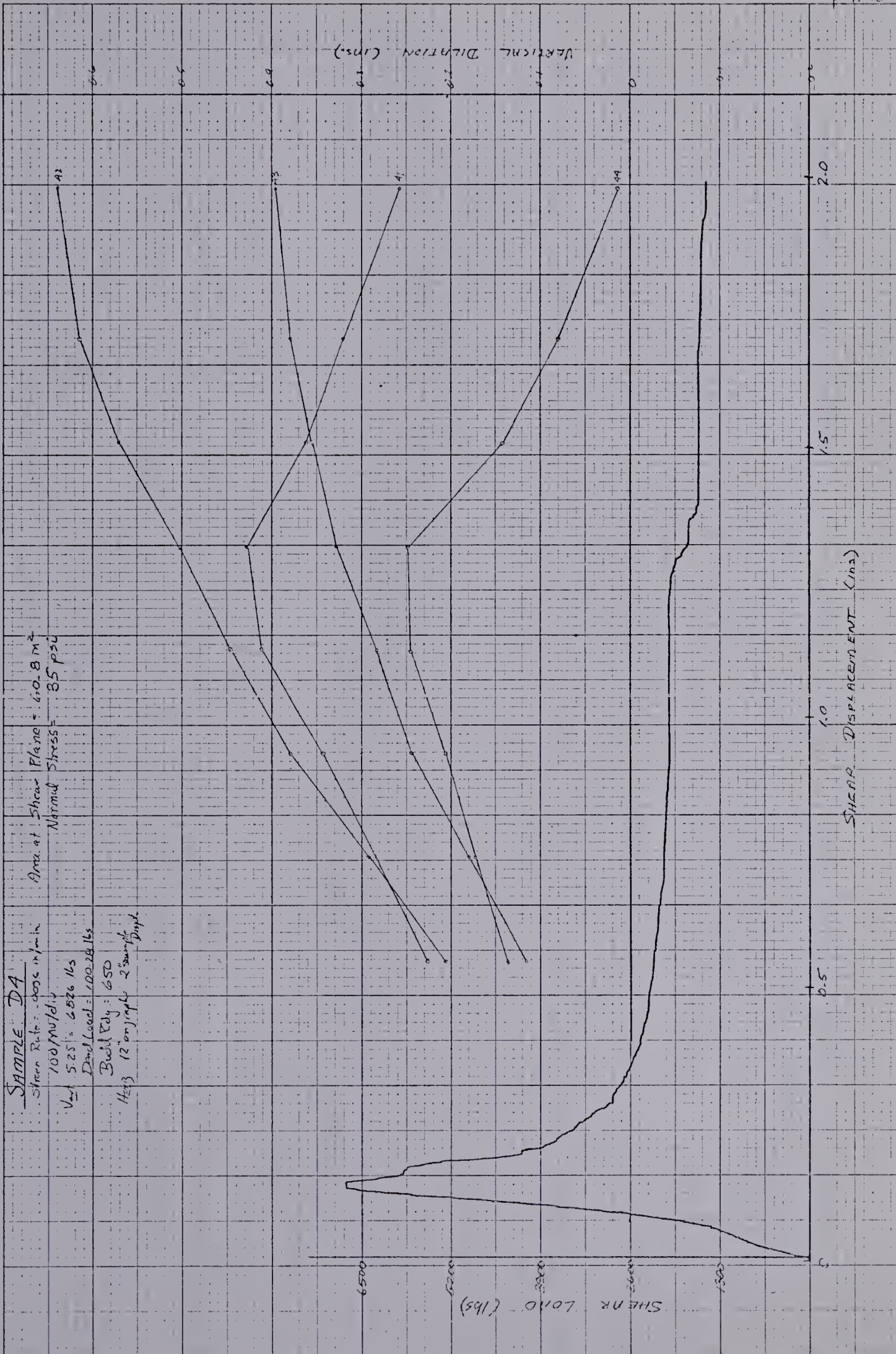
Area of Shear Plane = 59.7 in²
 Normal Stress = 60 psi

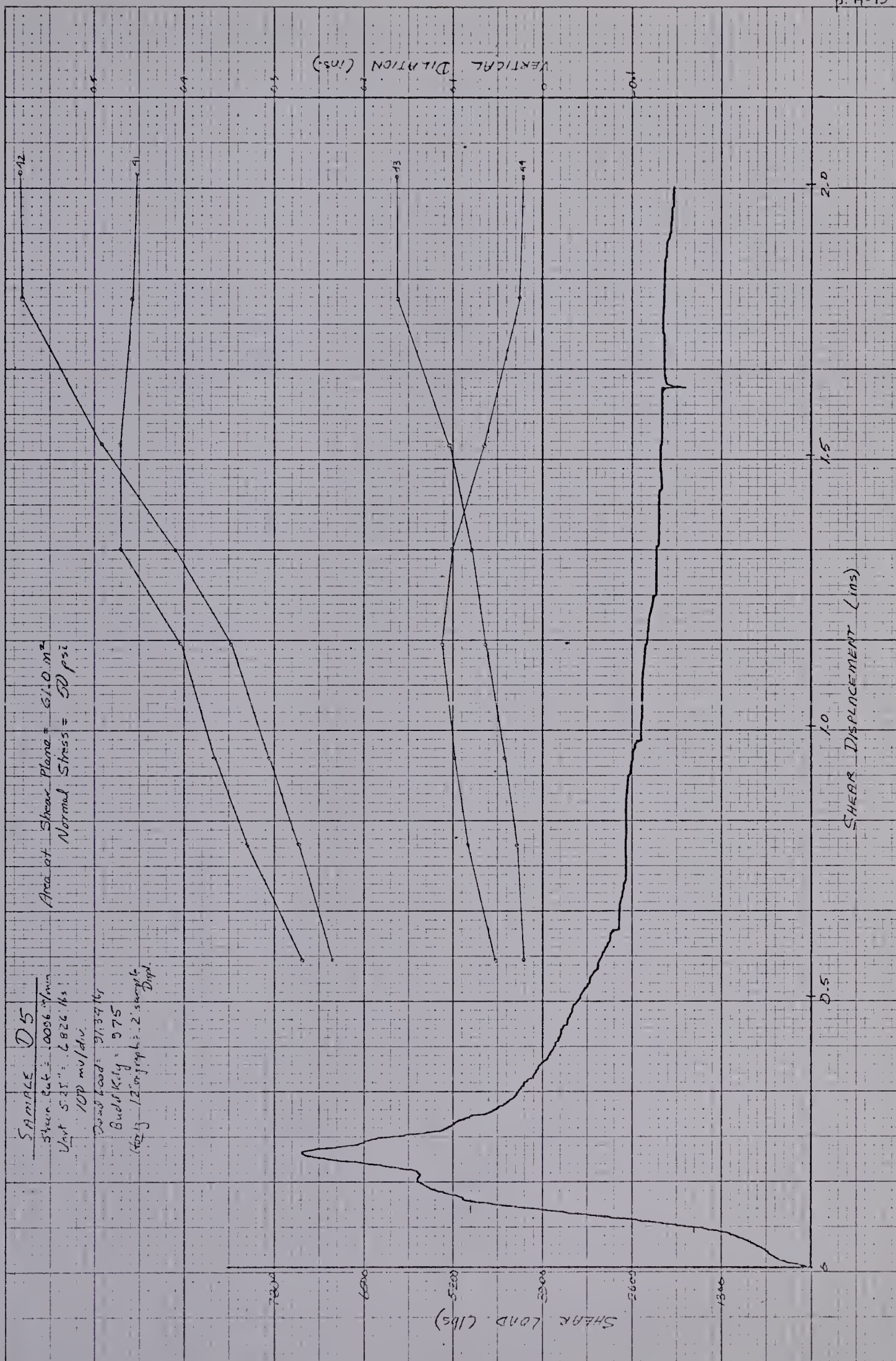


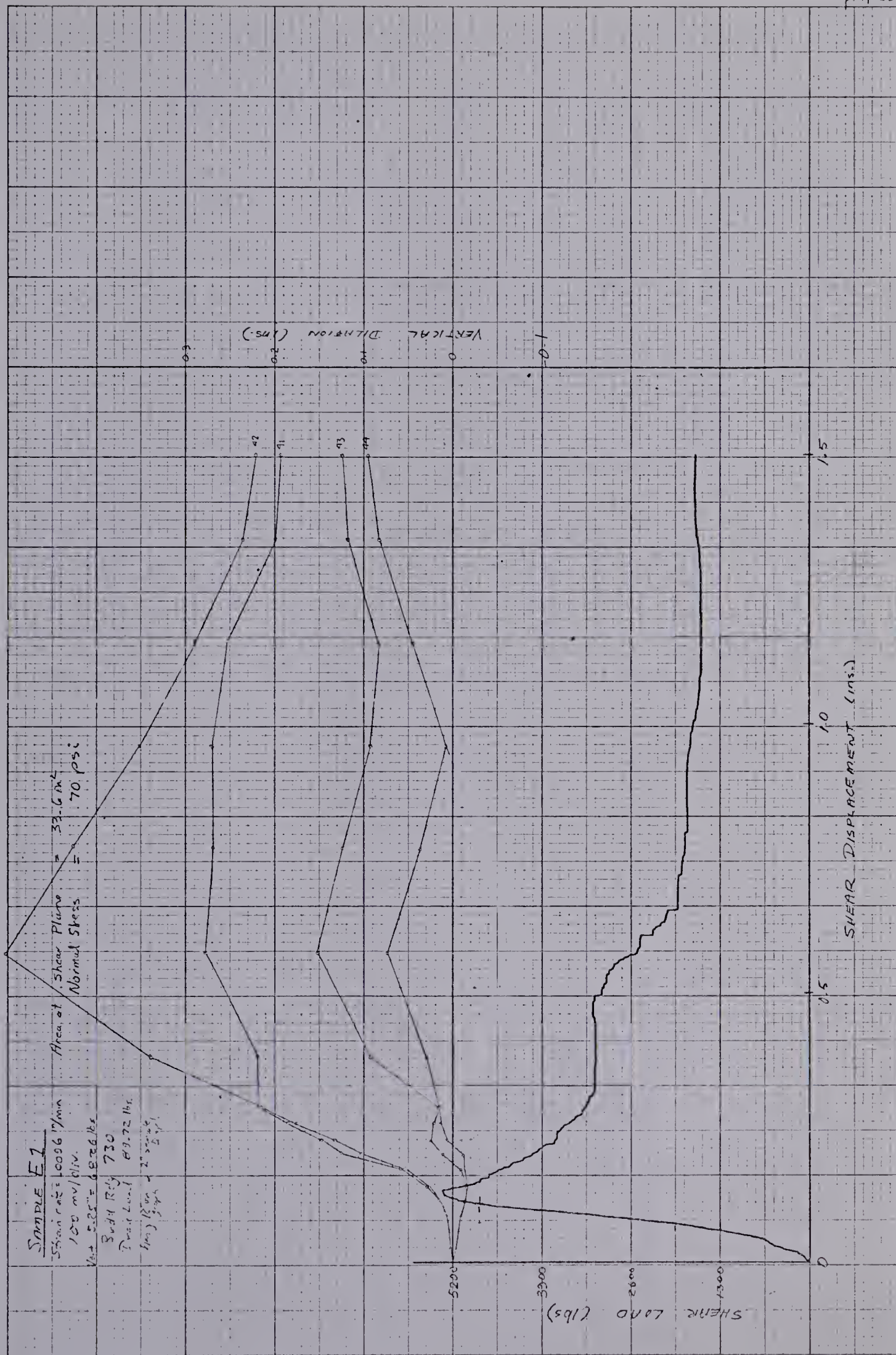


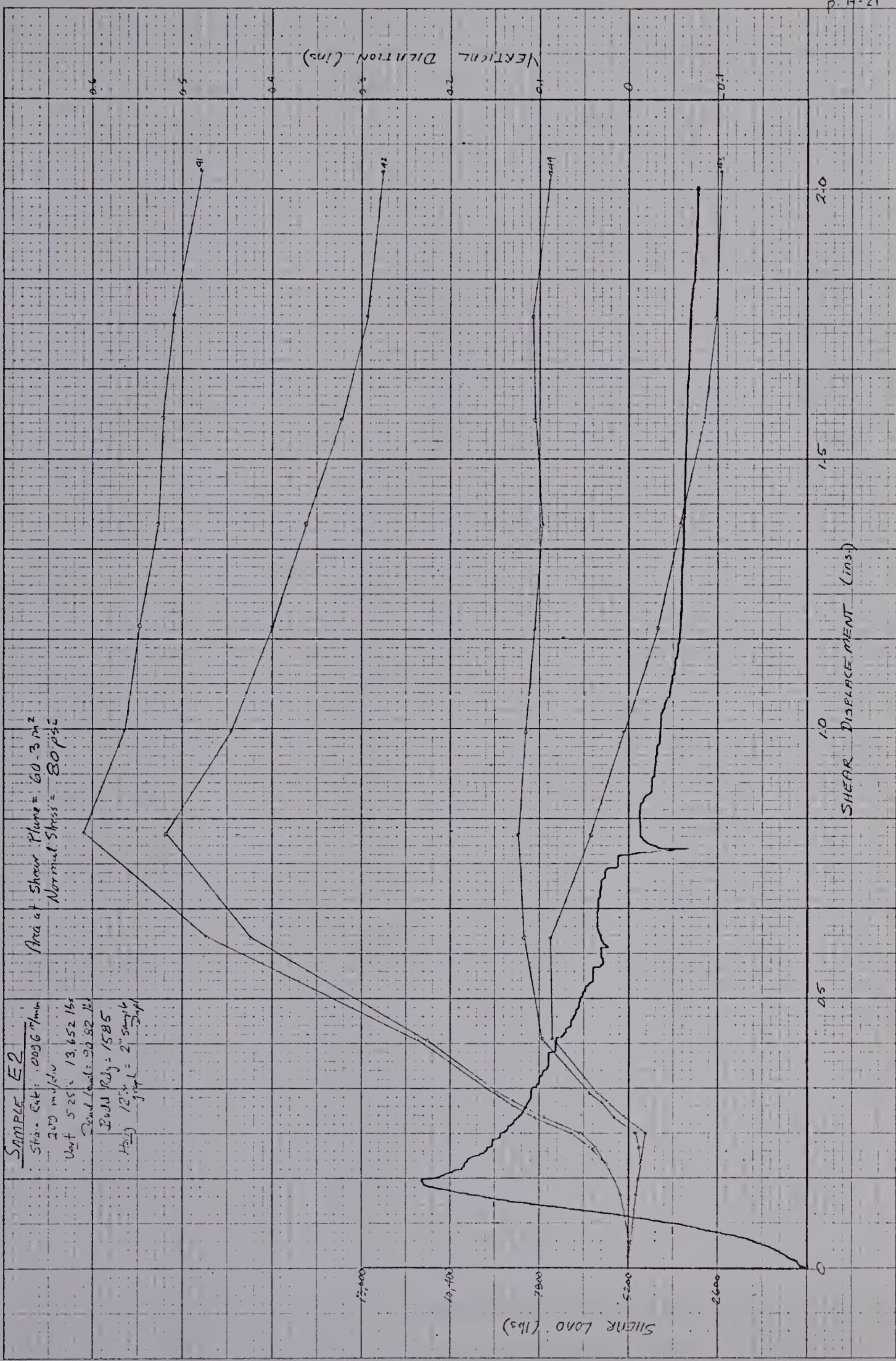




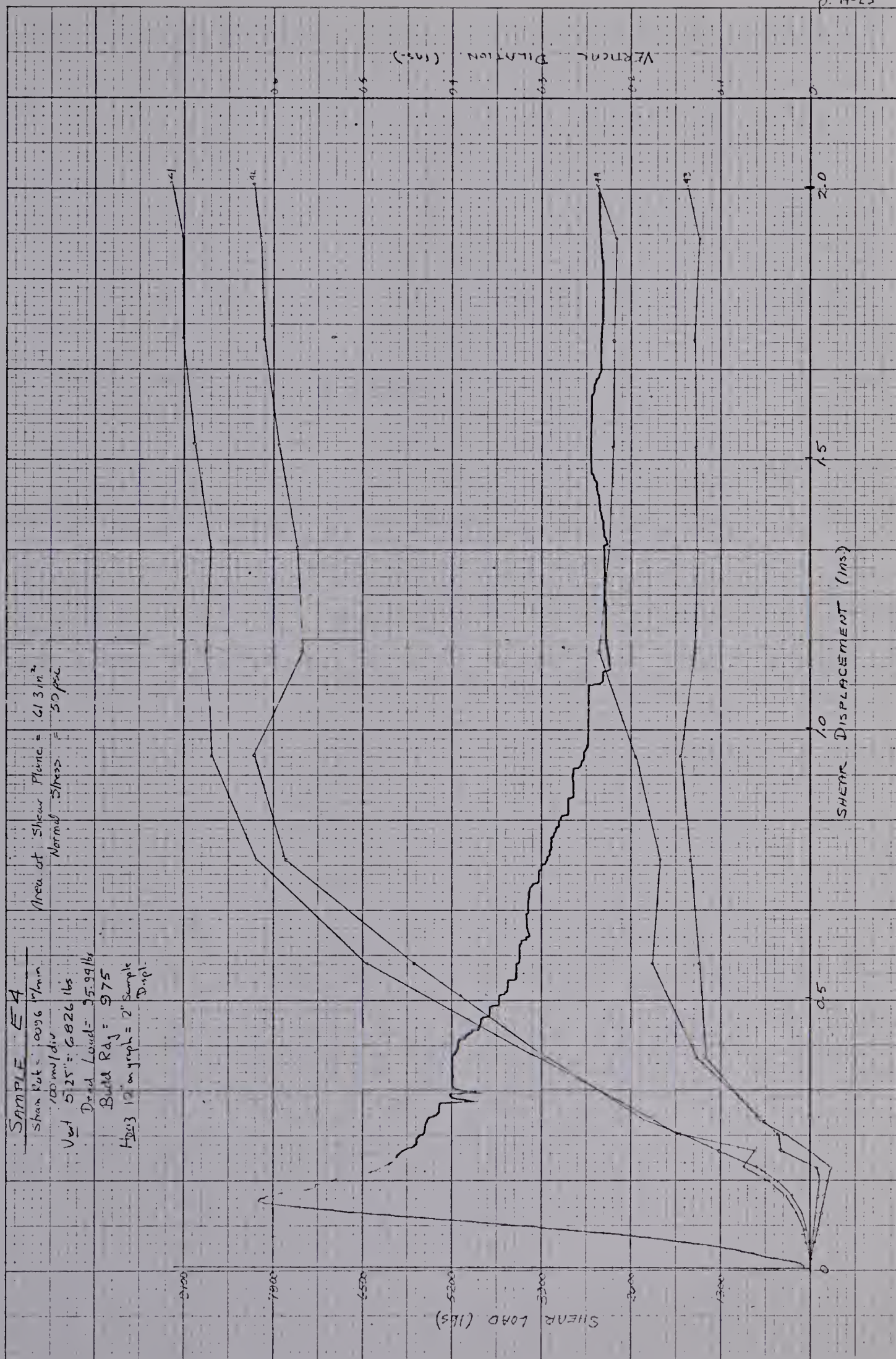


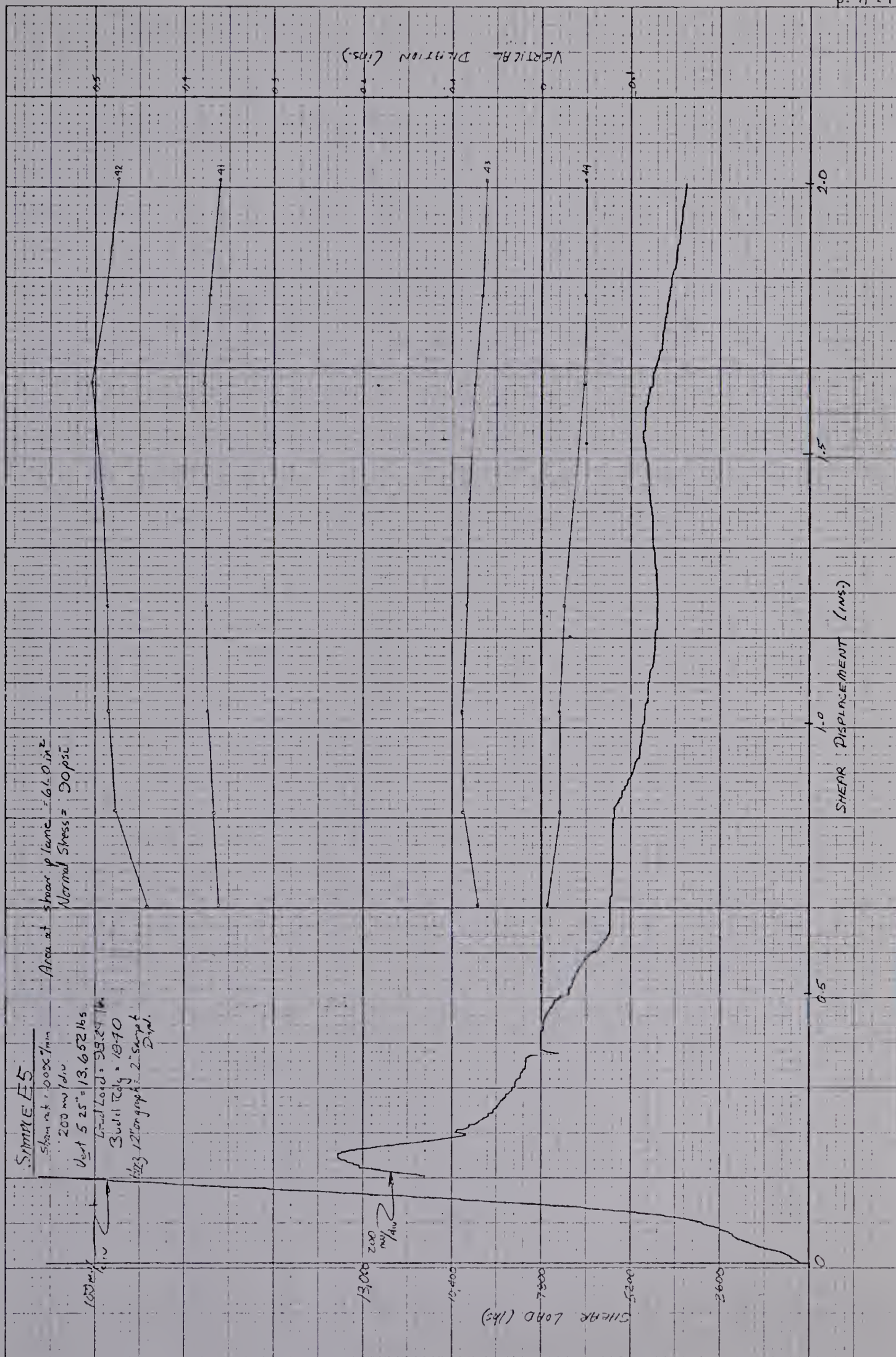


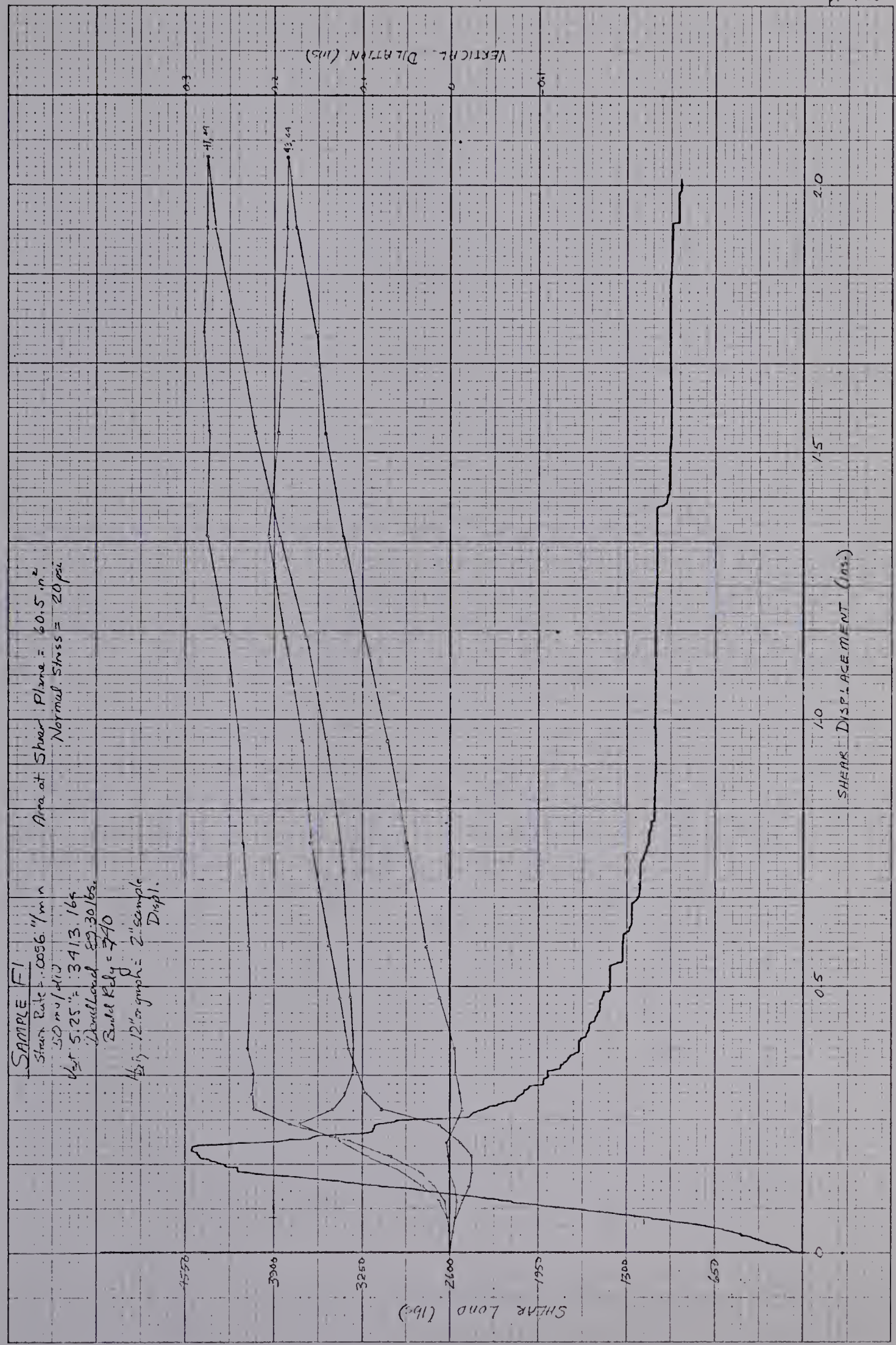


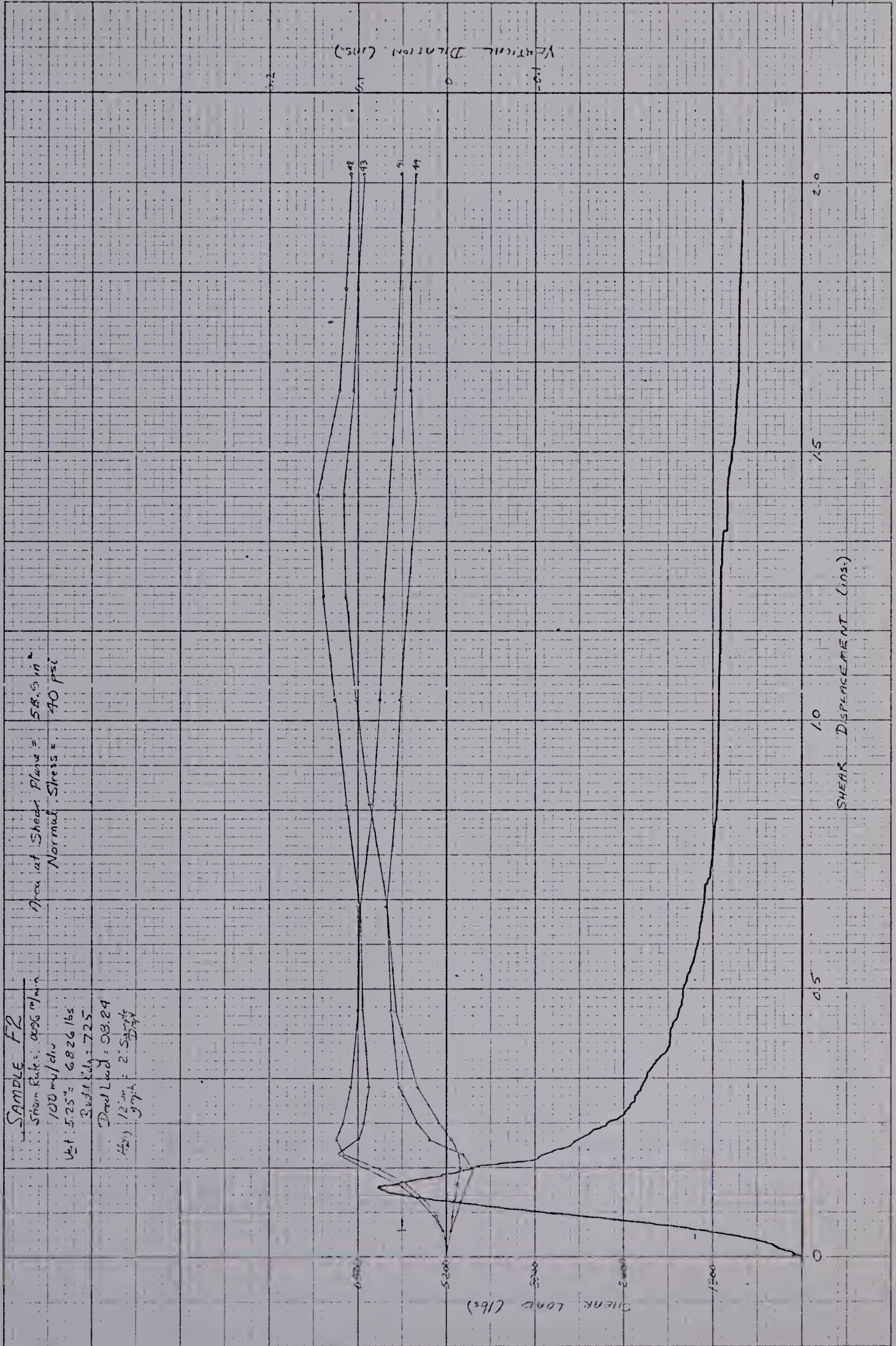


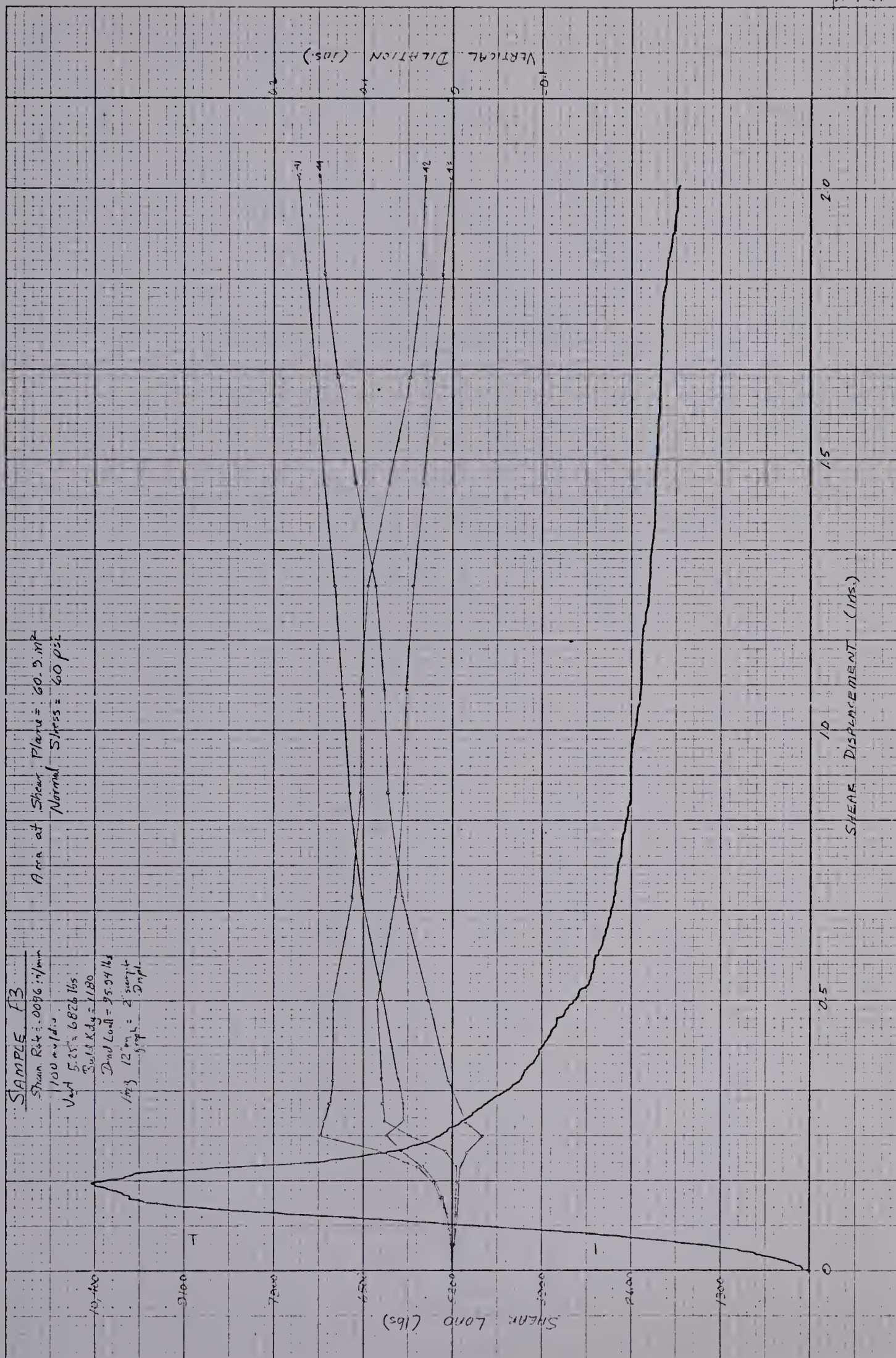


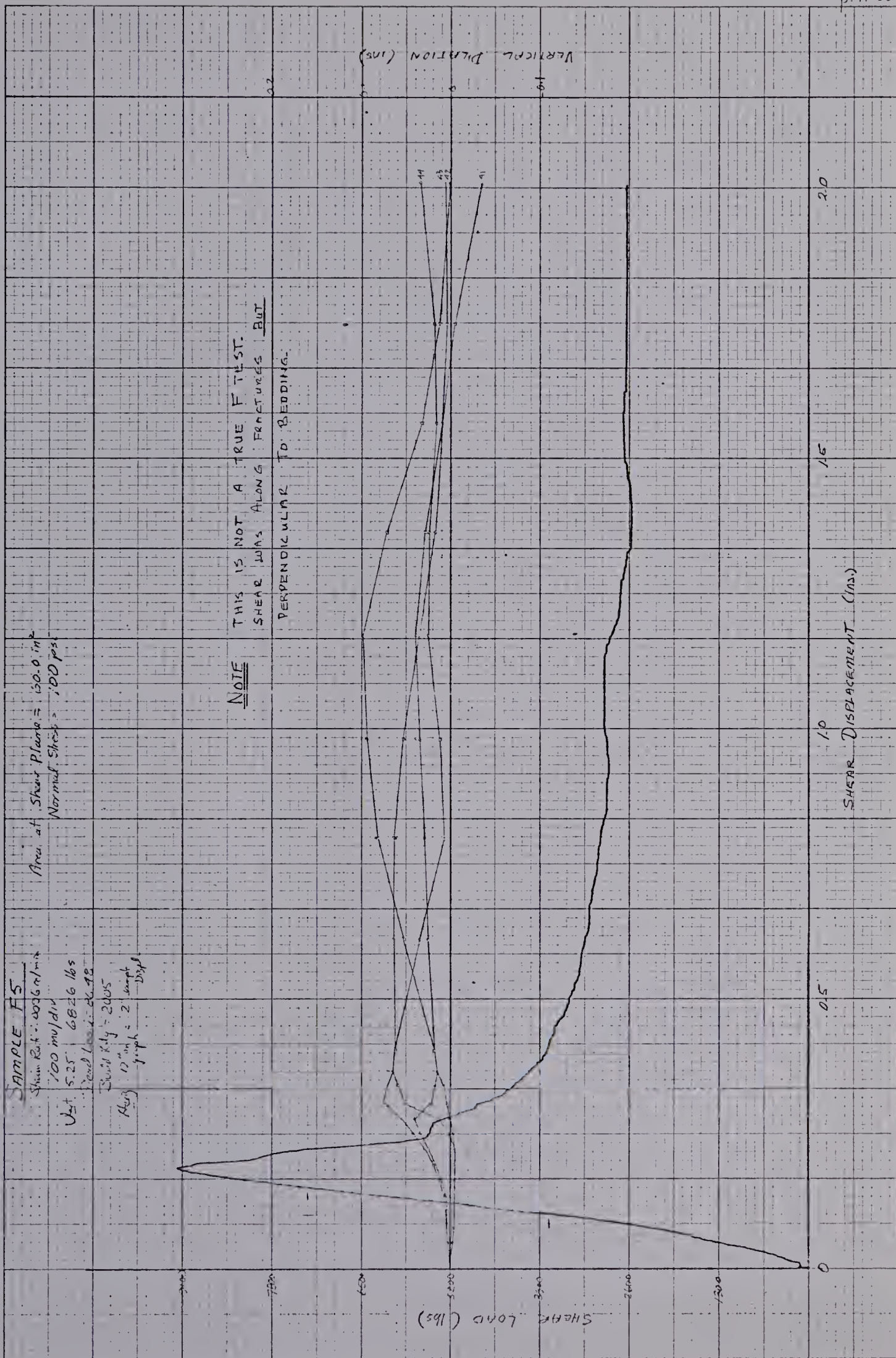


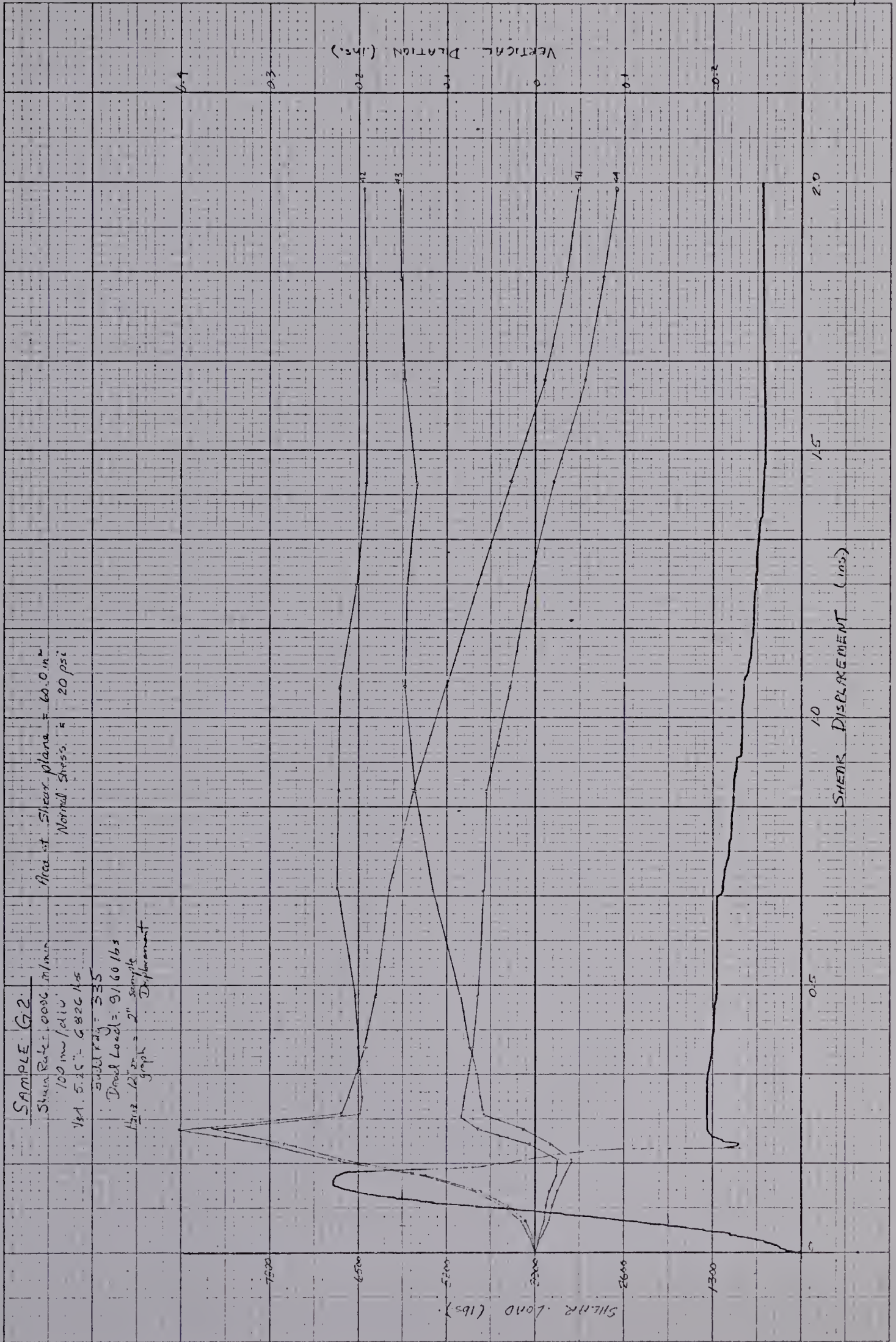


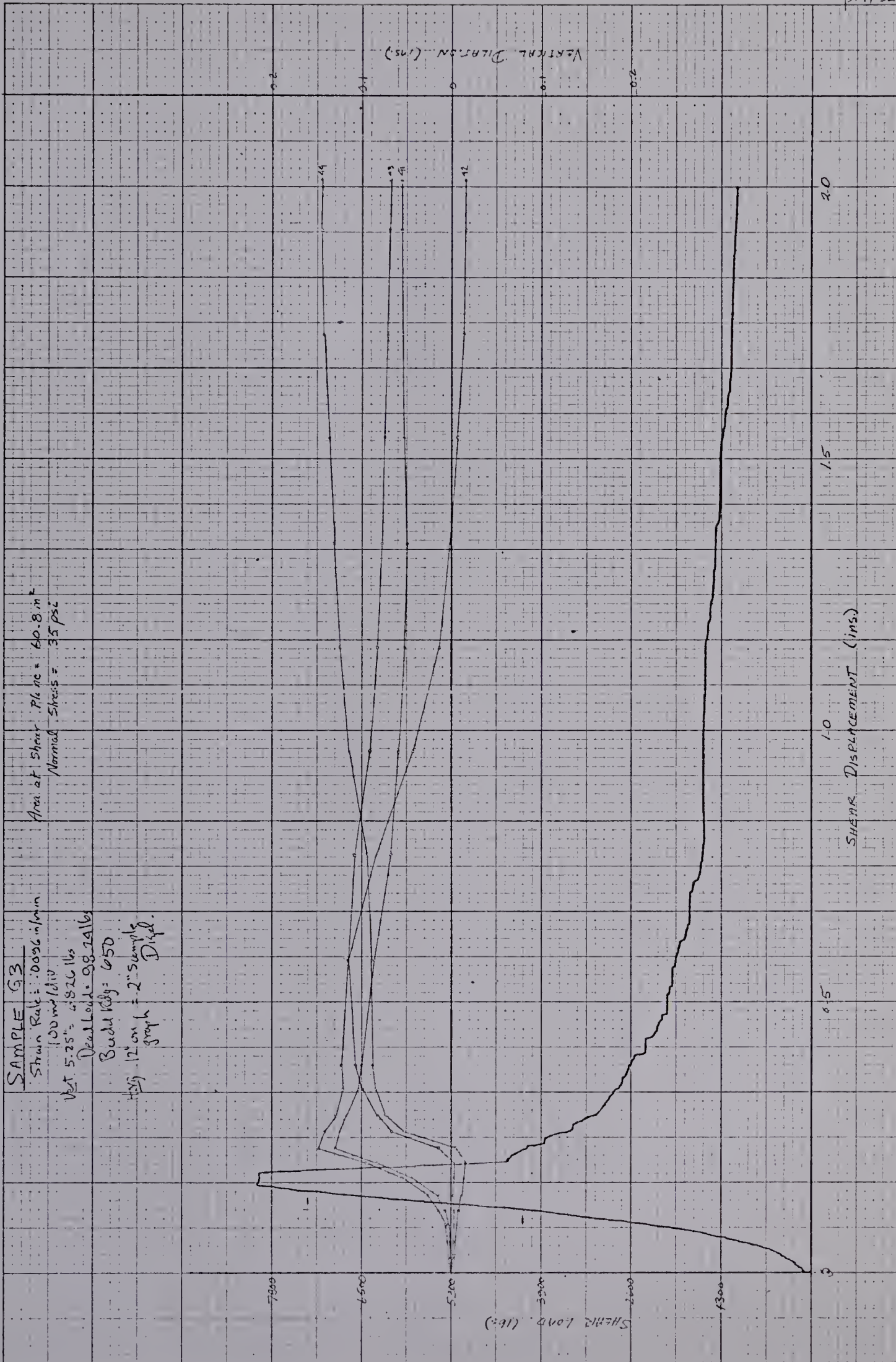


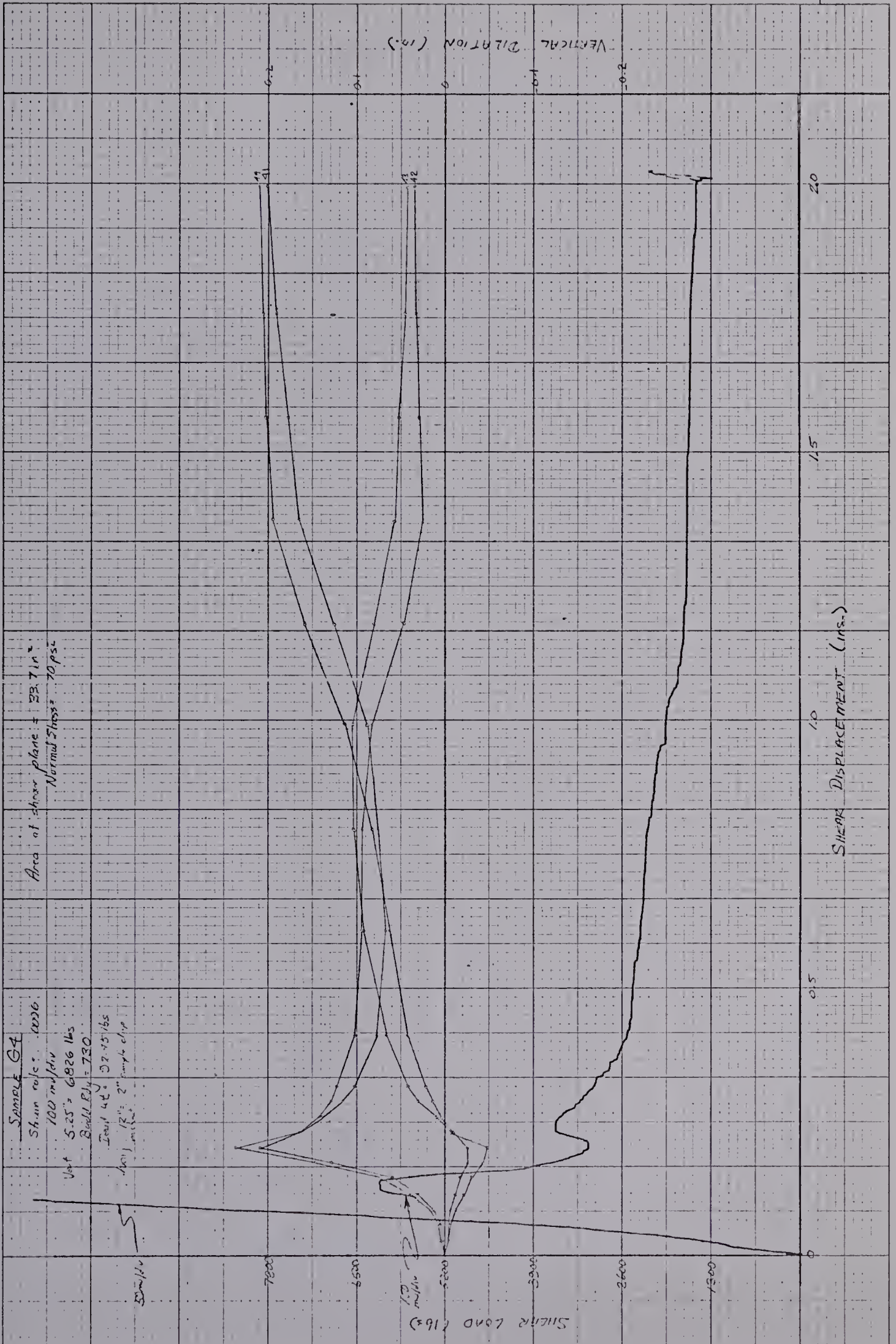












Appendix B

EXPERIMENTAL RELATIONSHIPS OF ϕ_r AND i

APPENDIX B

EXPLANATORY NOTES

The experimental relationship of $\phi_r + i$ with the independently determined values of ϕ_r and i are given in this appendix. The following notes are given to assist in the interpretation of the results.

1. The horizontal axis is given as a time scale in minutes because the results were all obtained at a set time during the test. Zero time corresponds to the point when shear loading was begun. The time scale can be converted to shear displacement by multiplying any required time by the constant strain rate imposed (0.0096 inches per minute).
2. The i values determined from each LVDT reading are shown as solid black lines along with the corresponding LVDT number.
3. The average i value is shown as a green line.
4. The $\phi_r + i$ line is shown as such by a solid black line.
5. The ϕ_r value determined from tests on samples with a pre-cut shear plane is shown by the blue line.
6. The results of subtracting the average i values (the green line) from the $\phi_r + i$ line is shown as

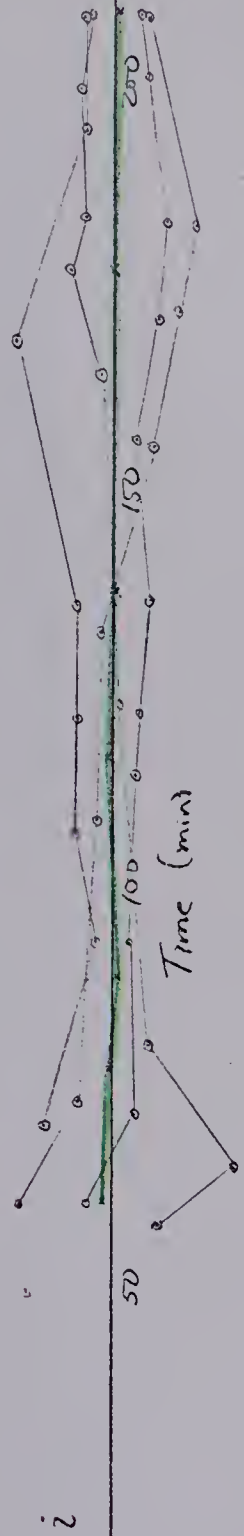
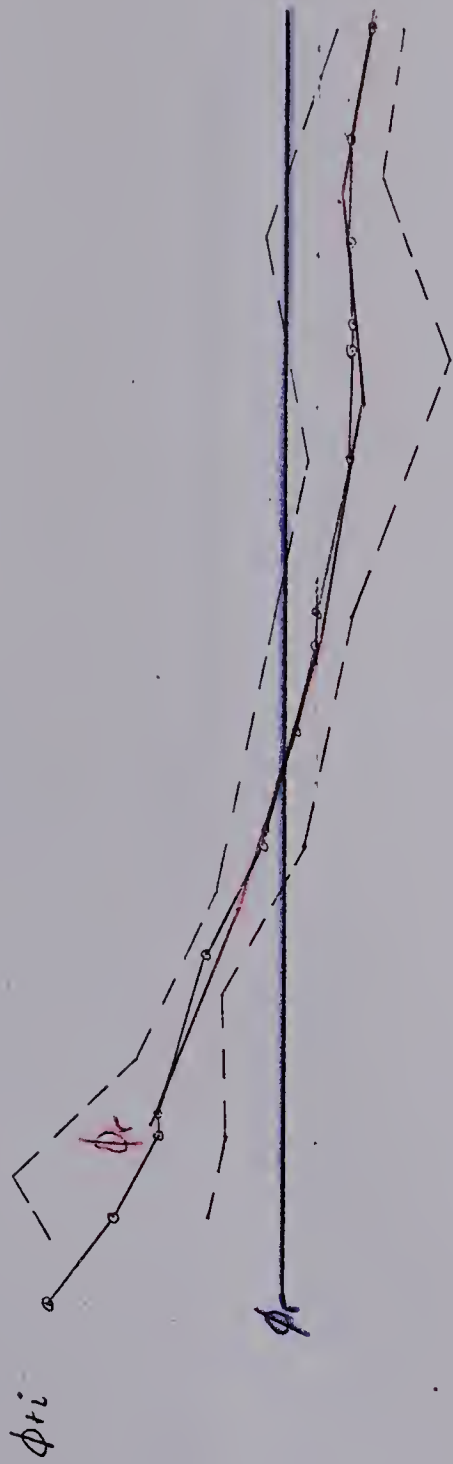
the red (\emptyset_r) line.

7. The result of subtracting the maximum i value from the $\emptyset_r + i$ line is shown as the lower dashed line.
8. The result of subtracting the minimum i value from the $\emptyset_r + i$ line is shown as the upper dashed line.

SAMPLE A2

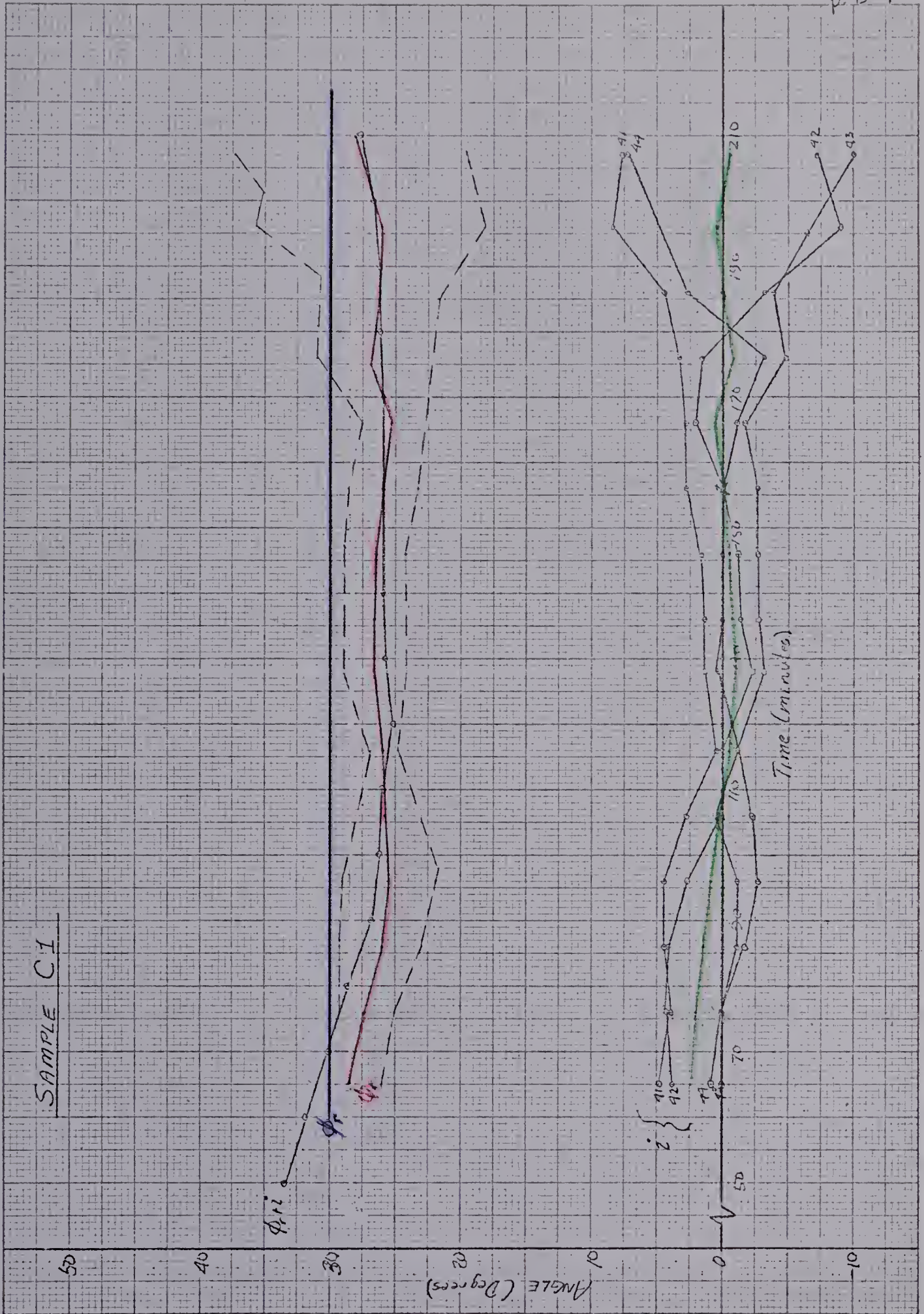


SAMPLE B1

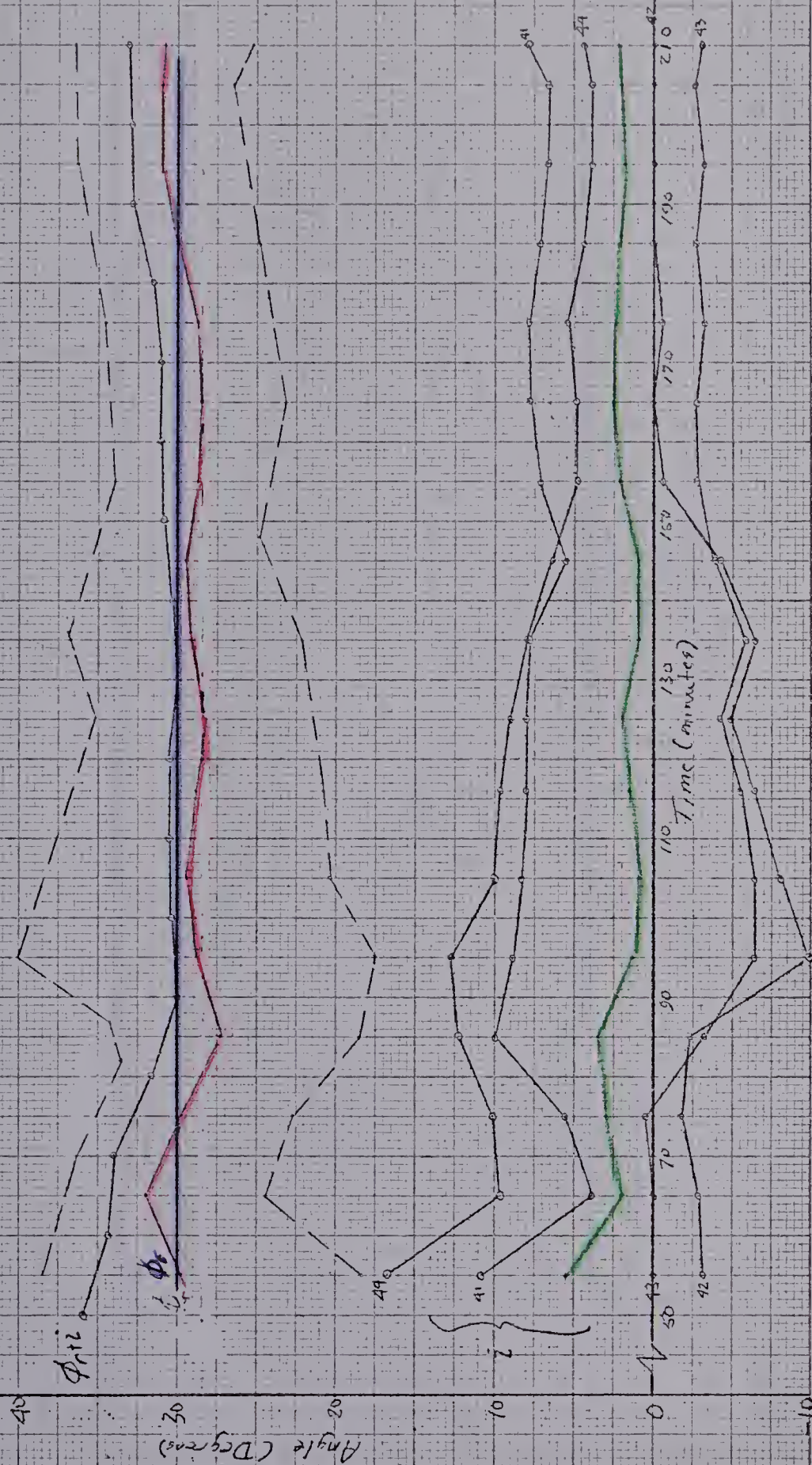




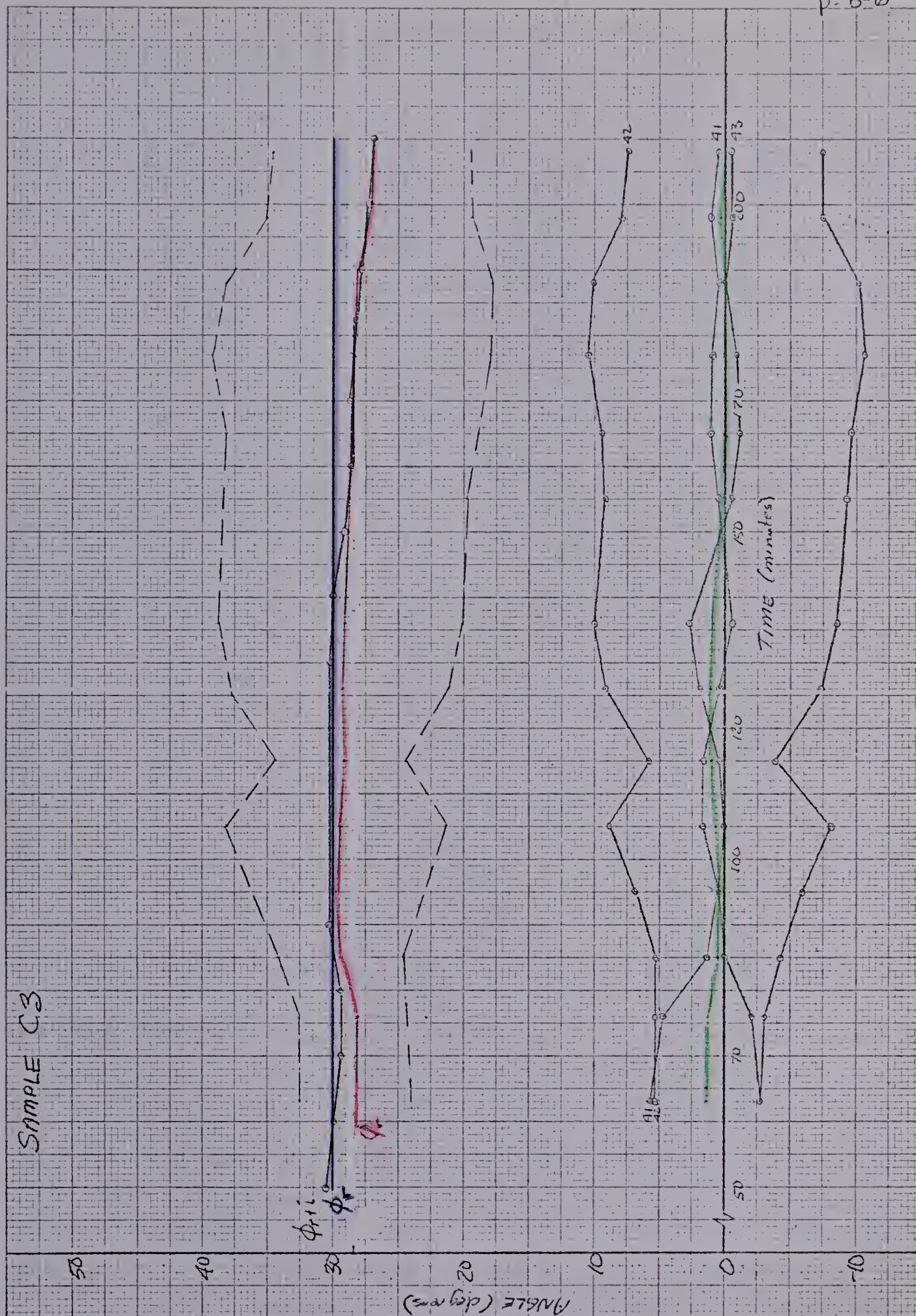
SAMPLE C-1



SAMPLE C2



SAMPLE C3

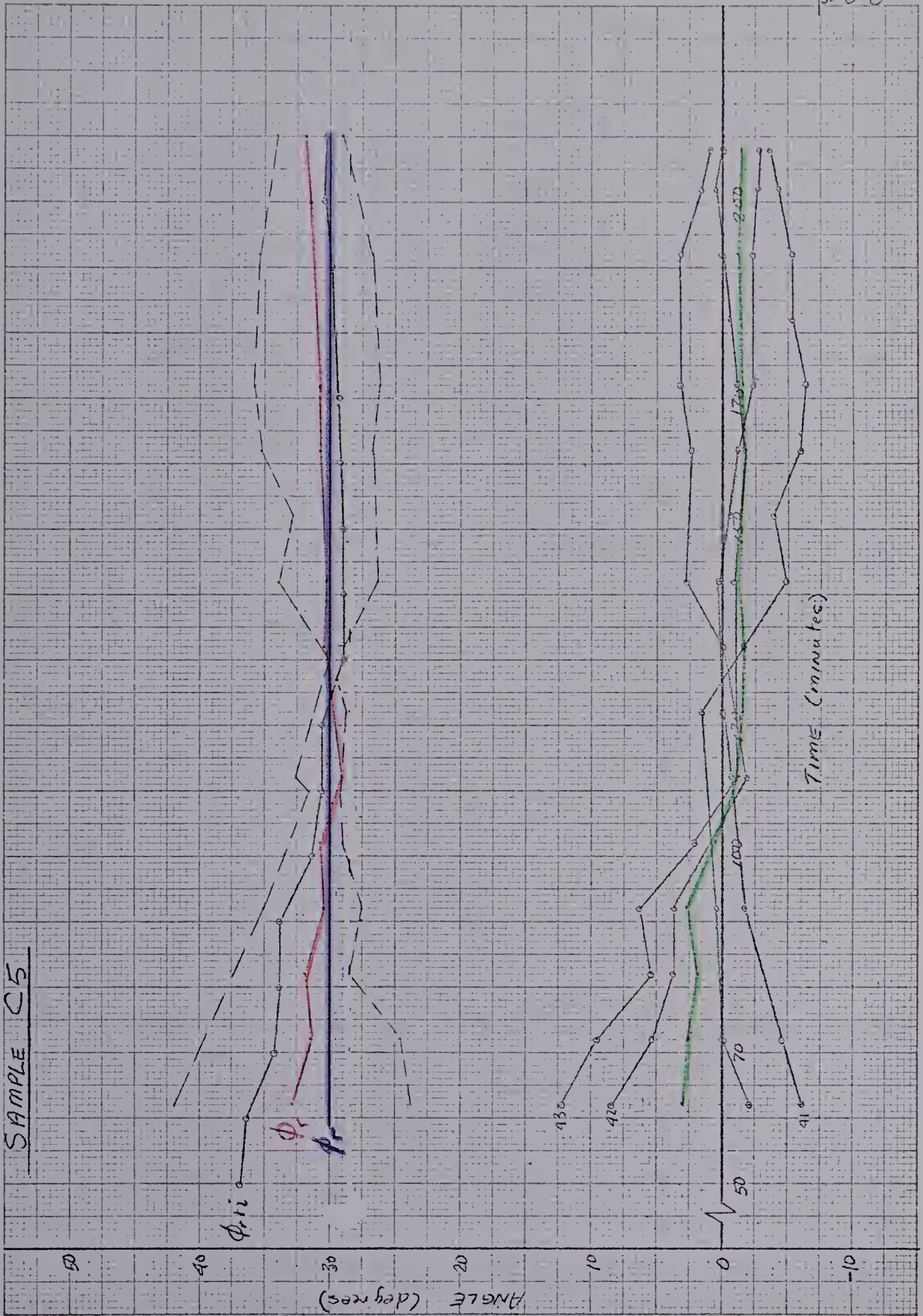


Sample C4

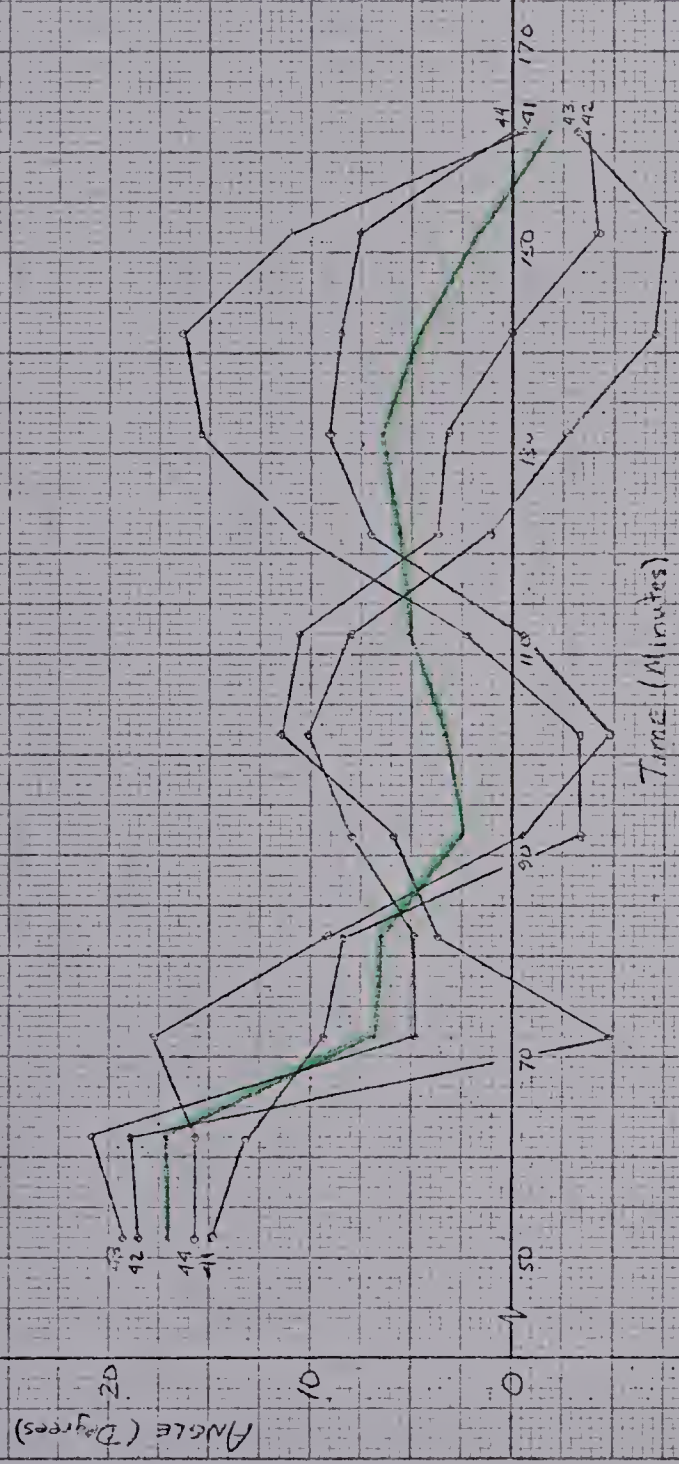
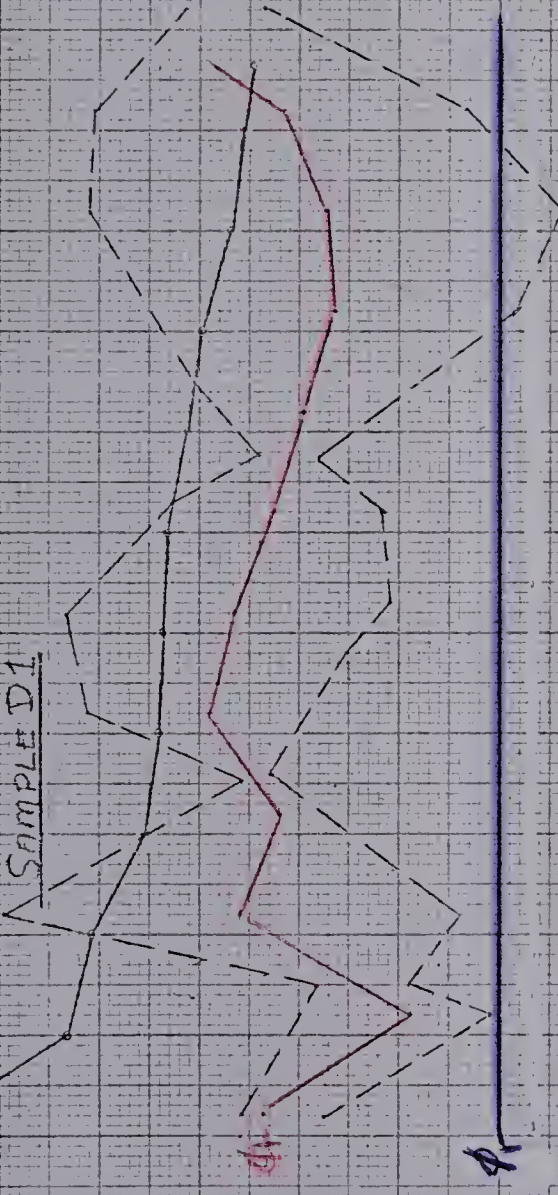


p. B-7

SAMPLE C5

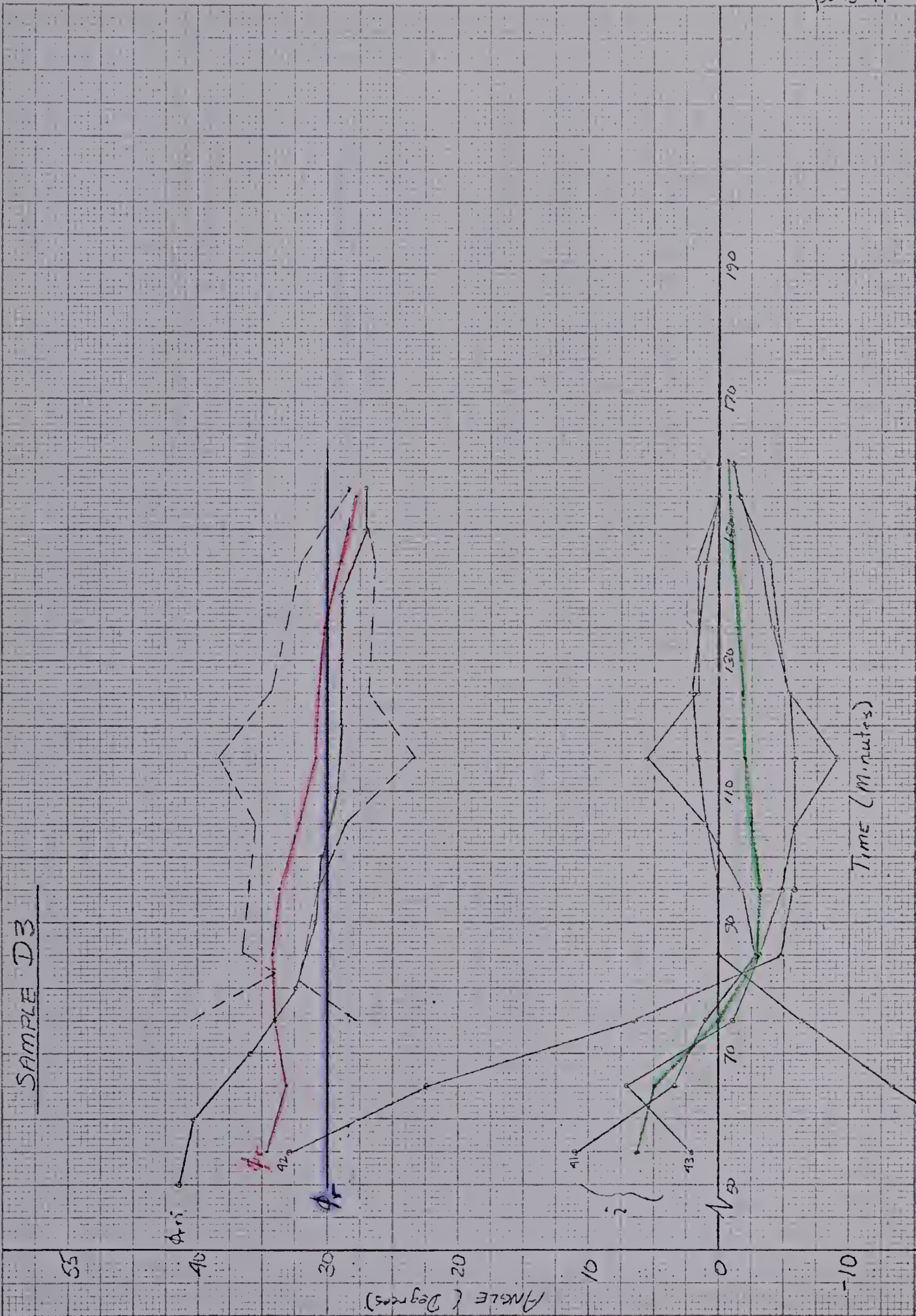


ϕ_{ti}
SAMPLE D1

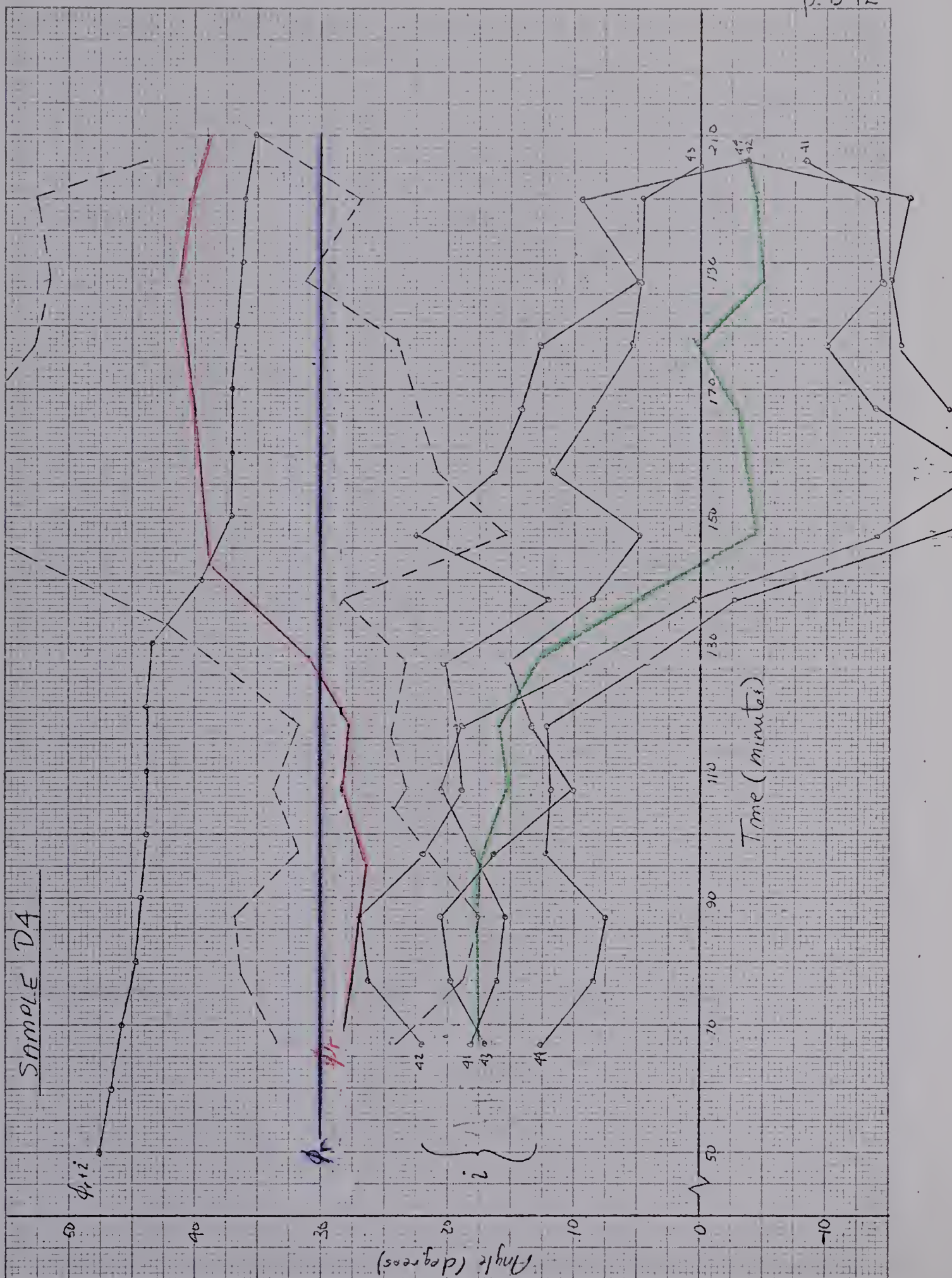




SAMPLE D3

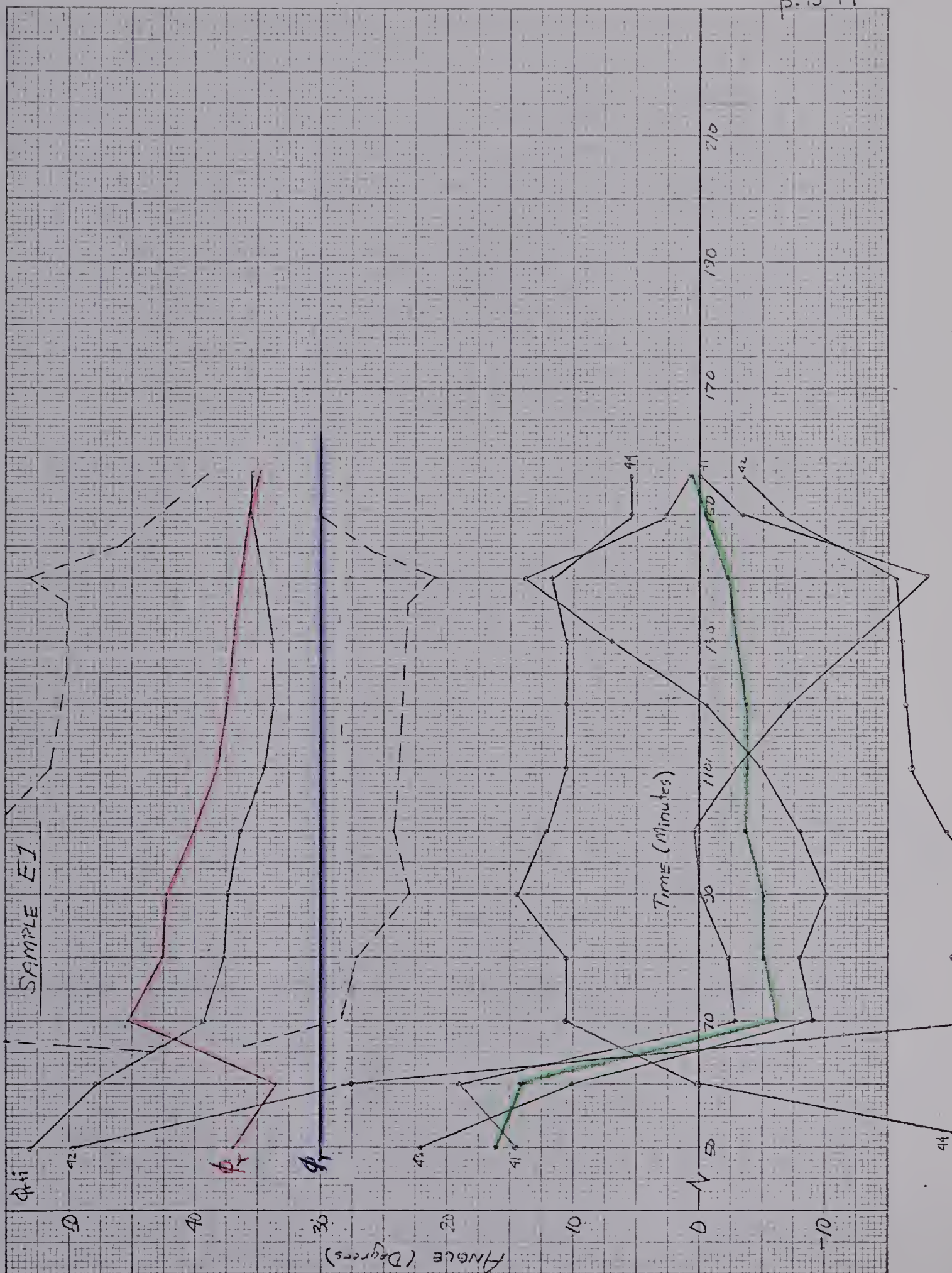


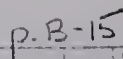
44

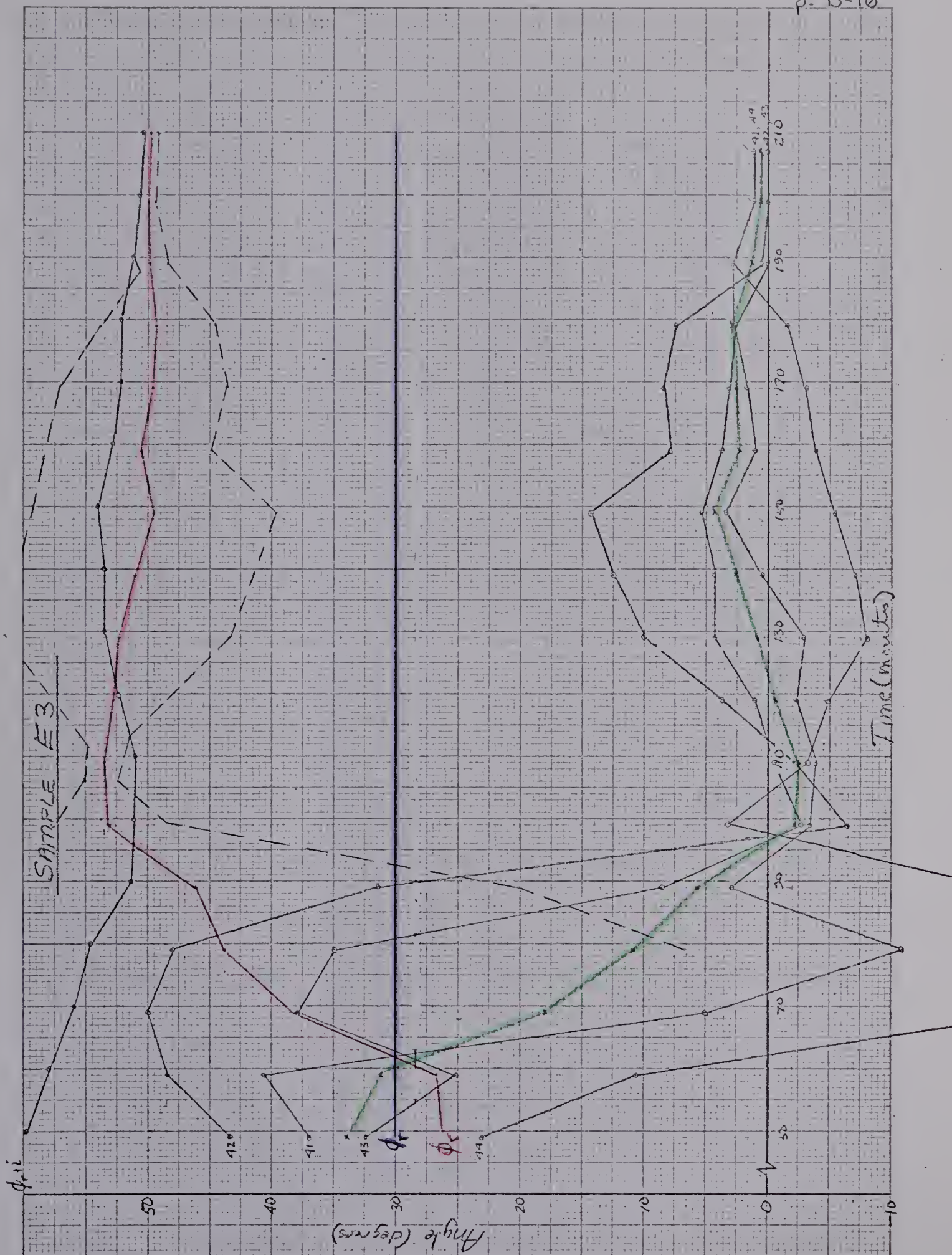


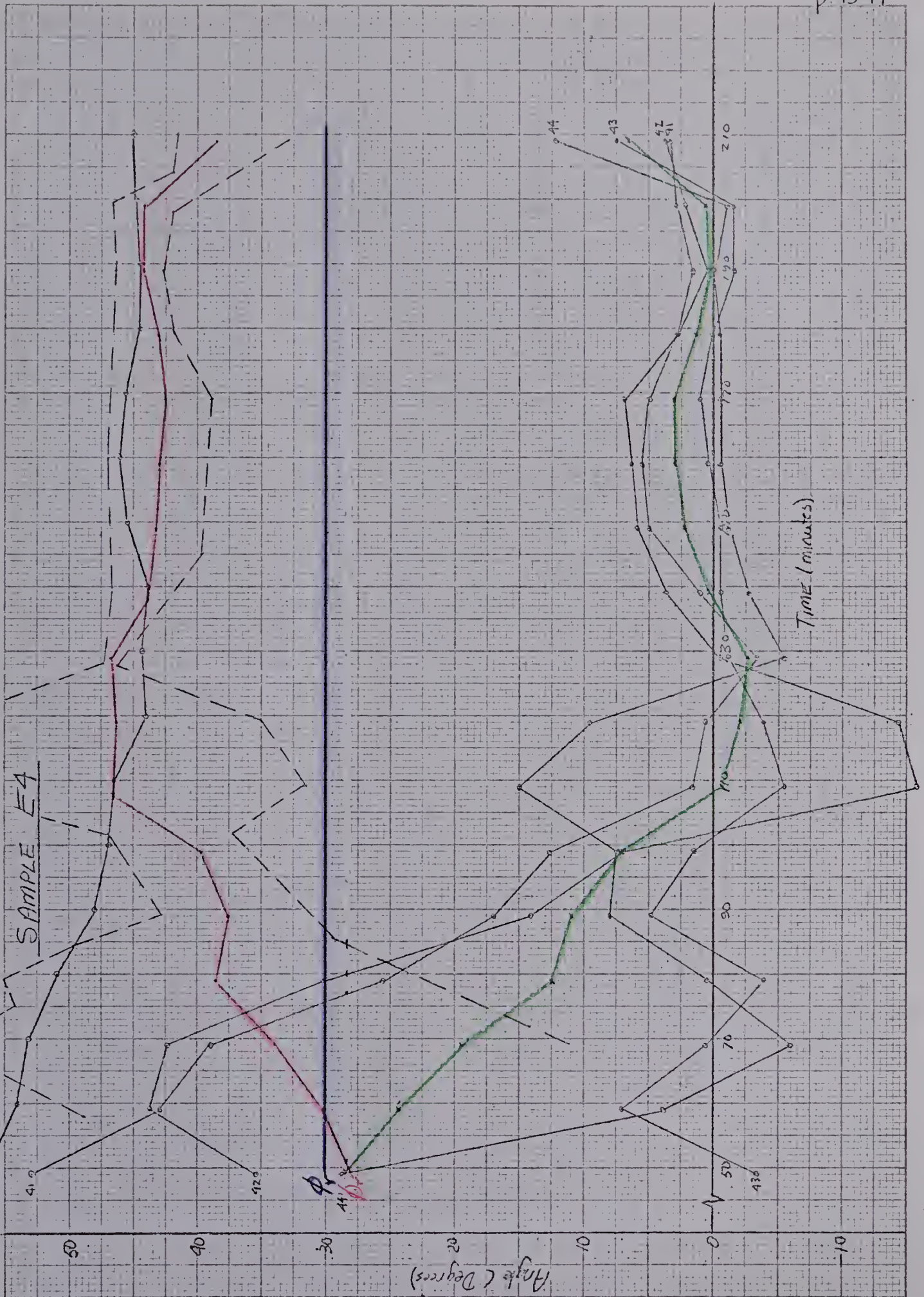
SAMPLE D5

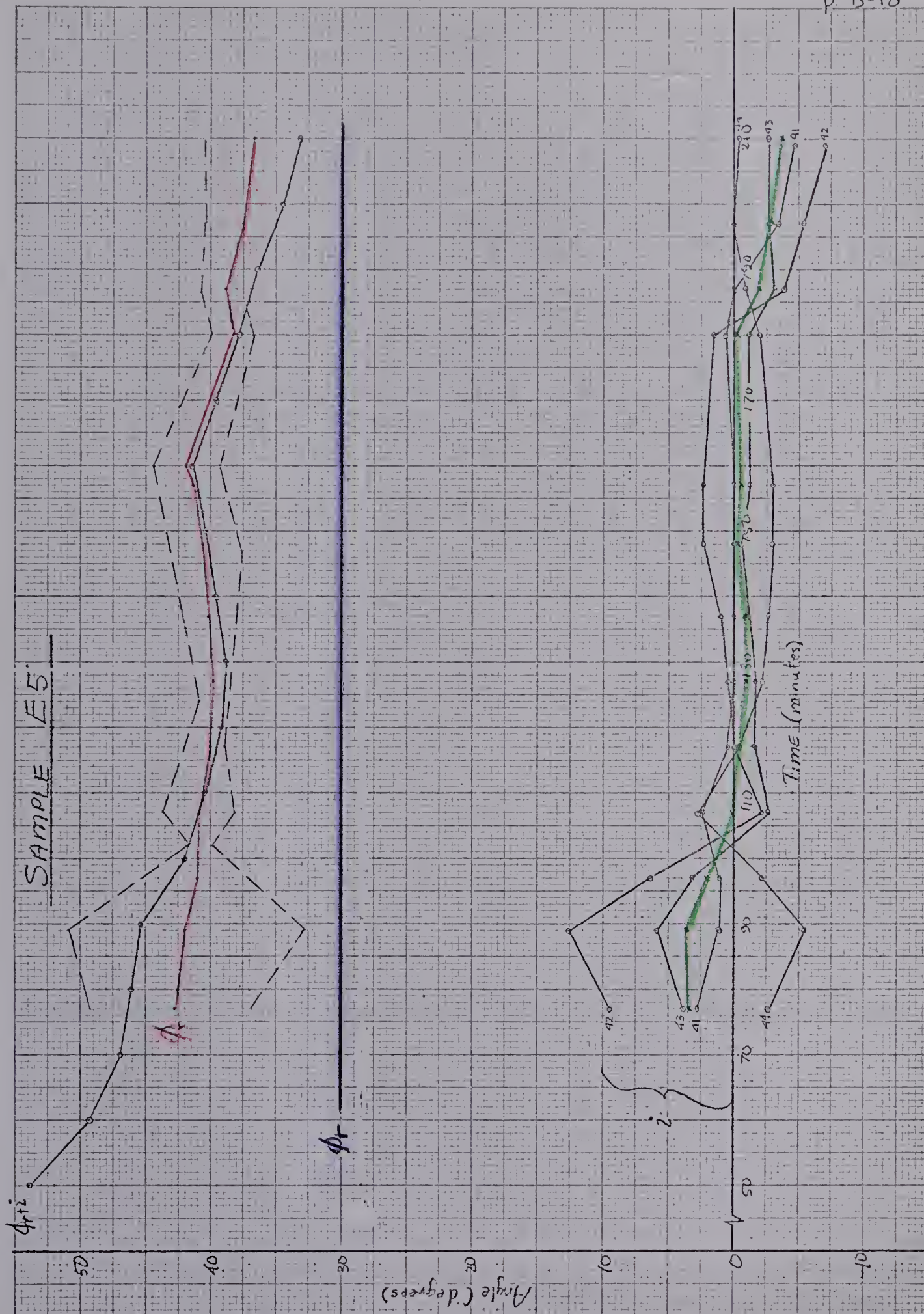


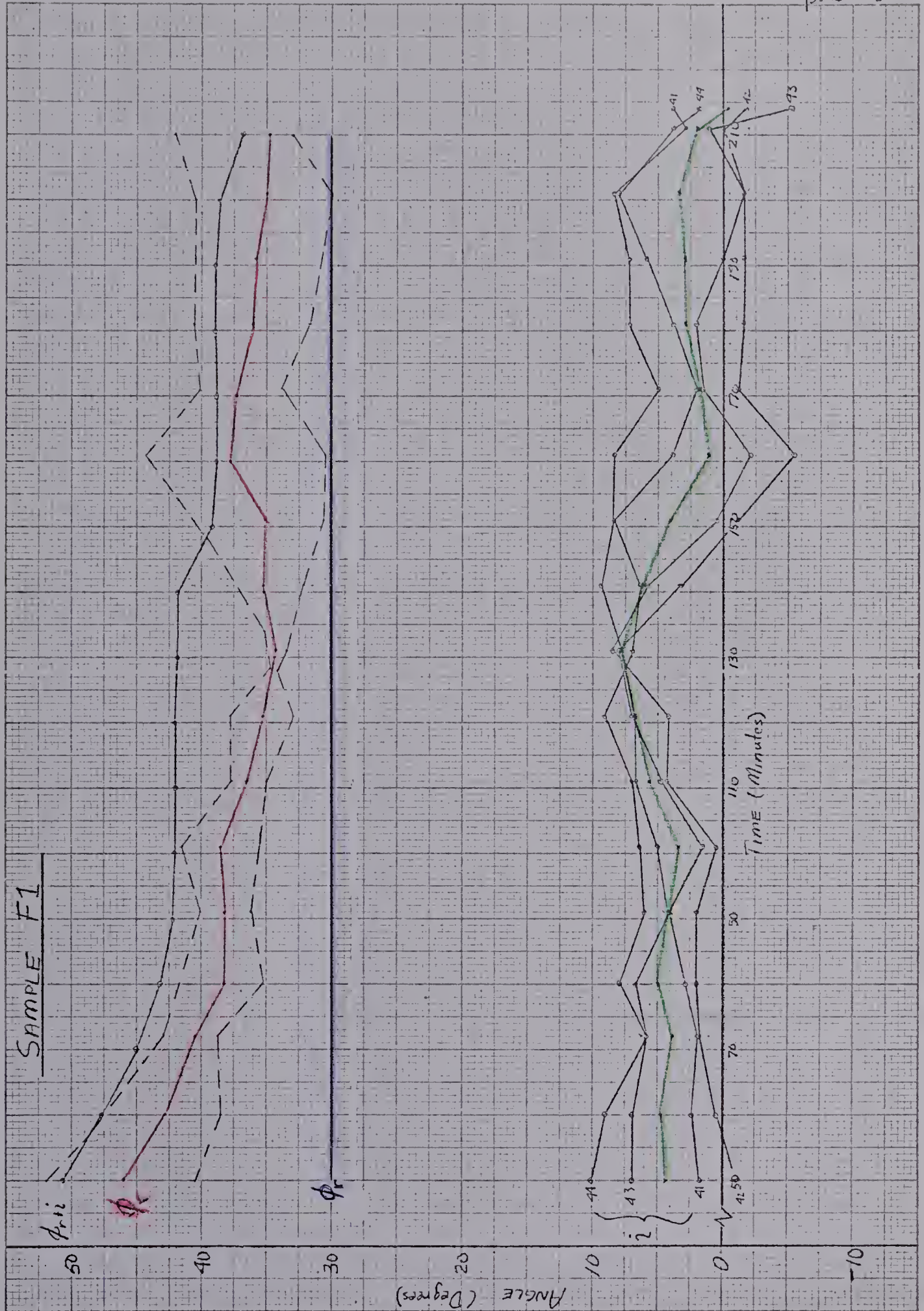




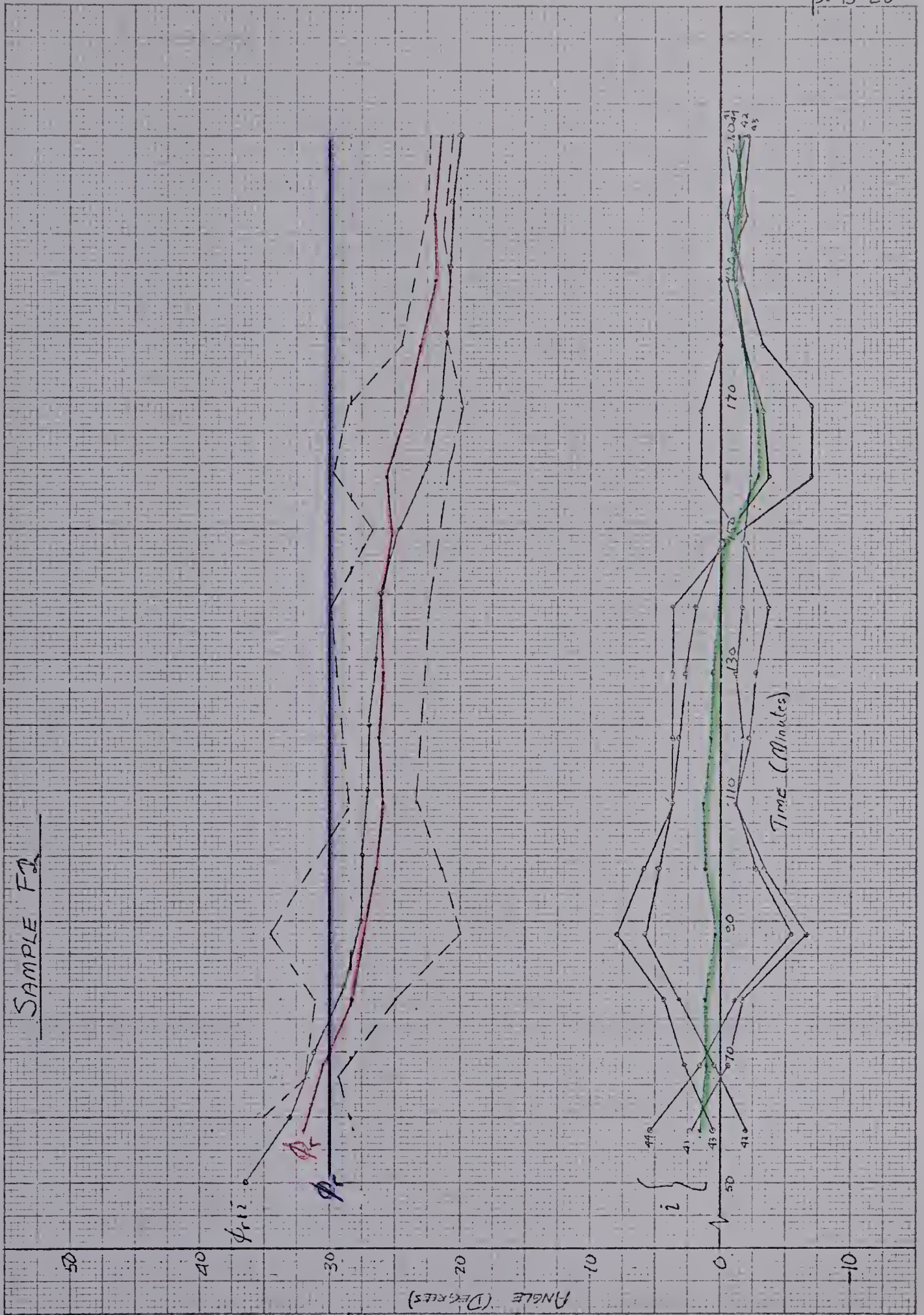








SAMPLE F2



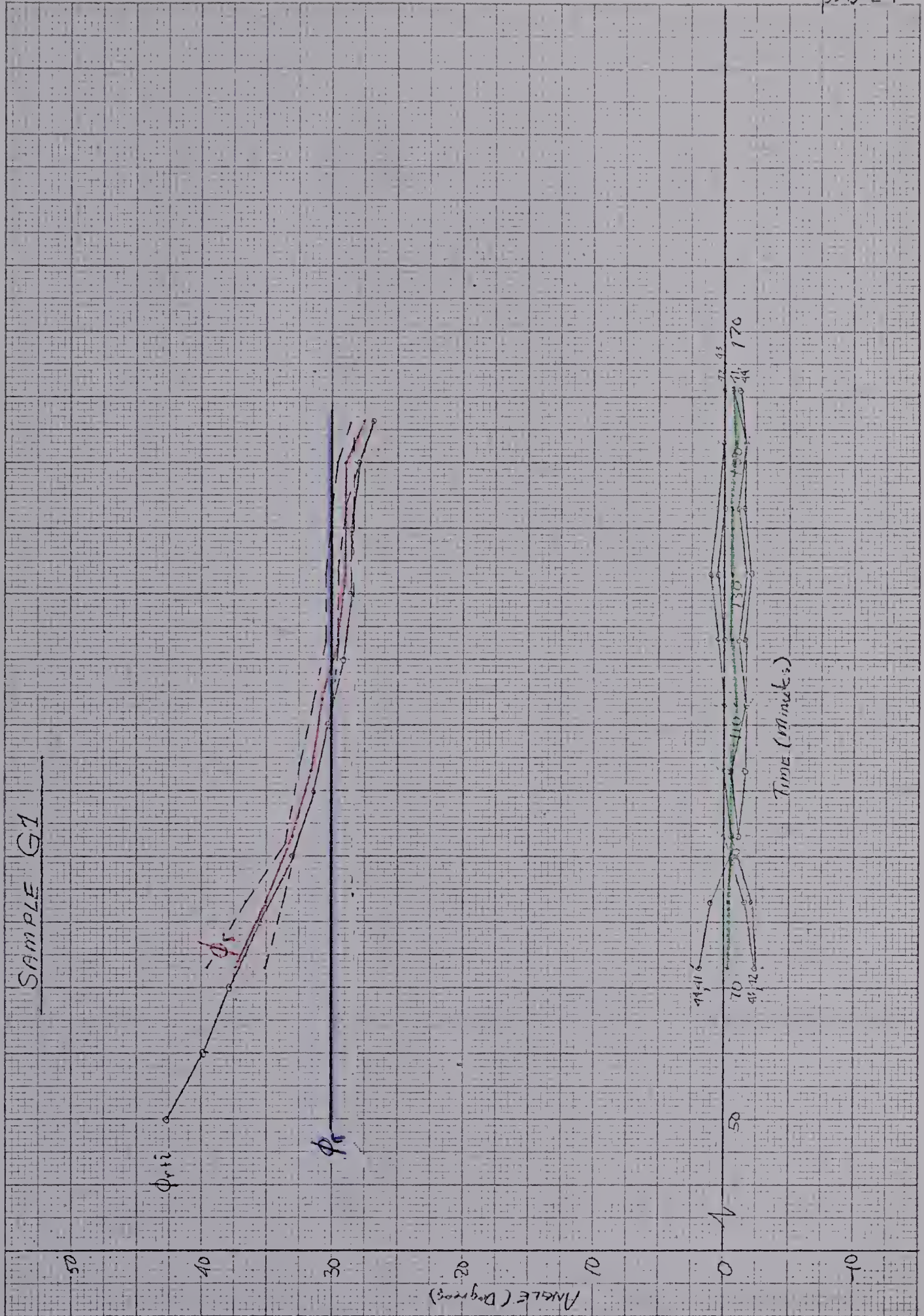


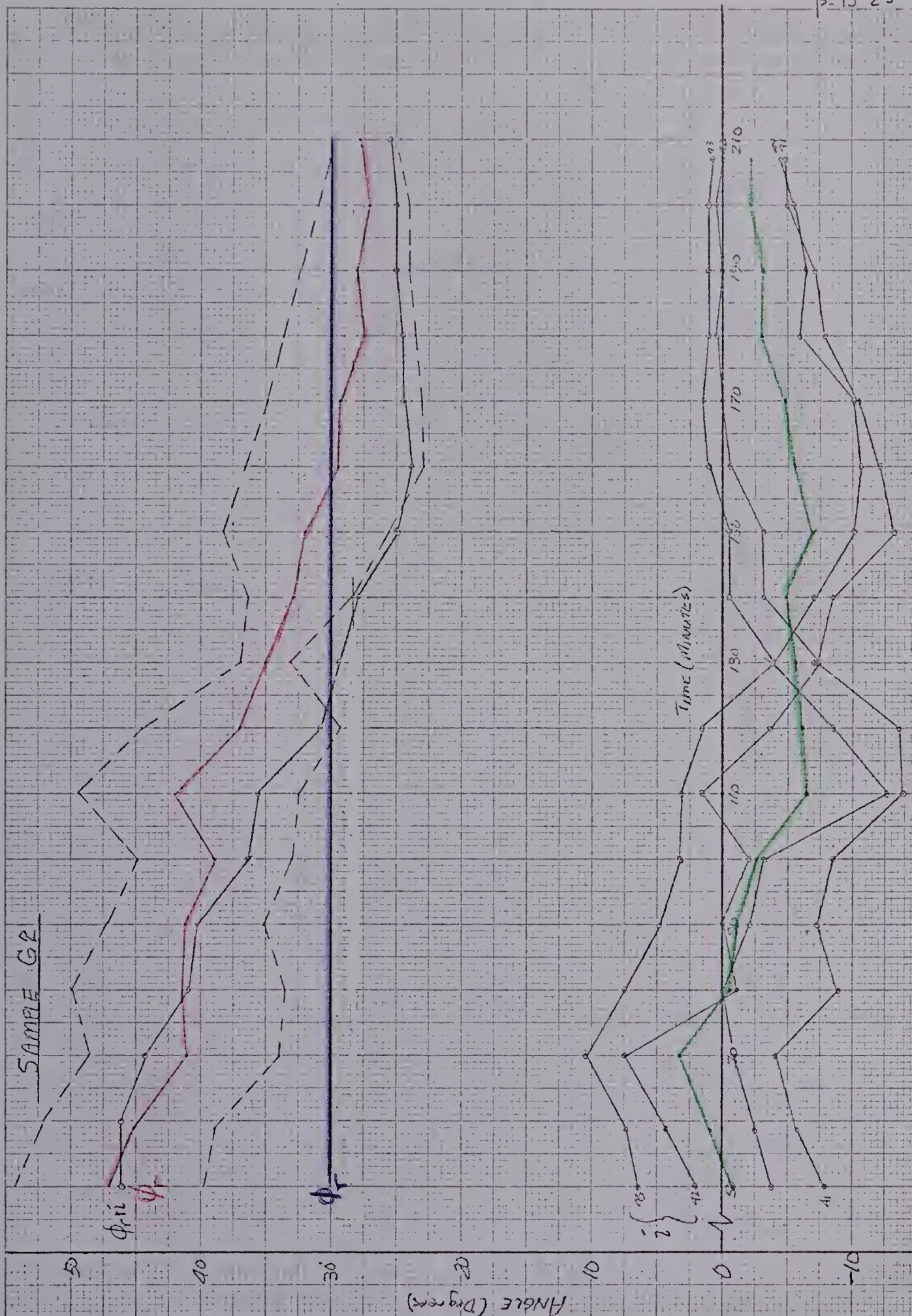


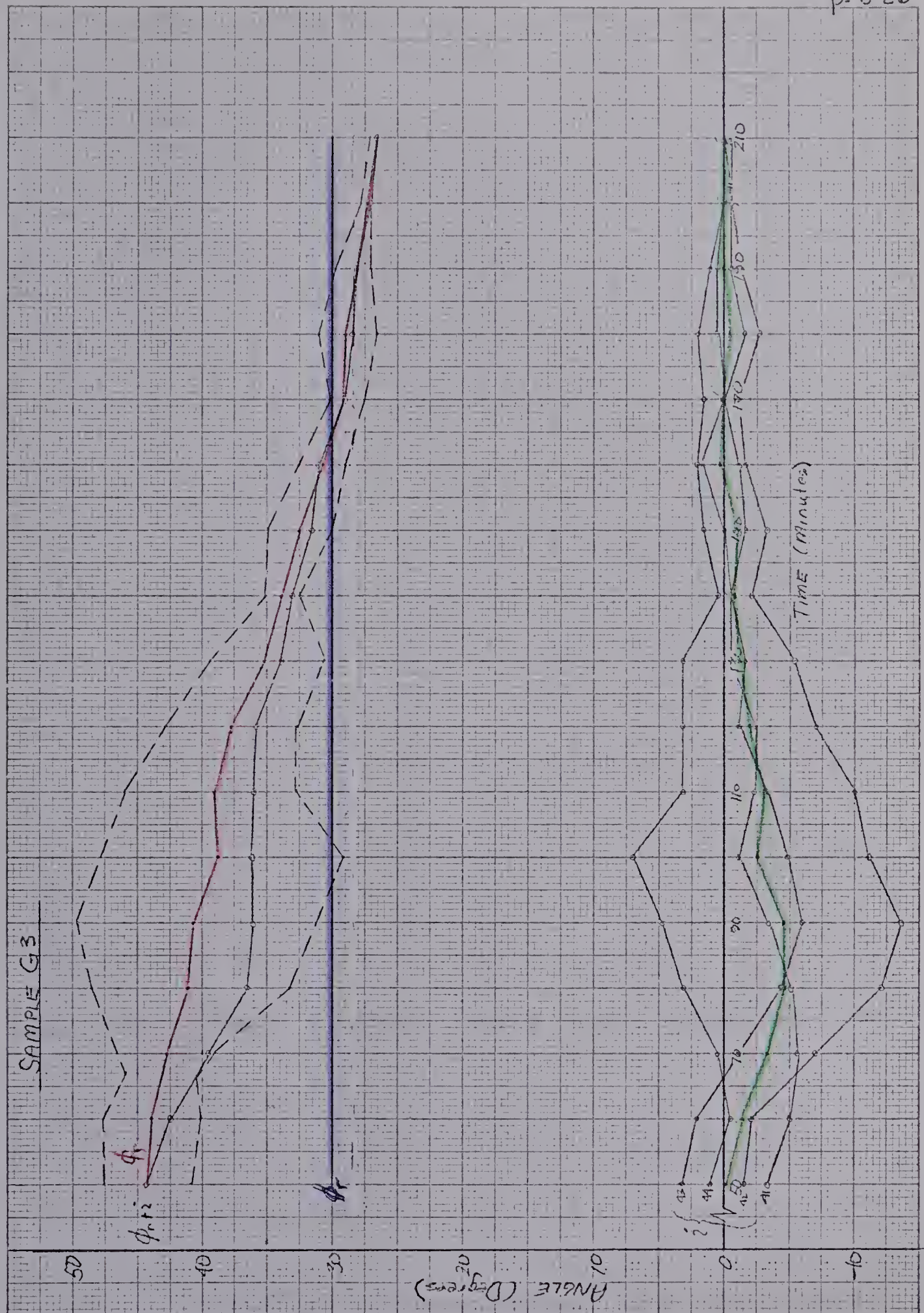
SAMPLE F5

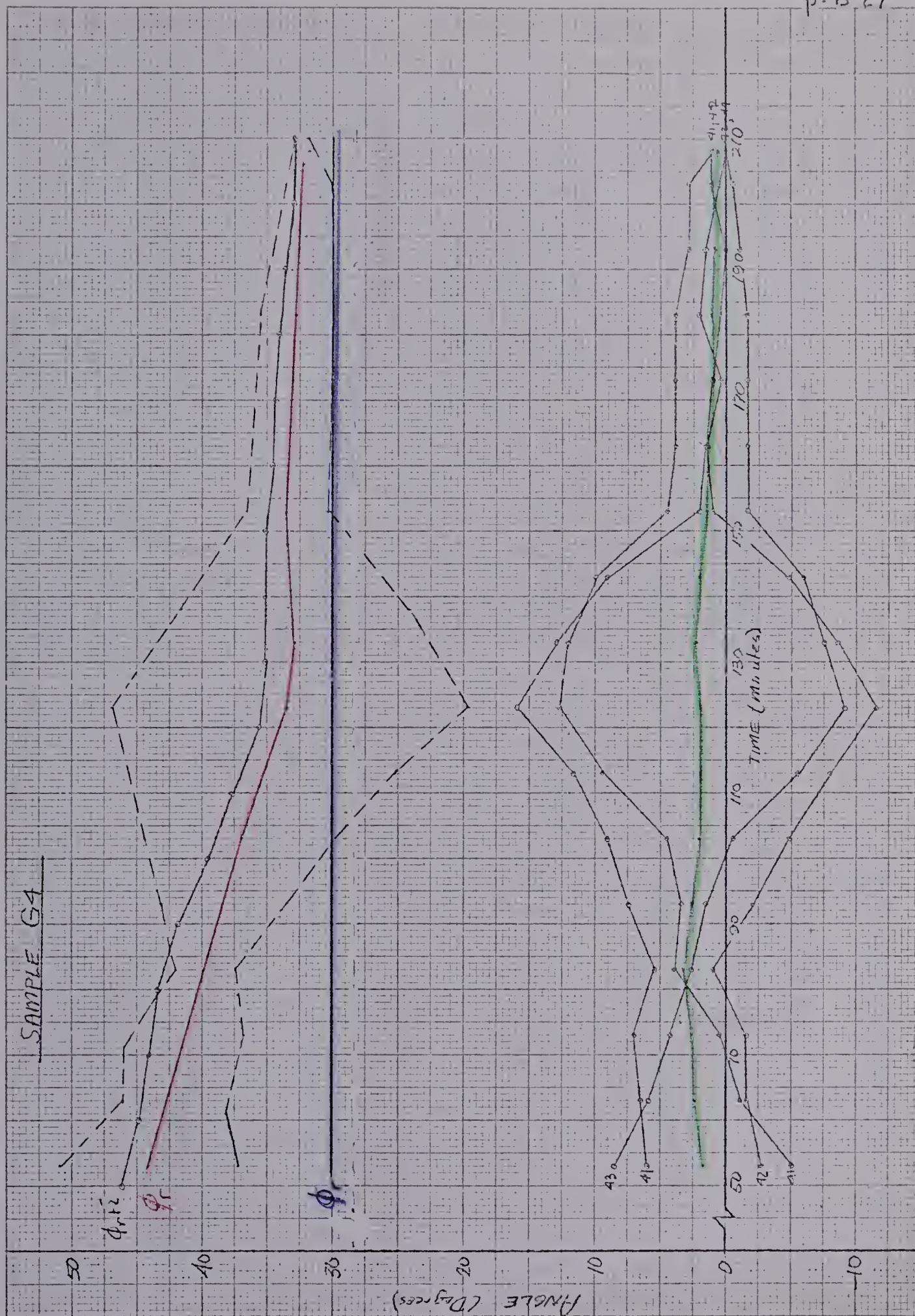


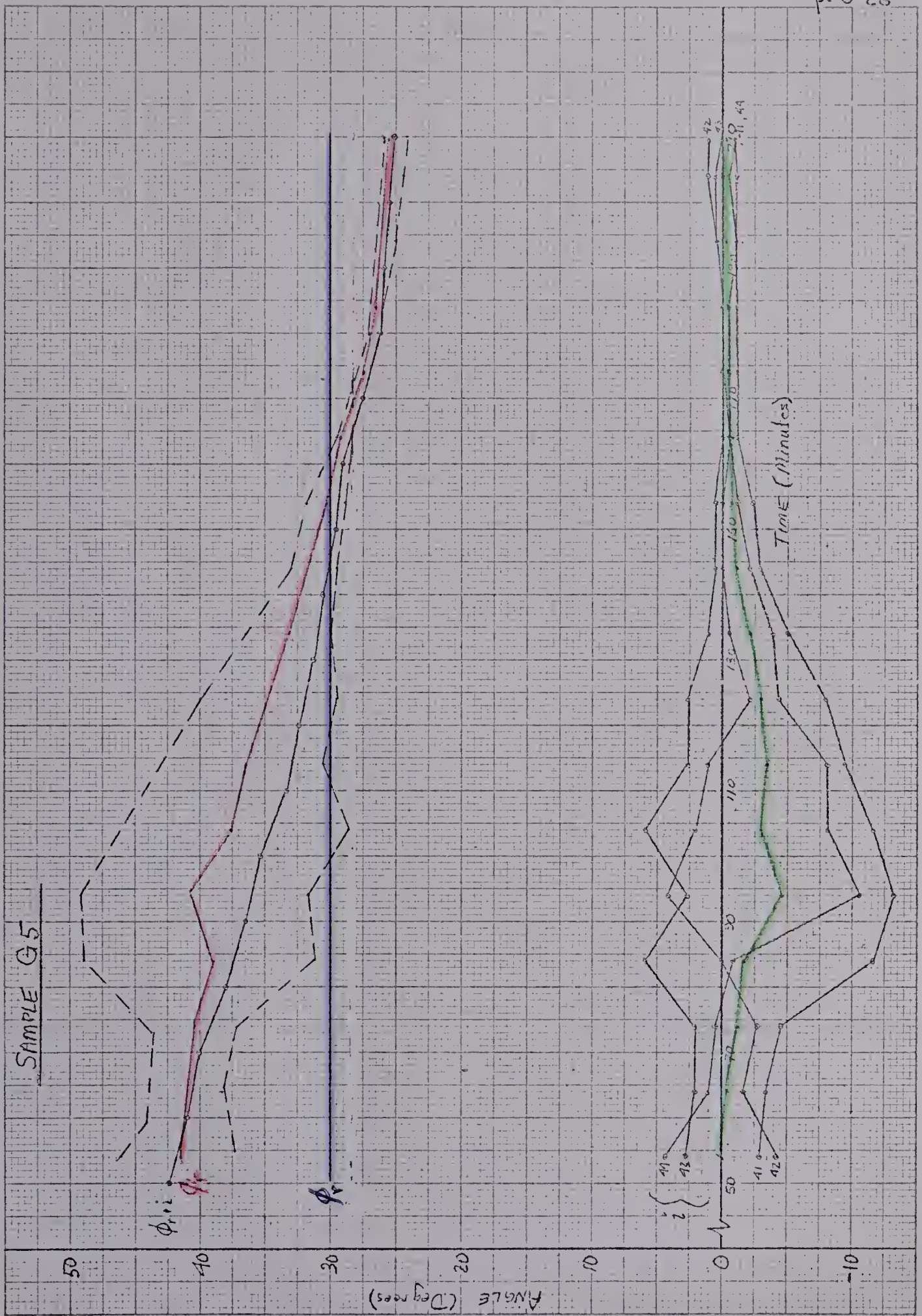
SAMPLE G1











B30015